# Tribology: The Story of Lubrication and Wear

Donald H. Buckley, William R. Jones, Jr., Harold E. Sliney,
Erwin V. Zaretsky, Dennis P. Townsend,
and Stuart H. Loewenthal
*Lewis Research Center*
*Cleveland, Ohio*

# CONTENTS

# Tribology

# TRIBOLOGY*

Donald H. Buckley
National Aeronautics and Space Administration
Lewis Research Center
Cleveland, Ohio 44135

Tribology is the study of the adhesion, friction, wear, and lubricated behavior of materials in solid-state contact. The function of tribological research is to bring about a reduction in the adhesion, friction, and wear of mechanical components to prevent their failure and provide long, reliable component life through the judicious selection of materials, operating parameters, and lubricants.

Mechanical systems such as bearings, gears, and seals are examples of components involving tribology. Wherever, however, two or more solid surfaces are in contact with relative motion between the surfaces, tribology is involved. Such mundane activities as a man's morning shave involve both friction and corrosive wear, and considerable tribological research has gone into increasing blade life and reducing friction and shaving discomfort. More complex tribological systems are gyro bearings and instrumentation gears requiring attention to many elements.

The objective of the present paper is to review the adhesion, friction, and wear properties of materials and some of the factors influencing these properties. The forms of lubrication and types of lubricants will also be discussed.

## ADHESION AND FRICTION

In a conventional atmospheric environment, the oxygen present in the air interacts with freshly generated metal and alloy surfaces to produce surface films; namely, oxides. These oxides play a very strong role in the adhesion, friction, and wear behavior of metals and alloys. In the absence of these oxides, very strong adhesion, high friction coefficients, and ultimately cold welding of materials from one surface to another are observed. If, for example, two normal metal surfaces are placed inside a vacuum environment with a system capable of achieving pressures to $10^{-10}$ torr, and the surfaces are very carefully cleaned with argon ion bombardment and then brought into touch contact, adhesion of one surface to the other will immediately occur. Attempts at tangential motion will cause a growth in the area adhered at the interface, that is, in the real contact area with an ultimate complete seizure of the surfaces one to another. With this occurrence, the surfaces are generally severely disrupted (refs. 1 and 2).

When adhered surfaces are separated, the adhesion at the interface between the two dissimilar solid surfaces is sufficiently strong to prevent fracture at the interface, but fracture does generally occur in the cohesively weaker

---

of the two materials in contact (ref. 3). An example of such behavior is shown in the photomicrograph of figure 1. This figure represents the results of an experiment conducted in a vacuum chamber where two solid surfaces were brought into contact; the surfaces had been cleaned in vacuum. Adhesion occurred at the interface, and when separation of the solid surface was attempted, fracture occurred in one of the two materials, leaving material transferred to the opposite surface.

The actual area of real contact at the interface can be seen in figure 1 by a careful examination of the interface region. There appear to be voids in the interface region where complete and intimate solid-state contact across the interface did not occur. However, a great portion of the interfacial area does reflect solid-to-solid contact in adhesive bonding. This adhesive bond was generated as a result of attempting to slide one surface over the other. This resulted in growth in the adhered junctions at the interface, leaving only a small are wherein no intimate contact of the two solid surfaces occurred. On separation, the adhesive bond at the interface remained intact and fracture occurred in one of the solids, as indicated in figure 1 by the rough piece which remained on the solid surface.

This type of adhesion and transfer behavior is observed for all clean metal surfaces and alloys in solid-state contact. That is, when the environmentally contributed surface films, namely the oxides, are removed, such adhesion is observed with strong bonding and friction coefficients measured in excess of 100 under such circumstances. The surfaces of solids such as metals and alloys are so sensitive to the contact region microenvironment that the admission of very small adsorbate concentrations from the environment to the solid surface can markedly reduce adhesion and friction. For example, fractions of a monolayer on the solid surface will produce a marked reduction in the adhesion and corresponding static friction coefficients for metal in contact (ref. 4).

In addition to metals and alloys, nonmentallic materials are also markedly influenced by the presence of the environment in their adhesion, friction, and wear behavior. The presence of adsorbates on ceramic materials such as aluminum oxide has a pronounced influence on the friction coefficients measured for aluminum oxide (ref. 5).

Polymeric materials are also affected by the presence of environmental constituents on their surfaces. For example, nylon serves as a good solid self-lubricanting material in certain mechanical applications. Nylon, however, depends upon the presence of adsorbed moisture for its effective lubrication; that is, for its low friction and wear properties. In the absence of moisture, nylon will not lubricate effectively and it becomes a poor tribological material (ref. 5). Carbon materials are heavily used in mechanical devices such as dynamic seals and are extremely sensitive to environment and environmental constituents.

The flying of aircraft at high altitudes results in excessive wear in carbon generator brush materials; this was established during the second World War. Careful analysis of the aircraft surfaces revealed that the excessive wear of carbon materials, carbon bodies at high altitudes, was due to a reduction in the ambient pressure, and more particularly with the reduction of moisture in the environment. Carefully controlled experiments in the laboratory subsequently demonstrated that carbon lubricates effectively in the

presence of moisture, exhibiting low friction, low wear, and little tendency to adhere. In the absence of moisture, however, carbon exhibits extremely heavy wear and becomes a very poor friction and wear material. In fact, by simply reducing the ambient pressure from 760 torr of air to an ambient pressure of approximately 1 torr, a 1,000-fold change in wear properties occurs. Thus, moisture is a lubricant and is needed on these surfaces and at the interface between two carbon bodies in relative contact and in motion, or between the carbon body and some other material in solid-state contact (ref. 5).

If one considers the environment not only as an ordinary air containing principally oxygen and nitrogen with some water vapor, but also considers vapors of hydrocarbons as constituents of the environment, then the particular hydrocarbon molecular structure that may be present in the environment can have a very pronounced influence upon the adhesion, friction, and wear behavior of materials in contact. For example, careful cleaning of iron surfaces in a vacuum environment will result in the generation of extremely energetic surfaces that will adhere one to another when brought into contact with cold welding occurring readily. If, however, a small amount of hydrocarbon gas is admitted to the vacuum chamber and allowed to absorb on the clean iron surface, a structure will develop which will provide that surface with a protective film.

Further, clean iron surfaces will chemisorb nearly all hydrocarbons (ref. 6). The hydrocarbon film will reduce adhesion, friction, and wear because the surface energy has been reduced by the hydrocarbon molecules on the surface. The energy on the clean iron surface available for bonding across the interface to another solid surface has been taken up in the interaction of the clean iron surface with the lubricating molecules absorbing on it. The particular molecular structure, however, of the adsorbing hydrocarbon will also affect the tribological behavior. That is, a slight modification in the molecule will produce sensitivities in adhesion, friction, and wear. These slight differences indicate extreme sensitivity in the tribological behavior of materials to environment and environmental constituents. This effect can be demonstrated by the adsorption of a simple hydrocarbon such as ethylene oxide onto an iron surface and exposure of that same surface to a different simple hydrocarbon with a slightly modified molecular structure, something such as ethylene chloride (or as it is commonly called, vinyl chloride).

If clean iron single crystal surfaces of the same orientation are exposed to equivalent concentrations of these two simple hydrocarbons, namely ethylene oxide and vinyl chloride, entirely different surface structures result. The differences can be seen in the LEED (Low Energy Electron Diffraction) patterns presented in figure 2.

LEED is a device which permits examination of the structural arrangement of atoms in the outermost atomic layer of the solid surface. Thus, in figure 2, we see the molecular arrangement in the diffraction pattern for the adsorbed ethylene oxide and vinyl chloride on the iron surface in the two patterns. Equivalent concentrations of each specie were provided. Thus, everything is constant except the particular molecular structure. The ethylene oxide exhibits the basic ethylene structure with oxygen present in the molecule. Vinyl choloride exhibits essentially the same structure as the ethylene, but chlorine is substituted for oxygen. This subtle difference in the structures, however, causes marked differences in surface coverage (see LEED patterns, fig. 2).

5

With the ethylene oxide, the six diffraction spots in a hexagonal array indicate that the ethylene oxide molecule completely masked or covered the iron surface. No diffraction spots are seen for the iron in the diffraction pattern of figure 2. A close packing of the molecules of ethylene oxide on the iron surface provides a very effective and continuous surface film.

In contrast to ethylene oxide, however, the vinyl chloride structure is much more open with less-than-complete surface coverage and bonding of vinyl chloride to the surface. The four bright diffraction spots with vinyl chloride adsorption, seen in a rectangular array in figure 2, are associated with the iron. Thus, vinyl chloride does not provide complete coverage, and nascent iron is still exposed at the surface.

As one might anticipate, differences in adhesion and friction behavior are observed with these two films present. With the ethylene oxide, the adhesive forces are appreciably reduced between two clean iron surfaces in contact. Further, the friction forces are less for the ethylene oxide on the iron surface than are observed with the vinyl chloride present. Thus, slight differences in the molecular structure of hydrocarbons present in the microenvironment of solid surfaces in contact can influence the tribological behavior of those surfaces.


## WEAR

Various recognized mechanisms cause surfaces to wear. The more common types are adhesion, abrasion, corrosion, erosion, cavitation, fretting, and fatigue. Some of these mechanisms will be briefly discussed.


### Adhesive Wear

Adhesion has already been discussed with reference to figure 1. The transfer resulting from the interfacial adhesion is adhesive wear. Material has been lost from one surface and transferred to another. Adhesive wear can occur for a wide variety of materials brought into contact. Abrasive wear, however, is limited to those situations where a very hard material contacts a softer material, or where hard particles are sandwiched between two softer surfaces (e.g., particles of sand in a bearing). Abrasion occurs when a softer surface is cut or micromachined by a harder surface or particle.


### Abrasive Wear

One might intuitively anticipate that the resistance of a material to abrasive wear is strongly a function of the hardness of the surface being abraded. The harder the surface, the greater should be the resistance to abrasion; this has been experimentally demonstrated (ref. 7).

In figure 3 resistance to wear is plotted as a function of hardness for the surface of various metals. The data of figure 3 indicate a direct relation between the hardness of the metal being abraded and its abrasive wear resistance.

The abrasion of solid surfaces involves wear to the abrasive as well as wear to the surface being abraded. For example, with such relatively hard abrasive materials as single crystal aluminum oxide (sapphire) and titanium dioxide (rutile), the resistance to wear is very much a function of their orientation. With certain atomic planes contacting steel, wear resistance of the abrasive substance is greater than for other orientations. This resistance is demonstrated in the data of figure 4 for titanium dioxide.

A marked variation in the wear rate of titanium dioxide (fig. 4) occurs with changes in orientation. Between the minimum and maximum it varies by a factor of seven times. Thus, abrasion can result in wear to the abrasive as well as to the surface being abraded; the latter can be minimized by giving consideration to the physical and mechanical properties of the abrasive material.

## Corrosive Wear

The surfaces of solids play an extremely important role in corrosive wear. In corrosive wear, material is lost from a solid as a direct result of chemical interactions of the solid surface with the environment. The active environmental constituent can be the lubricant, an additive, or a component of the surrounding atmosphere. The relative motion between solid surfaces in contact aggravates surface attrition by continuously exposing fresh surface for reaction.

Materials which are very effective lubricants under certain conditions can become extremely reactive under another set of conditions. The lubrication of alloys with halogen-containing lubricants is a good example.

In figure 5 for a cobalt alloy lubricated by a chlorinated fluorocarbon, wear at temperatures to 300 °C is extremely low. The values in figure 5 are 100 times less than those obtained for the unlubricated surfaces. Above 300 °C, however, the rate of wear begins to increase markedly. This increase is due to excessive chemical reactivity of the chlorine of the chlorinated fluorocarbon with the cobalt surface.

Examination of the cobalt alloy surface after sliding revealed copious quantities of cobalt chloride. This particular compound is an extremely good solid-film lubricant and accounts for the low wear to 300 °C. Above that temperature cobalt chloride continues to form, but in such large quantities that the cobalt alloys are consumed as a result of excessive surface reactivity. Thus, effective lubrication, with solid films of the type described here, is a matter of controlled corrosion. A reaction product should form to reduce friction and wear, as in figure 5, but that quantity should be limited.

The data of figure 5 also indicate that no correlation between friction and wear can be drawn from information about one or the other. Corrosive wear is an excellent example of this concept. Wear may increase due to the excessive reactivity, but friction may decrease because of the low shear strength of the reaction product formed.

Corrosive wear can be brought about by increasing temperature, as indicated in figure 5. Similar effects can be produced by both increased loading and increased rubbing speeds.

7

A wide variety of material properties affects wear behavior. As already indicated with reference to figure 4, the crystallographic orientation of materials affects wear. This property holds true not only for the wear of nonmetals, but for metals as well (ref. 8).

Crystal structure is another property of materials which influcences wear. Transformation in a metal from one crystal structure to another can result in notable changes in wear. This effect is indicated for tin in figure 6. The wear track width is plotted as a function of temperature, and is realtively constant until the temperature for the transformation of tin from a diamond structure (gray tin) to that of the tetragonal (white tin) is approached. At that point wear begins to increase. The tetragonal tin structure has greater ductility than the diamond form.

A further manifestation of the effect of crystal structure is observed when layer lamellar solids are in rubbing contact with metals. With these solids shear readily occurs along basal planes, and transfer to the metal surface is readily observed; this can be seen in table I. In the table pyrolytic boron nitride transfers to all metals except gold and silver; poor adhesion accounts for this failure.

In practical engineering applications, metals are not used in their elemental form, but rather as alloys. The alloying elements can have varying effects on wear. For example, in figure 7, adding 10-atomic-percent aluminum to copper does not affect its rate of wear. The addition of 10-atomic-percent of alloying element such as silicon, tin, or indium to copper does, however, appreciably reduce wear (fig. 7).

The wear behavior differences for copper alloyed with various elements are maintained even with variations in the concentration of the lubricant additive, as is indicated in figure 8 for the alloys copper-10-atomic percent aluminum and copper-10-atomic-percent indium. At all concentrations of stearic acid, wear is greater with aluminum alloyed with copper than it is for indium alloyed with copper.

LUBRICATION

Liquids

The purpose of lubrication is to separate surfaces in relative motion by a material which has a low resistance to shear so that the surfaces do not sustain major damage. This low-resistance material can be any of a variety of different species (e.g., adsorbed gases, chemical reactions films, liquids, solid lubricants), some of which have already been discussed.

Depending on the type of intervening film and its thickness, a number of lubrication regimes can be identified. A classical way of depicting some of these regimes is by use of the well-known Stribeck curve (fig. 9). Stribeck (ref. 9) performed comprehensive experiments on journal bearings around 1900. He measured the coefficient of friction as a function of load, speed, and temperature. He had difficulty, however, condensing this data into usable form. Some years later, Hersey (ref. 10) performed similar experiments and devised a plotting format based on a dimensionless parameter. The Stribeck curve, or more appropriately, the Stribeck-Hersey curve, takes the form of the

8

coefficient of friction as a function of the viscosity of the liquid (Z), velocity (N), and load (P) parameter, ZN/P.

At high values of ZN/P which occur at high speeds, low loads, and at high viscosities, the surfaces are completely separated by a thick (>0.25 μm) (>$10^{-5}$in.)) lubricant film. This area is that of hydrodynamic lubrication where friction is determined by the rheology of the lubricant. For non-conformal concentrated contacts where loads are high enough to cause elastic deformation of the surfaces and pressure-viscosity effects on the lubricant, another fluid film regime, elastohydrohynamic lubrication (EHL), can be identified. In this regime film thickness (h) may range from 0.025 to 2.5 μm ($10^{-6}$ to $10^{-4}$ in.).

As film thickness becomes progressively thinner, surface interactions start taking place. This regime of increasing friction, which combines asperity interactions and fluid film effects, is referred to as the mixed-lubrication regime.

Finally, at low values of the ZN/P parameter, one enters the realm of boundary lubrication. This regime is characterized by the following:

1. This regime is highly complex, involving metallurgy, surface topography, physical and chemical adsorption, corrosion, catalysis, and reaction kinetics.

2. The most important aspect of this regime is the formation of protective surface films to minimize wear and surface damage.

3. The formation of these films is governed by the chemistry of the film-forming agent, as well as the surface of the solid and other environmental factors.

4. The effectiveness of these films in minimizing wear is determined by their physical properties, which include shear strength, thickness, surface adhesion, film cohesion, melting point or decomposition temperature, and solubility.

Besides the Stribeck-Hersey curve (fig. 9) already described, an idealized plot of wear rate as a function of relative load can also delineate the various lubrication regimes and some wear transitions (fig. 10, ref. 11).

Region 0A of figure 10 encompasses the regimes of hydrodynamic and EHL, the latter as point A is approached. Since no surface interactions occur in this region except for startup of shutdown, little or no wear occurs. (This excludes rolling-element fatigue, which can occur without surface inter-actions.) Region AX is the mixed-lubrication regime where surface interactions begin to occur at A and become more prevalent as point X is approached. Wear is low because fluid film effects still exist.

Next there is region XY in figure 11, which is the region of boundary lubrication. The degree of metal-to-metal contact and the wear rate increase as the load increases. Wear is mild and tends to be corrosive to the left of B and adhesive to the right of B. The location of B is quite variable and depends on the corrosivity of the lubricant formulation. For a noncorrosive lubricant, adhesive wear can occur at X. On the other hand, a corrosive

9

additive can extend the boundary regime to $Z^1$ before boundary film failure occurs. Region YZ is the regime of severe wear where severe adhesion and scoring occur. Machinery cannot operate successfully in this region, and, therefore, the location of this transition point is quite important. At point Z total surface failure occurs, followed by seizure.

In the boundary lubrication regime many properties of the liquid lubricant become important. These include shear strength, film thickness, melting point, and chemical reactivity with the surface. Operating variables which will affect lubricant film-performance include load, speed, temperature, and atmosphere, as already discussed. Additives present in the lubricant to serve specific functions will also affect behavior. These additives include antiwear, antifoam, antioxidants, viscosity improvers, and others. A good review of boundary lubrication can be found in reference 12.

## Solids

At temperatures below which liquid lubricants become solid, and above which they either thermally or oxidatively decompose, solids are used. The solids include inorganic compounds, polymers, and low-shear-strength metals. A review of the subject can be found in reference 13.

Of solid lubricants, those most widely used and studied are the layer-lattice inorganic compounds. These materials have a hexagonally layered crystal structure. Their shear properties are anisotropic with preferred planes for easy shear parallel to the basal planes of the crystallites. In some of the compounds such as molybdenum disulfide ($MoS_2$), a low shear strength is intrinsic to the pure material, which in others, notably graphite, the presence of absorbed gases or intercalated "impurities" between the basal planes appears to be necessary to develop desirable friction characteristics. The most common representatives of this class of lubricants are graphite and the dichalcogenides, notably $MoS_2$ and $WS_2$.

The maximum useful temperatures for solid lubricants depend strongly upon the composition of the ambient atmosphere, the required life at temperature, factors such as oxygen availability at the lubricated surface (is the coating openly exposed to the atmosphere, or shielded within conforming bearing surfaces?), air flow rates, lubricant particle size, and the influence of adjuvants and binders.

## Dichalcogenides

The maximum temperature for lubrication with $MoS_2$ in an air atmosphere is limited by oxidation to about 400 °C under favorable conditions. Some oxidation kinetics data for loosely compacted $MoS_2$ powders of 1$\mu$ average particle size are given in figure 11(a) from reference 13. At a modest airflow rate over the compact, 50 percent of the $MoS_2$ was oxidized to molybdic oxide ($MoO_3$) in 1 hr at 400 °C. At a six-times-higher airflow rate, the temperature for an oxidation half-life of 1 hr was reduced to 300 °C. Figure 1(b) compares the oxidation kinetics of $MoS_2$ and $WS_2$ at the lower airflow rate. The curves for $MoS_2$ and $WS_2$ intersect, with $MoS_2$ oxidizing more rapidly above about 340 °C.

Friction experiments were conducted with a pin-on-disk apparatus using a hemispherically tipped pin in sliding contact with the flat surface of a rotating disk. A comparison of the oxidation data of figure 11 and the friction data of figure 12(b) (ref. 13) shows that the loss of lubricating ability of $MoS_2$ and $WS_2$ in air coincides with the temperatures at which rapid conversion to the oxides occurs.

Figure 12(a) also shows that both compounds lubricate to much higher temperatures in a nonreactive argon atmosphere. In an inert gas or vacuum, the maximum useful temperature is a function of the thermal dissociation rates, rather than the oxidation rates of the lubricants. Thermal dissociation rates and the friction coefficients of molybdenum and tungsten disulfides, diselenides, and ditellurides in vacuum have been systematically studied (ref. 14). The major results, summarized in table II, indicate that the disulfides are the most stable, the diselenides are intermediate, and the ditellurides are the least stable. However, thin, burnished films of the diselenides with their higher densities evaporate more slowly than the disulfides. Apparently, for the very thin, burnished films, the evaporation rates were the controlling factor in determining the maximum temperature for effective lubrication. The limiting temperatures for a significant wear life of these coatings ranged from 600 to 700 °C.

Vacuum-deposited coatings are increasingly being used in tribological applications; these fall into two main composition categories: soft-lubricating coatings, and very hard, wear-resistant coatings. The methods of application are also in two principal categories: sputtering and ion-plating. These techniques have been rapidly adopted by industry especially for aerospace applications. A very large variety of these vacuum-deposited coatings is becoming available for lubrication application.

The most common vacuum-deposited tribological coatings are the sputtered dichalogenides, especially $MoS_2$ and ion-plated soft metals such as gold. These coatings are often very thin, on the order of 2000 to 5000 Å in thickness. Compounds such as $MoS_2$ are usually applied by sputtering, because with proper procedures, pure, essentially stoichiometric, compounds can be deposited. In contrast, ion-plating tends to dissocate chemical compounds. However, ion-plating is an appropriate technique for the deposition of elemental metals because (1) dissociation is obviously not a problem; (2) high ion-impact energies can be used to enhance adhesion; (3) excellent throwing power is achieved when coating parts with complex shapes; and (4) rapid deposition rates can be achieved.

Sputtered hard coats are used primarily for wear control. The oxidation temperatures and hardness of some important carbides and nitrides are presented in table III. Coatings of all of the compounds listed are hard enough to be expected to have good wear resistance, assuming adequate bond to the substrate can be achieved. However, a considerable variation in oxidation resistance exists. Chromium carbide, boron carbide, silicon nitride, and silicon carbide are oxidatively stable to at least 1000 °C, while tungsten and titanium carbides oxidize during long-duration exposure in air at temperatures above about 540 °C. Tungsten carbide tends to oxidize more rapidly than titanium carbide because its oxides are volatile at high temperature, and their sublimation tends to accelerate the oxidation.

Titanium nitride is another promising hard-coat material, but it too will convert to the oxide above 550 °C.  However, some TiC- and TiN-sputtered coatings have shown surprisingly good resistance to oxide conversion at higher temperatures than those listed in table III.  Oxidation occurs, but the rate is very low, probably because of high coating density and the passivating nature of the initially formed oxide films, which protect the coating against catastrophic oxidation.

## CONCLUDING REMARKS

The adhesion, friction, and wear behavior of materials in solid-state contact are strongly dependent upon material properties and environmental factors.  Adsorbed surface films and oxides on metals markedly influence tribological behavior.

Relatively subtle differences in the molecular structure of hydrocarbons can profoundly influence adhesion and friction.  With liquid lubrication, distinct regimes of lubrication are identified.  Both the physical properties of the lubricant and operating variables affect lubricant performance.

With solids as high-temperature lubricants, both thermal and oxidative stability are important, as well as the lubricating properties of the solids over a broad temperature range.  Techniques such as ion-plating and sputtering are being increasingly used for the application of solid film lubricants.

## REFERENCES

1.  Buckley, D.H.; and Johnson, R.L.:  Friction and Wear of Hexagonal Metals and Alloys as Related to Crystal Structure and Lattice Parameters in Vacuum.  ASLE Trans., vol. 9, no. 2, 1966, pp. 121-135.

2.  Tabor, O.:  Junction Growth in Metallic Friction:  The Role of Combined Stresses and Surface Contamination.  Proc. Roy. Soc. (London), A, vol. 251, 1959.

3.  Buckley, D.H.:  Definition and Effect of Chemical Properties of Surfaces in Friction, Wear and Lubrication.  NASA TM-73806, 1978.

4.  Wheeler, D.R.:  Effect of Adsorbed Chlorine and Oxygen on the Shear Strength of Iron and Copper Junctions.  J. Appl. Phys., vol. 47, no. 3, Mar. 1976, pp. 1123-1130.

5.  Buckley, D.H.:  Friction, Wear and Lubricating in Vacuum.  NASA SP-277, 1971.

6.  Buckley, D.H.:  Adsorption of Ethylene Oxide and Vinyl Chloride on an Iron (011) Surface and Effect of these films on Adhesion.  NASA TN D-5999, 1970.

7.  Khruschov, M.M.:  Resistance of Metals to Wear by Abrasion, as Related to Hardness.  Proceedings of the Conference on Lubrication and Wear. Institution of Mechanical Engineers, London, 1957, pp. 655-659.

8. Buckley, D.H.; and Johnson, R.L.: Friction and Wear of Hexagonal Metals and Alloys as Related to Crystal Structure and Lattice Parameters in Vacuum. ASLE Trans., vol. 9, 1966, pp. 121-135.

9. Stribeck, R.: Characteristics of Plain and Roller Bearings. Z.V.D.I., vol. 46, (1902).

10. Hersey, M.D.: The Laws of Lubrication of Horizontal Journal Bearings. J. Wash. Acad. Sci., vol. 4, 1914, pp. 542-52.

11. Beerbower, A.: Boundary Lubrication. Scientific and Technical Applications Forecasts, Department of the Army, DAHC-19-69-C-0033, 1972.

12. Jones, W.R., Jr.: Boundary Lubrication Revisited. NASA TM-82858, 1982.

13. Sliney, H.E.: Solid Lubricant Materials for High Temperature - A Review. Dry Bearings, Tribology International Journal, 1982.

14. Brainard, W.A.: The Thermal Stability and Friction of the Disulfides and Ditellurides of Molybdenum and Tungsten in Vacuum. ($10^{-9}$ to $10^{-6}$ torr). NASA TN D-5141, 1969.

CS-32218

Figure 1. - Severe surface welding resulting from unlubricated sliding.
(2% Al-Ni alloy from $10^{-9}$ mm Hg vacuum experiment.)

14

$$\overset{\displaystyle O}{\underset{\displaystyle CH_2 - CH_2}{\diagup \ \diagdown}}$$
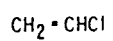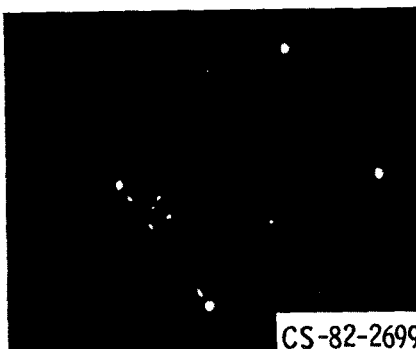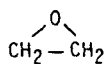
CS-82-2699

$CH_2 \cdot CHCl$

Figure 2. - Leed patterns obtained with two polymer forming
hydrocarbons on iron (011) surface.  100 L exp.
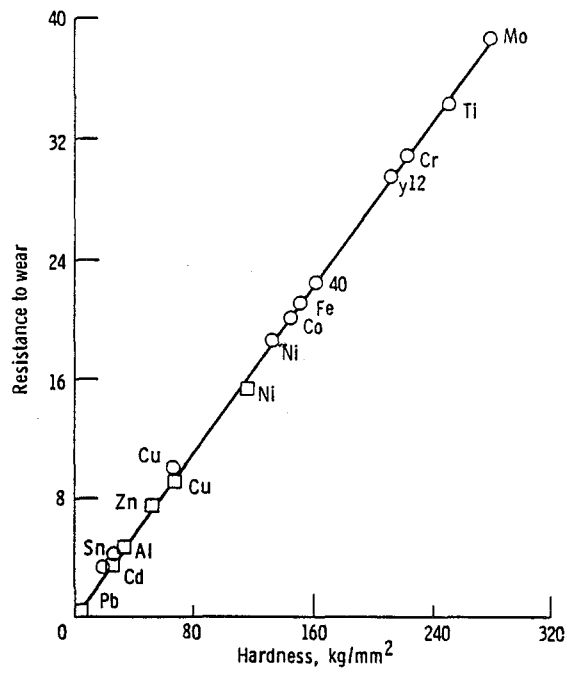
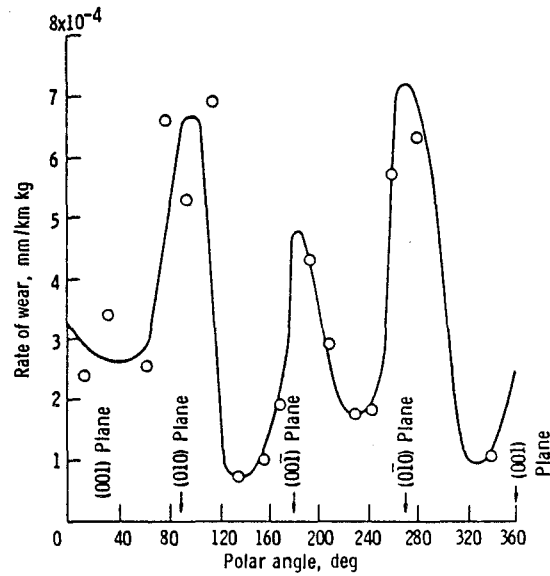Figure 3. - Resistance to wear as function of hardness
(ref. 7).



Figure 4. - Rate of wear of rutile single-crystal
sphere on great circle in plane of a- and c-
axes. The c-axis is normal to plane of sliding
at 0° and 180°. Sliding direction is in plane of
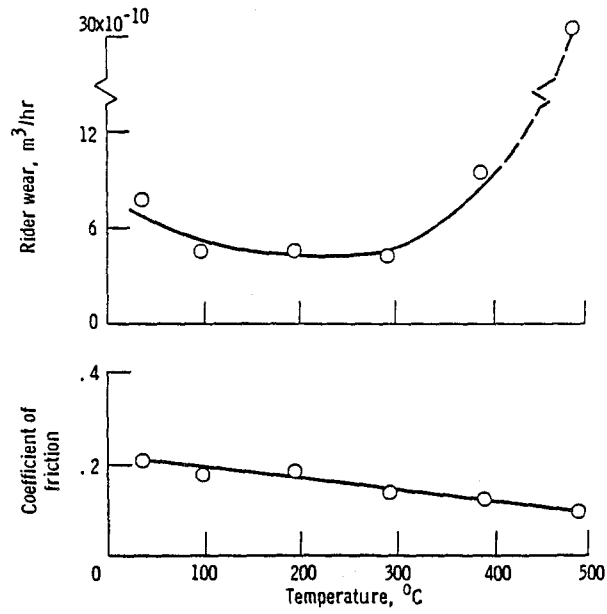great circle.

Figure 5. - Friction and wear of cobalt alloy sliding on itself at various temperatures and lubricated with chlorinated fluorocarbon.
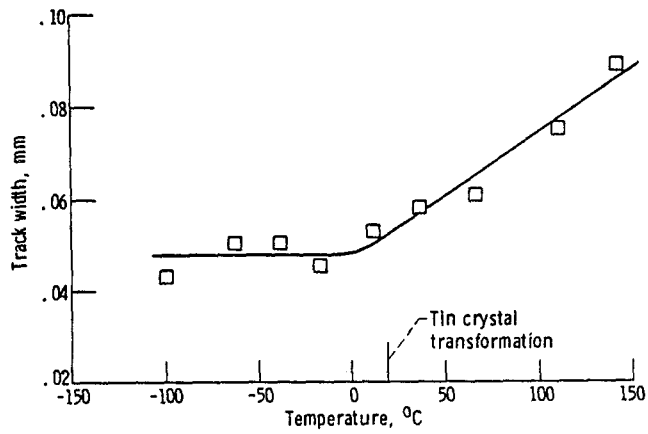


Figure 6. - Track width on tin single-crystal surface as function of temperature. Sliding velocity, 0.7 mm/min; load, 10 g; pressure, $10^{-8}$ N/m$^2$; rider, iron (110); single pass.
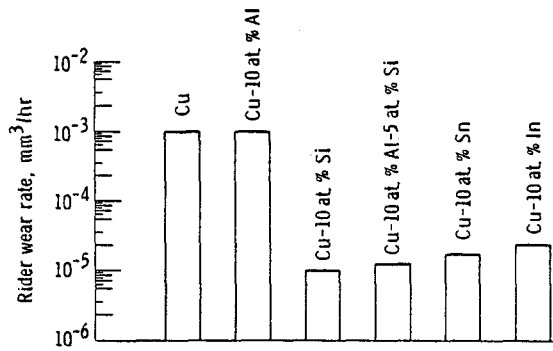
17

Figure 7. - Rider wear for various copper alloys sliding
on themselves in hexadecane containing 0.1 vol %
stearic acid. Load, 250 g; sliding velocity, 300 cm/
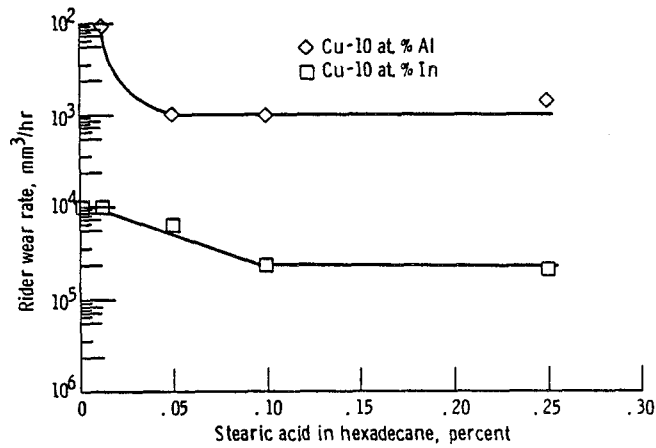min; temperature, 25 °C.



Figure 8. - Rider wear rate for two copper alloys sliding on themselves
with various concentrations of stearic acid in hexadecane as lubri-
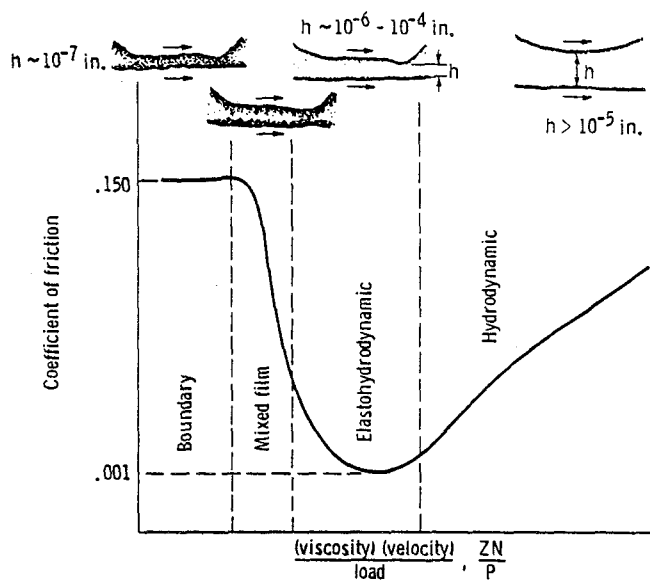cant. Load, 500 g; sliding velocity, 300 cm/min; temperature, 25 °C.

Figure 9. - Coefficient of friction as function of viscosity-velocity-load parameter (Stribeck-Hersey curve) (ref. 9).
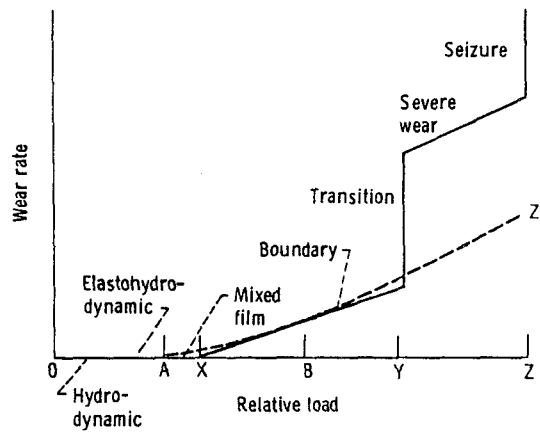


Figure 10. - Wear rate as function of relative load depicting various regimes of lubrication (ref. 11).
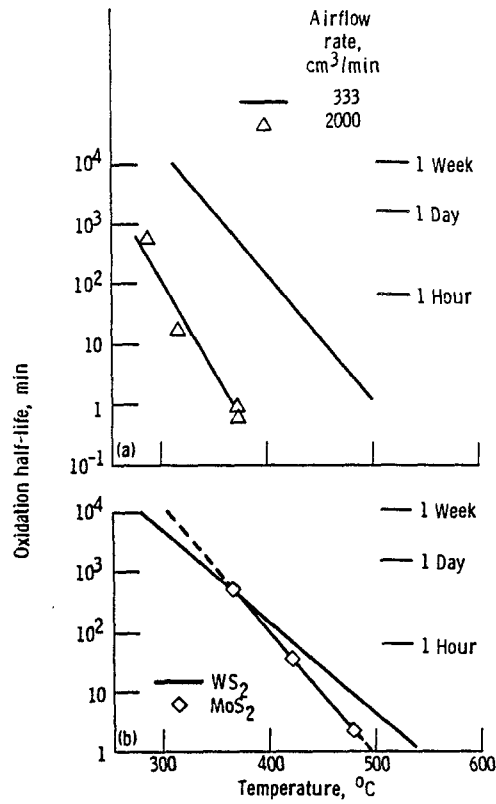
(a) Oxidation characteristics of $MoS_2$ at two airflow rates.
(b) Comparative oxidation of $WS_2$ and $MoS_2$ at airflow rate of 1/3 liter/min.

Figure 11. - Oxidation kinetics of $MoS_2$ and $WS_2$. Average particle size, 1 μm; compact density, 50 percent.
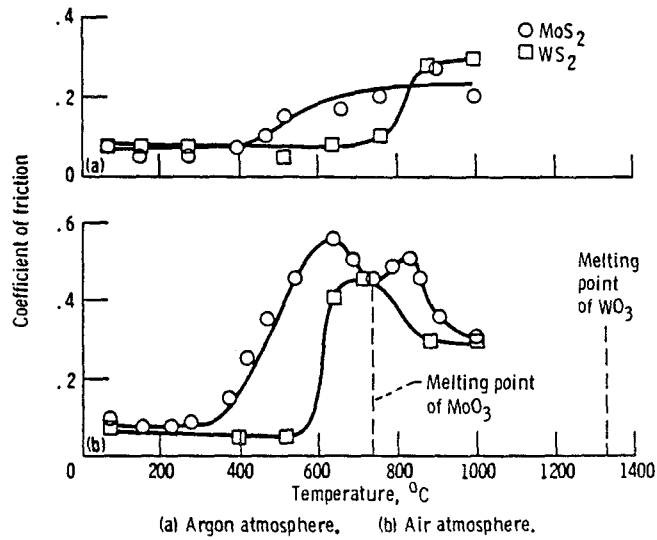


(a) Argon atmosphere.     (b) Air atmosphere.

Figure 12. - Friction characteristics of $MoS_2$ and $WS_2$ in argon and in air.

20

# Lubrication

Liquids
Solids

# BOUNDARY LUBRICATION - REVISITED*

William R. Jones, Jr.
National Aeronautics and Space Administration
Lewis Research Center
Cleveland, Ohio 44135

A review of the various lubrication regimes, with particular emphasis on boundary lubrication, is presented. The types of wear debris and extent of surface damage is illustrated for each regime. The role of boundary surface films along with their modes of formation and important physical properties are discussed. In addition, the effects of various operating parameters on friction and wear in the boundary lubrication regime are considered.

## INTRODUCTION

The purpose of lubrication is to separate surfaces in relative motion by a material which has a low resistance to shear so that the surfaces do not sustain major damage. This low resistance material can be a variety of different species (e.g., adsorbed gases, chemical reaction films, liquids, solid lubricants, etc.).

Depending on the type of intervening film and its thickness, a number of lubrication regimes can be identified. A classical way of depicting some of these regimes is by use of the well known Stribeck curve (fig. 1). Stribeck (ref. 1) performed comprehensive experiments on journal bearings around 1900. He measured the coefficient of friction as a function of load, speed, and temperature. However, it was difficult to condense this data into usable form. Some years later, Hersey (ref. 2) performed similar experiments and devised a plotting format based on a dimensionless parameter. The Stribeck curve, or more appropriately, the Stribeck-Hersey curve takes the form of the coefficient of friction as a function of the viscosity (Z), velocity (N), and load (P) parameter, ZN/P.

At high values of ZN/P which occur at high speeds, low loads, and at high viscosities, the surfaces are completely separated by a thick (>0.25 μm) (>10-5 in.) lubricant film. This is the area of hydrodynamic lubrication where friction is determined by the rheology of the lubricant. For nonconformal concentrated contacts where loads are high enough to cause elastic deformation of the surfaces and pressure-viscosity effects on the lubricant, another fluid film regime, elastohydrodynamic lubrication (EHD) can be identified. On this regime film thicknesses (h) may range from (0.025 to 2.5 μm) ($10^{-6}$ to $10^{-4}$ in.).

As film thickness becomes progressively thinner, surface interactions start taking place. This regime of increasing friction in which there is a combination of asperity interactions and fluid film effects is referred to as the mixed lubrication regime.

---

Finally, at low values of the ZN/P parameter, one enters the realm of boundary lubrication, the primary subject of this paper. This regime is characterized by the following (ref. 3):

1. It is a highly complex regime involving metallurgy, surface topography, physical and chemical adsorption, corrosion, catalysis, and reaction kinetics.

2. The most important aspect of this regime is the formation of protective surface films to minimize wear and surface damage.

3. The formation of these films is governed by the chemistry of both the film former as well as the surface and other environmental factors.

4. The effectiveness of these films in minimizing wear is determined by their physical properties which include: shear strength, thickness, surface adhesion, film cohesion, melting point or decomposition temperature, and solubility.

At is obvious that a concise definition of boundary lubrication is not possible. For the purposes of this vaper, the following general definition will be used. Boundary lubrication is lubrication by a liquid under conditions where there is appreciable solid-solid interactions. Friction and wear are determined predominantly by interactions between the solid surfaces and between the surfaces and the liquid. The viscous properties of the liquid play little or no part in this process.

The purpose of this paper is to summarize the present knowledge about boundary lubrication. There is no intent to provide an exhaustive survey of the literature. A number of adequate surveys already exist (refs. 3 to 8).

## Lubrication Regimes

Besides the Stribeck-Hersey curve (fig. 1) described in the introduction, an idealized plot of wear rate as a function of relative load can also delineate the various lubrication regimes as well as some wear transitions (fig. 2) (ref. 8).

Region OA. - This region encompasses the regimes of hydrodynamic and elastohydrodynamic lubrication (EHD), the latter as point A is approached. Since there are no surface interactions in this region except for startup or shutdown, little or no wear occurs. This is excluding rolling element fatigue which can occur without surface interactions.

Region AX. - Region AX is the mixeu lubrication regime where surface interactions begin to occur at A and become more prevalent as point X is approached. Wear is low because there are still fluid film effects.

Region XY. - This is the region of boundary lubrication. The degree of metal to metal contact and the wear rate increase as the load increases. Wear is mild and tends to be corrosive to the left of B and adhesive to the right of B. The location of B is quite variable and depends on the corrosivity of the lubricant formulation. For a noncorrosive lubricant, adhesive wear can occur at X. On the other hand, a corrosive additive can extend the boundary regime to $Z^1$ before boundary film failure occurs.

Region YZ. - This is the regime of severe wear where scuffing and scoring occur. Machinery cannot operate successfully in this region and, therefore, the location of this transition point is quite important. At point Z, there is total surface failure and seizure occurs.


## Wear Particles and Surface Damage

The types of wear particles and surface damage generated during these lubrication regimes has been reported by Reda, et al. (ref. 9). On that study, wear particles were generated in sliding steel contacts and were isolated by Ferrographic analysis (ref. 10). Basically, this technique involves pumping a quantity of used lubricant across a glass slide which sits on top of an electromagnet (fig. 3). The ferromagnetic wear particles are magnetically precipitated onto the slide and can then be observed microscopically. Surface damage can also be observed by microscopic examination.

Hydrodynamic and EHD regimes. - Since the surfaces are completely separated in these regimes, no wear or surface damage should be evident. This is the case with a featureless surface (fig. 4(a)) and only a few isolated wear particles (fig. 4(b)).

Mixed and boundary lubrication regimes. - These are mild wear regimes where penetration of the boundary film occurs.

This produces the surface damage as illustrated in figure 5(a). Wear particles are generated in a thin surface layer that is continuously removed and reformed during the sliding process. In Ferrographic terminology the wear particles generated in these regimes are referred to as normal rubbing wear particles. These flake-like particles are released into the lubricant by an exfoliation or fatigue-like process. The rate of removal of this surface layer is less than its rate of formation. Wear occurs continuously but at a low rate.

These wear particles are arranged in strings by the magnetic field of the Ferrograph (fig. 5(b)). A scanning electron micrograph (fig. 6) (ref. 11) at a higher magnification illustrates their flake-like nature. Typically, for steel surfaces, these particles are 0.75 to 1.0 $\mu$m in thickness with a major dimension of less than 15 $\mu$m.

The transition from the EHD regime into the mixed and boundary regimes is dramatically illustrated by Ferrographic analysis (fig. 7) (ref. 12). In this figure the Ferrogram density is plotted as a function of the $\Lambda$ ratio. Ferrogram density is a measure of the amount of wear particles. The $\Lambda$ ratio is the ratio of the film thickness to the composite surface roughness. This data was generated by sliding steel balls of three different roughnesses against a sapphire plate. As can be seen, the amount of wear debris increases sharply at $\Lambda$ values of one and below where surface interactions begin taking place. The comparable curve for the friction coefficient (f) as a function of the $\Lambda$ ratio appear in figure 8 (ref. 12). Here the corresponding increase in the friction with increasing surface interactions is evident. This is analogous to the rising portion of the Stribeck-Hersey curve (fig. 1) in the mixed film regime.

Transition to severe wear. - As load is increased, there is some point (Y) (fig. 2) where the rate of removal of the surface layer starts to exceed its

rate of formation. A transition from mild to severe wear occurs. Surface damage becomes more extensive (fig. 9(a)). As the surface film starts to fail, much larger metallic wear particles (up to 150 μm in major dimension) are formed (fig. 9(b)).

Mild oxidative wear. - Under certain conditions a mild form of oxidative wear occurs. Here the majority of wear particles are iron oxide of the $\alpha Fe_2O_3$ type (hematite). The surfaces appear oxidized and grooved to depths of 20 μm (fig. 10(a)). The wear particles appear reddish-orange in reflected white light (fig. 10(b)).

Severe oxidative wear. - As load is further increased, a transition from mild to severe oxidative wear occurs. The surfaces are now grooved to depths of 100 μm and black oxide appears on the surface (fig. 11(a)). The generation of black oxide particles consisting of $\gamma-Fe_2O_3$, $Fe_3O_4$ and FeO predominates (fig. 11(b)).

Both of these oxidative wear regimes are most commonly observed during unlubricated conditions. However, both regimes have been observed during lubricated sliding which is indicative of very poor, perhaps starved, lubrication.

Seizure. - Finally, at very high loads, complete breakdown of the wear surface occurs. Considerable smearing and tearing of the surface is evident with grooving to 200 μm (fig. 12(a)). Free metallic particles having dimensions up to 1 mm are generated (fig. 12(b)).


## Boundary Film Formation

As discussed in the introduction, the most important aspect of boundary lubrication is the formation of surface films (from additives or the lubricant itself) which will protect the contacting surfaces. Basically, there are three mechanisms of boundary film formation: physical adsorption, chemisorption and chemical reaction (ref. 13).

Physical adsorption. - Physical adsorption involves intermolecular forces analogous to those involved in condensation of vapors to liquids. Physical adsorption is usually rapid, reversible, and nonspecific. Energies involved in physical adsorption are in the range of heats of condensation. Physical adsorption may be monomolecular or multilayer. There is no electron transfer in this process. An idealized example of the physical adsorption of hexadecanol on an unreactive metal is shown in figure 13. Because of the weak bonding energies involved, physically adsorbed species are not very effective boundary lubricants.

Chemisorption. - Chemisorption of a species on a surface is usually specific, may be rapid or slow and is not always reversible. Energies involved in chemisorption are large enough to imply that a chemical bond has formed (i.e., electron transfer has taken place). Chemisorption is a monomolecular process. It also may require an activation energy as opposed to physical adsorption which requires none. A species may be physically adsorbed at low temperatures and chemisorbed at higher temperatures. In addition, physical adsorption may occur on top of a chemisorbed film. An example of the chemisorption of stearic acid on an iron oxide surface to form iron stearate is illustrated in figure 14.

26

Chemical reaction. - Although chemisorbed films involves a chemical reaction, this section mainly deals with inorganic reaction products on surfaces. This process is also specific, may be rapid or slow (depending on temperature, reactivity and other conditions), and is irreversible. Films can be unlimited in thickness. An idealized example of a reacted film of iron sulfide on an iron surface is shown in figure 15.

Another chemical reaction of import to boundary lubrication is "friction polymer" formation. In 1958, Hermance and Egan (ref. 14) reported on the occurrence of organic deposits on electrical relay contacts and coined the term "friction polymer." Since that time many investigators have observed the presence of this material in lubricated contacts. Although little is known about its mode of formation or its chemical structure, it can, in some cases, act as a boundary lubricant (ref. 14). An example of "friction polymer" debris generated by a polyphenyl ether appears in figure 16 (ref. 15). A summary of the importance of friction polymers in lubricated contacts appears in reference 16.

## Physical Properties of Boundary Films

The physical properties of boundary films that are important in determining their effectiveness in protecting surfaces include: melting or decomposition temperature, shear strength, thickness, surface adhesion, cohesion and solubility in the bulk lubricant.

Melting point. - The melting point of boundary films is probably the most common property which correlates with film failure. The literature is replete with such examples. Russell, et al., (ref. 17) reported friction transitions for copper lubricated with pure hydrocarbons. Friction data for two hydrocarbons (mesitylenes and dotriacontane) appear in figure 17 as a function of temperature. Here boundary film failure occurs at the melting point of each hydrocarbon. Although data for only two hydrocarbons are shown in figure 17, the same phenomenon occurred for several other compounds. Obviously, the films of these nonpolar materials, which are not chemically bound to the copper surface, provide little protection in the liquid state.

In contrast, chemisorption of fatty acids on reactive metals yields failure temperature based on the softening point of the soap rather than the melting point of the parent fatty acid. Examples of transition temperatures for several fatty acids appear in figure 18 (ref. 18).

Chemically reacted inorganic surface films such as oxides and sulfiues do not have failure transitions that correlate with their melting points. These materials often have very high melting points (>1000 °C) and other factors (such as decomposition or physical removal) may limit their effectiveness at temperatures well below their melting point.

Shear strength. - The shear strength of a boundary lubricating film should be directly reflected in the friction coefficient. In general, this is true with low shear strength soaps yielding low friction while high shear strength salts yield high friction (ref. 5). However, the important parameter in boundary friction is the ratio of the shear strength of the film to that of the substrate (ref. 5). This relationship is illustrated in figure 19. Shear strength is also affected by both pressure and temperature. For example, shear stress as a function of load (pressure) for stearic acid is shown in figure 20

(ref. 19). A compilation of similar data for inorganic compounds appears in reference 20.

Boundary-film thickness. - Boundary film thicknesses can vary from a few angstroms (adsorbed gas) to thousands of angstroms (chemical reaction film). The effect of thickness on friction has been discussed in detail by Kragelskii (ref. 21). In general, as the thickness of a boundary film increases, the coefficient of friction decreases (fig. 21(a)). However, continued increases in thickness may result in an increase in friction (fig. 21(b)). This figure has the general form of the familiar Stribeck-Hersey curve (fig. 1). Another point of interest: shear strength of all boundary films decreases as their thickness increases, which may be related to the above.

For physically adsorbed or chemisorbed films, surface protection is usually enhanced by increasing film thickness (ref. 18). The frictional transition temperature of multilayers also increases with increasing number of layers (ref. 3). ·

For thick chemically reacted films there is an optimum thickness for minimum wear which depends on conditions. The relationship between wear and lubricant (or additive) reactivity is shown in figure 22. Here, if reactivity is not great enough to produce a thick enough film, adhesive wear occurs. On the other hand, if the material is too reactive, very thick films are formed and corrosive wear ensues. Lubricant or additive reactivity is also a function of temperature (fig. 23) (ref. 22) and concentration (fig. 24) (ref. 7).

## Effect of Operating Variables on Friction

Load. - As mentioned in the earlier discussion on the Stribeck-Hersey curve (fig. 1), in the boundary lubrication regime, the coefficient of friction is essentially constant with increasing load. This is a statement of Amonton's law which says that the coefficient of friction is independent of load. This law is amazingly well obeyed for most systems if there is no boundary film failure. This is illustrated in figure 25 (ref. 23) for copper surfaces lubricated with two fatty acids. At loads (>50 g) the coefficientlent of friction is essentially constant. The increasing friction at decreasing loads is probably related to molecular orientation effects and the fact that film penetration does not occur.

Speed. - In general, in the absence of viscosity effects, friction changes little with speed over a sliding speed range of 0.005 1.0 cm/sec (ref. 4). Where viscosity effects do come into play, two types of behavior are observed. These are illustrated in figure 26 (ref. 24). Here, relatively nonpolar materials such as mineral oils show a decrease in friction with increasing speed while polar fatty acids show the opposite trend. In addition, the mineral oil behavior is usually associated with stick-slip phenomena. This is of practical importance since a good boundary lubricant does not lead to stick-slip behavior.

At high speeds, viscous effects will be present and increases in friction are normally observed (fig. 27) (ref. 25). This portion of the friction curve is analogous to the rising portion of the Stribeck-Hersey curve (fig. 1) as one approaches hydrodynamic lubrication.

Temperature. - It is impossible to generalize about the effect of temperature on boundary friction. So much depends on the other conditions and the type of materials present. Temperature can cause disruption, desorption, or decomposition of boundary films. It can also provide activatelon energy for chemisorption or chemical reactions. The frictional transition temperatures of figure 18 show the effect of temperature on the melting of the chemisorbed fatty acids.

Atmosphere. - The presence of oxygen and water vapor in the atmosphere can greatly affect the chemical processes that occur in the boundary layer. These processes can, in turn, affect the friction coefficient. The importance of atmospheric and adsorbed oxygen is illustrated in figure 28 (ref. 26). Here, the "EP" activity of tricresylphosphate (TCP) is totally absent in a dry nitrogen atmosphere. In contrast, normal "EP" activity is present in dry air.


## Effect of Operating Variables on Wear

Load. - It is generally agreed that wear increases with increasing load but no simple relationship seems to exist. This refers to the situation where no transition to severe wear has occurred. At this point, a discontinuity on wear versus load occurs which is illustrated in figure 2. Figure 29 illustrates the increase in wear scar radius with increasing load (ref. 4).

Speed. - For practical purposes, wear rate in the boundary lubrication regime is essentially independent of speed. Obviously, this does not hold if one moves into the EHD regime with increasing speed. This also assumes no boundary film failure due to contact temperature rise. An example of wear rate as a function of sliding speed appears in figure 30 (ref. 28). These data indicate that fluid film effects are negligible only at 25 and 50 rpm and a 1 kg load.

Temperature. - As was the case for friction, there is no way to generalize the effect of temperature on wear. The same statements that pertain to friction also pertain to wear. A good example of the effect of temperature on wear is presented in figure 23.

Atmosphere. - The effects of atmospheric oxygen and moisture on wear has been studieo by many investigators. Oxygen has been shown to be an impcrtant ingredient in boundary lubrication experiments involving load carrying additives (refs. 4, and 29 to 33). For example, the presence of oxygen or moisture in the test atmosphere has a great effect on the wear properties of lubricants containing aromatic species (figs. 31 and 32) (refs. 27 and 33).


## Additive Behavior of Boundary Lubricated Systems

!n discussing figure 2, it was stated that the boundary lubrication regime could be extended to higher loads by proper formulation of the lubricant with additives. A discussion of the variety of boundary additives is outside the scope of this paper. However, the general behavior of the two common types of boundary additives, namely, antiwear and "EP", is illustrated in figure 33 (ref. 34). In figure 33 wear rate (K) is plotted as a function of load (F). There is a wear transition when boundary film failure occurs. The presence of an antiwear additive reduces wear ($\Delta K$) but may have little or no effect on

the wear transition load. On the other hand, an "EP" additive yields an increase in the load carrying capacity ($\Delta F$) with little or no effect on the wear rate below the original base oil wear transition.

The most common antiwear additives are those which contain the element phosphorus. Typical examples include the metal dialkyldithiophosphates, organic phosphates and phosphites. "EP" additives include compounds containing sulfur and chlorine. A review of these two additive classes appears in reference 35.

## CONCLUDING REMARKS

In conclusion, the boundary lubrication regime has been shown to be a complex arena of a variety of competing chemical and physical processes. The ultimate unuerstanding of this regime will come when these processes and their interrelationships are completely identified.

## REFERENCES

1. Stribeck, R.: "Characteristics of Plain and Roller Bearings", Ziet. V.D.I., Vol. 46 (1902).

2. Hersey, M.D.: "The Laws of Lubrication of Horizontal Journal Bearings", J. Wash. Acad. Sci., 4 1914, pp. 542-52.

3. Godfrey, U.: "Review of Usefulness of New Surface Analysis Instruments In Understanding Boundary Lubrication," Fundamentals of Tribology, ed. by N. P. Suh and N. Saka, MIT Press (1980), pp. 945-967.

4. Ling, F.F., Klaus, E.E., and Fein, R.S.: Boundary Lubrication, an Appraisal of the World Literature. American Society of Mechanical Engineers (1969).

5. Godfrey, D.: "Boundary Lubrication," in Interdisciplinary Approach to Friction and Wear, NASA SP-181, ed. by P.M. Ku (1968), p. 335-384.

6. Fein, R. S., "Chemistry in Concentrated-Conjunction Lubrication," Interdisciplinary Approach to the Lubrication of Concentrated COntacts, NASA SP-237, ed. by P.M. Ku (1970), p. 489-527.

7. Rowe, C.N.: "Wear-Corrosion and Erosion," Interdisciplinary Approach to Liquid Lubricant Technology, NASA SP-318, ed. by P.M. Ku (1973), p. 527-568.

8. Beerbower, A.: "Boundary Lubrication," Scientific and Technical Applications Forcasts, Department of the Army, DAHC-19-69-C-0033 (1972).

9. Reda, A.A., Bowden, R., and Westcott, V.C.: "Characteristics of Particles Generated at the Interface Between Sliding Steel Surfaces," Wear, 34, pp. 261-273 (1975).

10. Seifert, W.W. and Westcott, V.C.: "A Method for the Study of Wear Particles in Lubricating Oil," Wear, 21, 27-42 (1972).

11. Jones, W.R. Jr.: "Elucidation of Wear Mechanisms by Ferrographic Analysis," NASA TM-82737 (1981).

12. Jones, W.R., Jr., Nagaraj, H.S., and Winer, W.O.: "Ferrographic Analysis of Wear Debris Generated in a Sliding Elastohydrodynamic Contact," ASLE Trans., 21 (3), 181-190 (1978).

13. Adamson, A.W.: Physical Chemistry of Surfaces, John Wiley and Sons, 2nd. ed. (1967).

14. Hermance, H.W. and Egan, T.F., "Organic Deposits on Precious Metal Contacts," Bell Syst Tech. J., 37, 739-76 (1958).

15. Jones, W.R., Jr., "Ferrographic Analysis of Wear Debris from Boundary Lubrication Experiments with a Five Ring Polyphenyl Ether," ASLE Trans., 18 (3), 153-62 (July 1975).

16. Lauer, James L.; Jones, William R., Jr.; and Wedeven, Lavern D.: Assessment of Lubricated Contacts - Friction Polymer, Proposed NASA TM.

17. Russell, J.A., Campbell, W.E., Burton, R.A., and Ku, P.M.: "Boundary Lubrication Behavior of Organic Films at Low Temperatures," ASLE Trans., 8(1), 48 (1965).

18. Bowden, F.P., and Tabor, D.: The Friction and Lubrication of Solids, Part 1, Oxford University Press (1971) p. 182.

19. Akhmatov, A.S.: Molecular Physics of Boundary Friction, Israel Program for Scientific Translations (1966), p. 248.

20. Bridgman, P.W.: "Shearing Phenomena at High Pressures, Particularly in Inorganic Compounds", Proceedings of the Amer. Acau. of Arts and Sciences, 71 (9), 387-460 (1937).

21. Kragelski, I.V.: Friction and Wear, Butterworths (1965), pp. 158-163.

22. Jones, William R., Jr.: Boundary Lubrication of Formulated C-Ethers in Air to 300 °C," Lubr. Eng., 32, (10), 530-538 (1976).

23. Whitehead, J.R.: "Surface deformation and Friction of Metals at Light Loads," Proc. R. Soc. London Ser. A, 201 (1064) 109-124, (1950).

24. Clayton, D.: An Introduction to Boundary and Extreme Pressure Lubrication. Physics of Lubrication, Br. J. Appl. Phys. 2, Suppl. 1, 1951, p. 25.

25. Forrester, P.G.: "The Influence of Sliding Velocity and Other Variables on Kinetic Friction in or near the Boundary Region," Proc. R. Soc. London, Ser. A, 187 (1011), 439-463 (1946).

26. Faut, O.D.; and Wheeler, D.: On the Mechanism of Lubrication by Tricresyl Phosphate (TCP). I. The Coefficient of Friction as a Function of Temperature for TCP on M-50 Steel, NASA TP in process.

27. Jones, W.R., Jr. and Hady, W.F.: "Effect of Humidity and a Wettability Additive on Polyphenyl Ether Boundary Lubrication of Steel in Air and Nitrogen to 350 °C," NASA TN D-6055 (1970).

28. Loomis, W.R., and Jones, W.R., Jr.: "Steady-State Wear and Friction in Boundary Lubrication Studies," NASA TP-1658 (1980).

29. Godfrey, D., "The Lubricatiopn Mechanism of Tricresyl Phosphate on Steel," ASLE Trans. 8 (1), 1-11 (1965)."

30. Goldblatt, I.L., and Appeldorn, J. K.: The Antiwear Behavior of TCP in Different Atmospheres and Different Base Stocks," ASLE Trans. 13, (3), 203-214 (1970).

31. Wheeler, D.R., "Surface Chemistry of Iron Sliding in Air and Nitrogen Lubricated With Hexadecane and Hexadecane Containing Dibenzyl-Disulfide," NASA TP-1545 (1979).

32. Vinogradov, G.V., Arkarova, V. V., and Petrov, A. A.: "Antiwear and Antifrictionlon Properties of Hydrocarbons Under Heavy Loads", Wear, 4, (4) 274-291 (1961).

33. Jones, W.R., Jr.: "The Effect of Oxygen Concentration on the Boundary-Lubricating Characteristics of a C-Ether and a Polyphenyl Ether to 300 °C," Wear, 73, 123-136 (1981).

34. Czichos, H.: "Tribology, a Systems Approach to the Science and Technology of Friction," Lubrication and Wear, Elsevier (1978).

35. Forbes, E.S.: "Antiwear and Extreme Pressure Additives for Lubricants," Tribology, 3, 145-152 (1970).
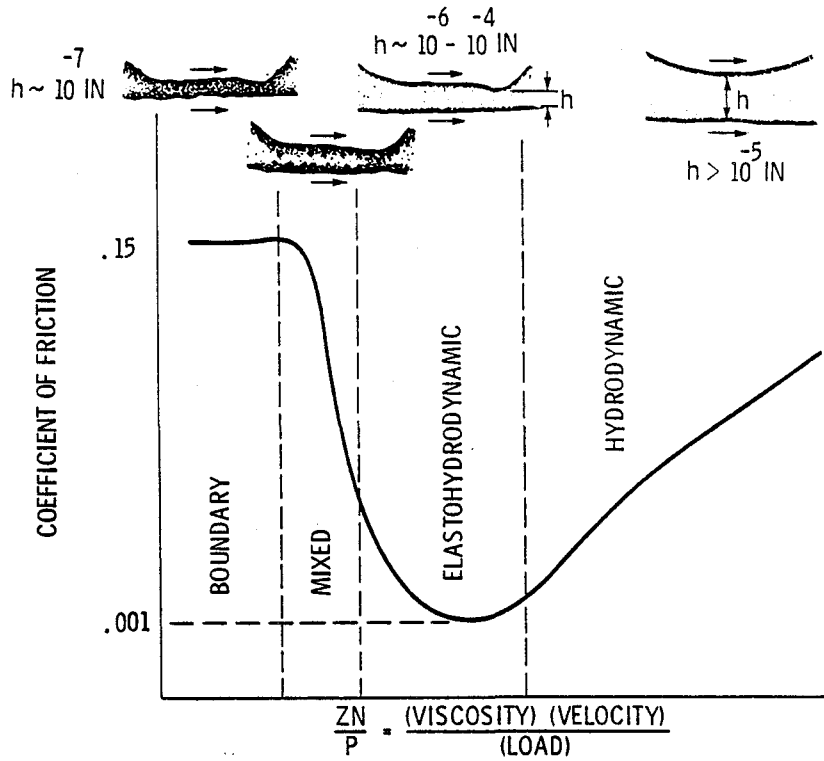
Figure 1. - Coefficient of friction as a function of speed-velocity-load parameter (Stribeck-Hersey curve).(ref. 1).

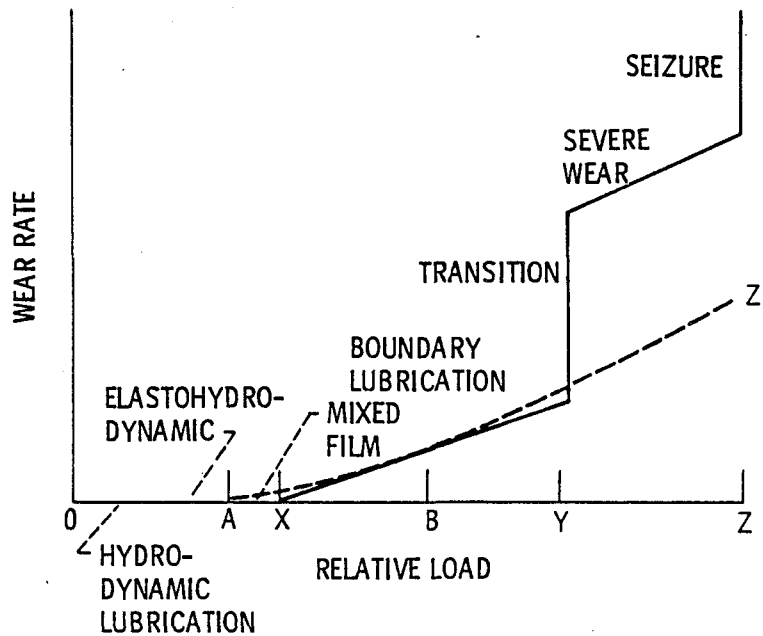$$\frac{ZN}{P} = \frac{(VISCOSITY)\ (VELOCITY)}{(LOAD)}$$



Figure 2. - Wear rate as a function of relative load depicting the various regimes of lubrication (ref. 8).

33

OIL INLET

OIL SAMPLE

FERROGRAM SLIDE
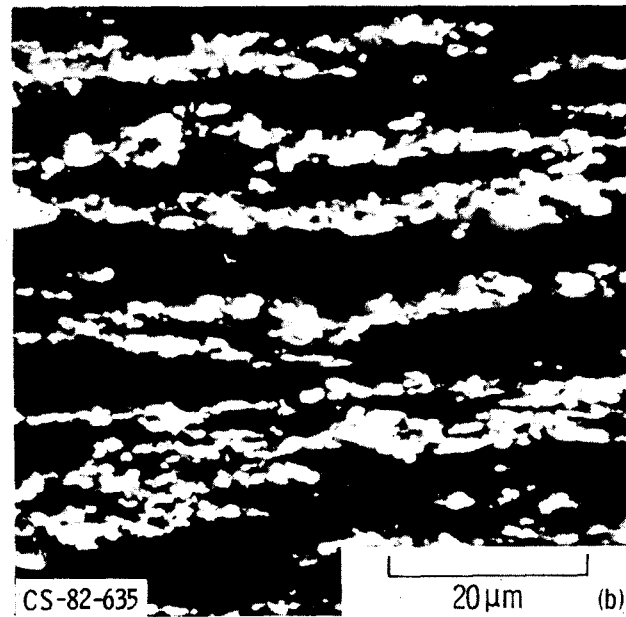
ENTRY POSITION
(55-56 mm)

10 mm
POSITION

MAGNET
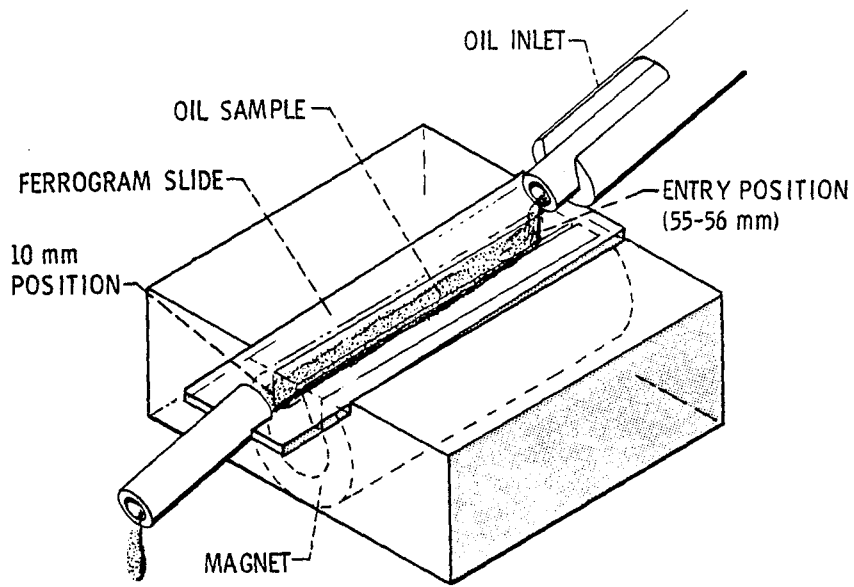
Figure 3. - Ferrograph analyzer.

40 µm   (a)

CS-82-638          20 µm   (b)
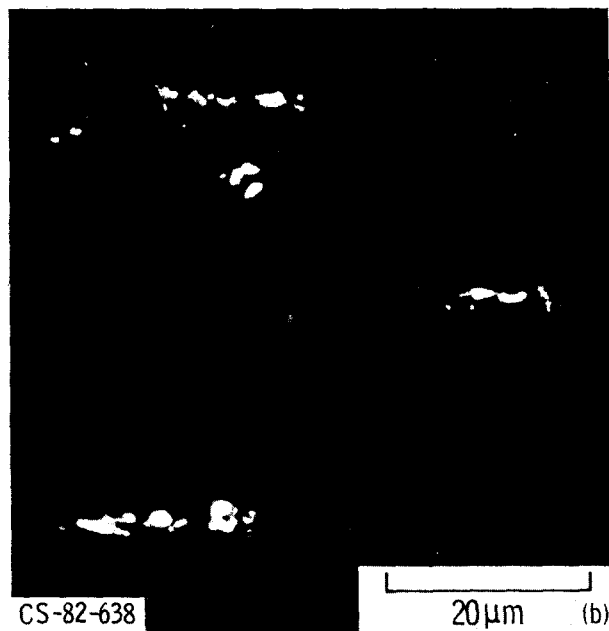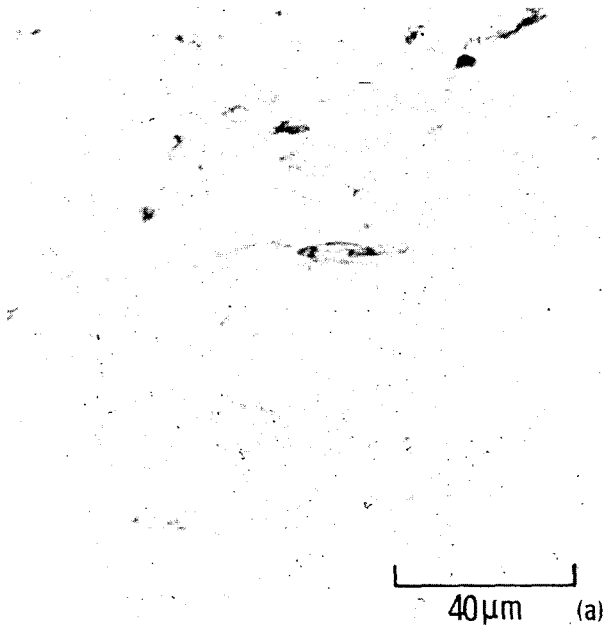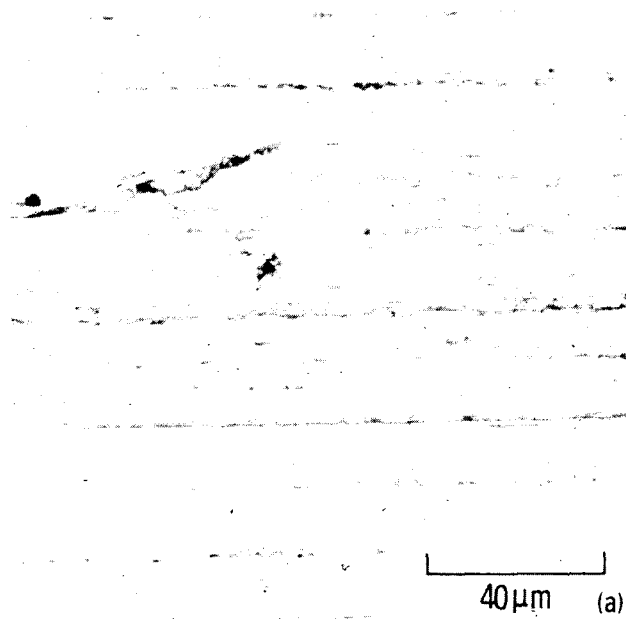
(a) Wear surface.

(b) Wear particles (ref. 9).

Figure 4. - Hydrodynamic or elastohydrodynamic
lubrication regime.

35

40 μm     (a)



CS-82-635                    20 μm     (b)

(a) Wear surface.

(b) Wear particles (ref. 9).

Figure 5. - Boundary lubrication regime.

36
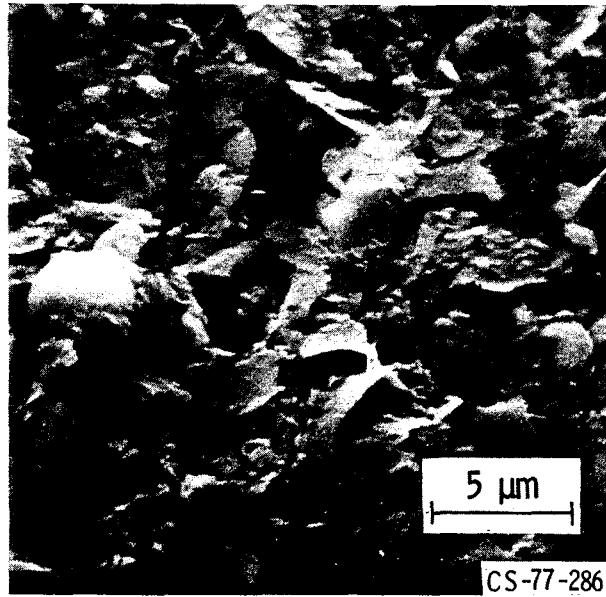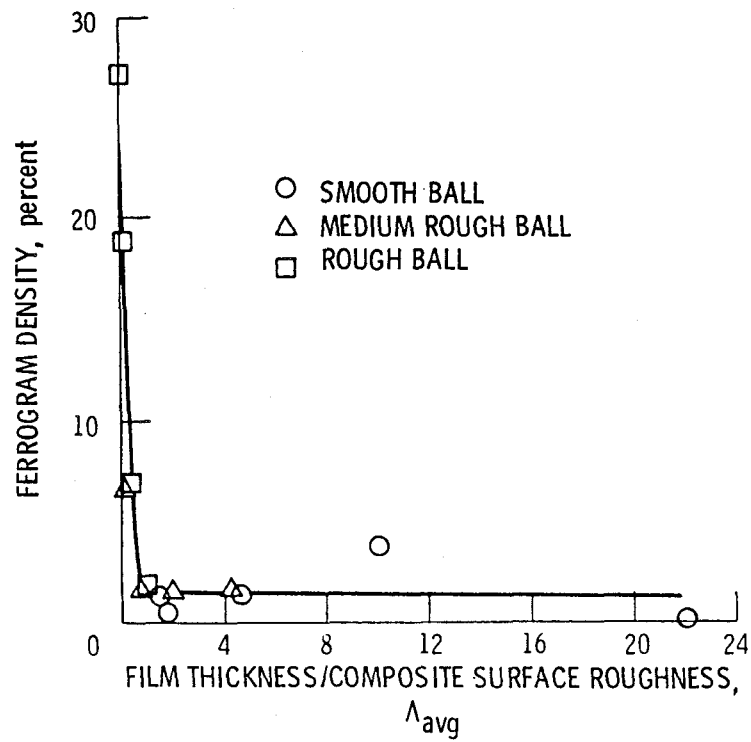
Figure 6. – Normal rubbing wear particles (from ref. 11).



○  SMOOTH BALL
△  MEDIUM ROUGH BALL
□  ROUGH BALL

FILM THICKNESS/COMPOSITE SURFACE ROUGHNESS, $\Lambda_{avg}$

FERROGRAM DENSITY, percent

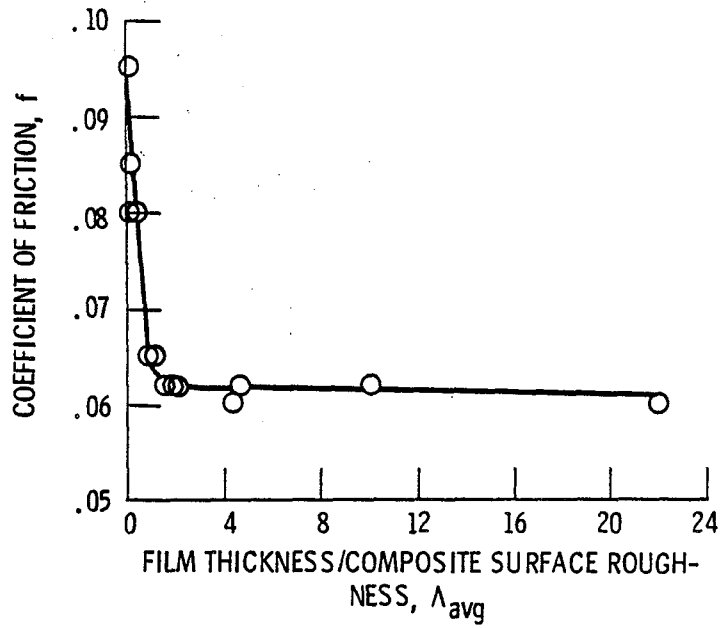Figure 7. – Ferrogram density versus average $\Lambda$ ratio (ref. 12).
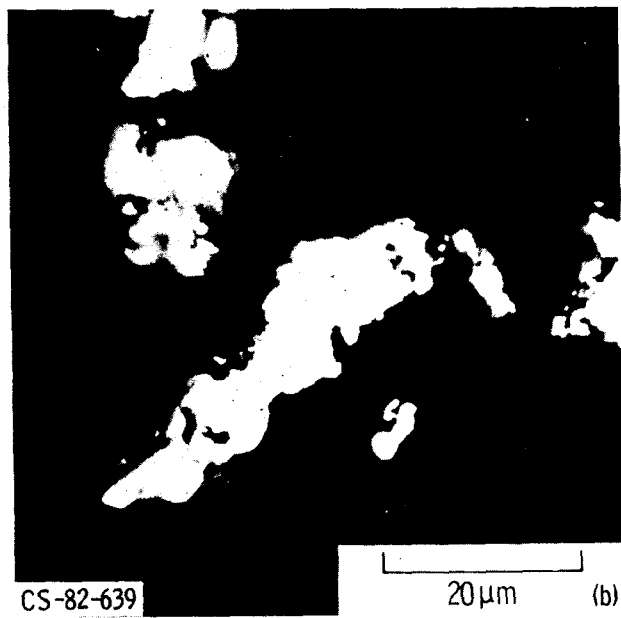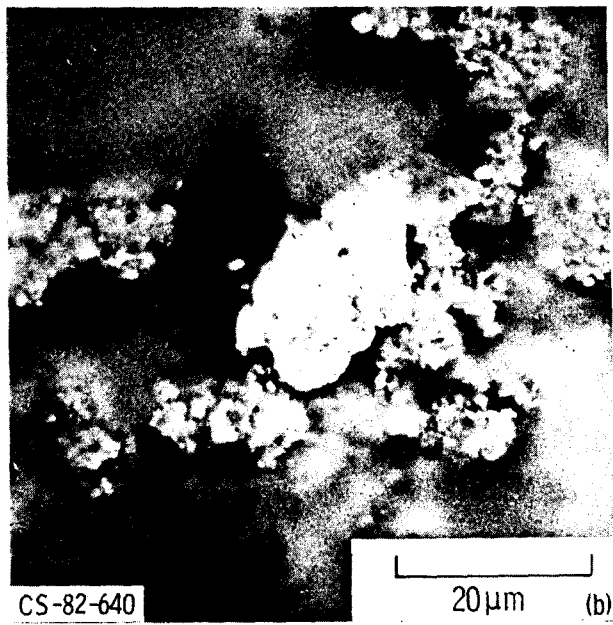
Figure 8. - Friction versus average $\Lambda$ ratio (ref. 12).

(a) Wear surface.

(b) Wear particles (ref. 9).

Figure 9. – Transition to severe wear.
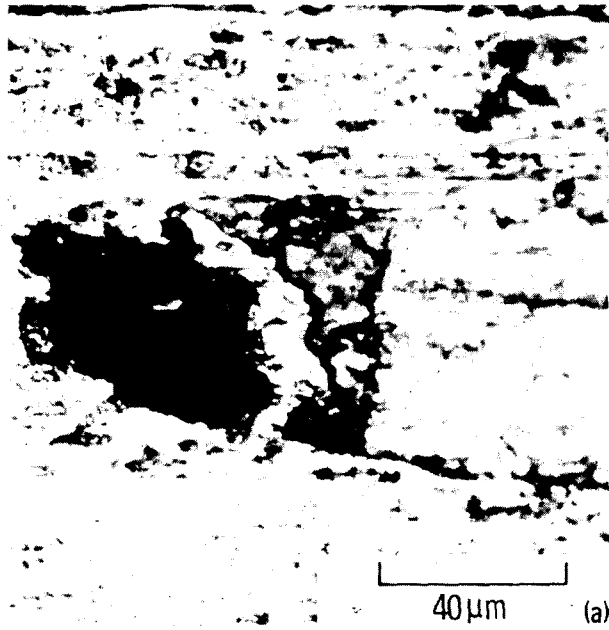
(a) Wear surface.

(b) Wear particles (ref. 9).

Figure 10. – Severe wear regime–mild oxidative wear.

40

40 μm  (a)

CS-82-637  20 μm  (b)
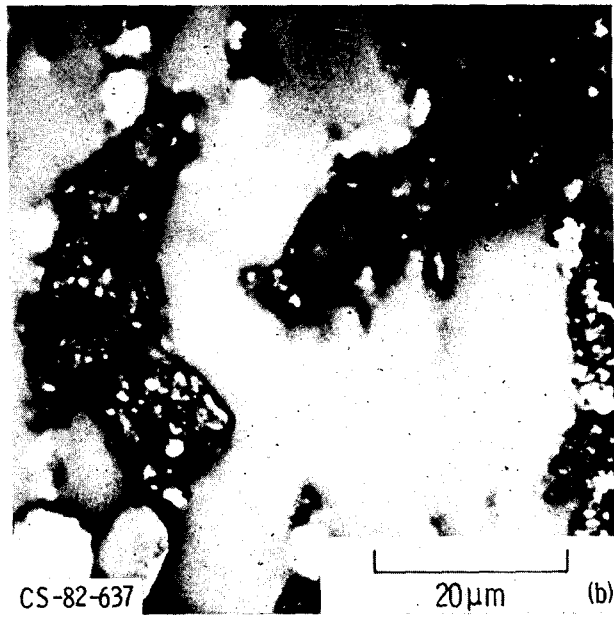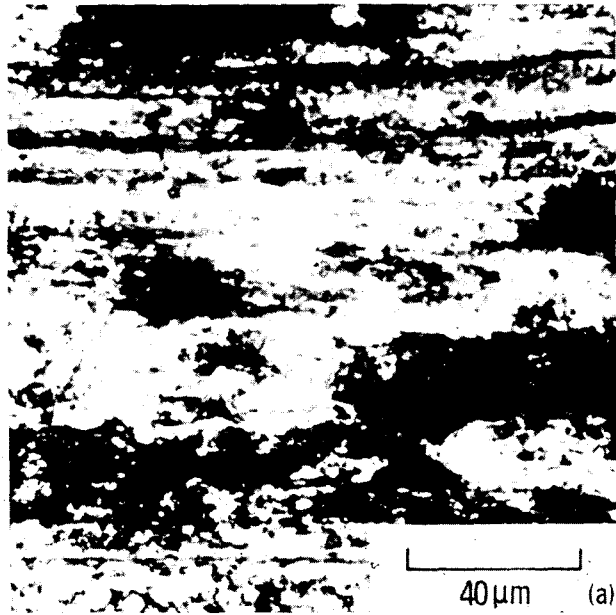
(a) Wear surface.

(b) Wear particles (ref. 9).

Figure 11. – Severe wear regime–severe oxidative wear.

41

40 μm (a)

CS-82-636                    20 μm (b)
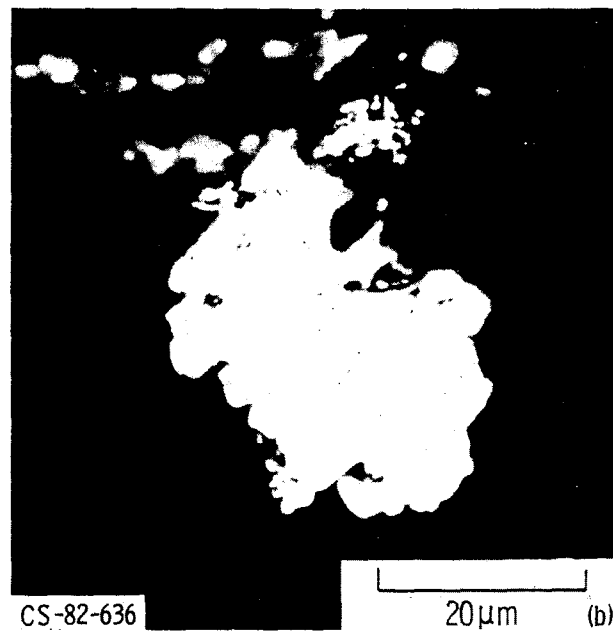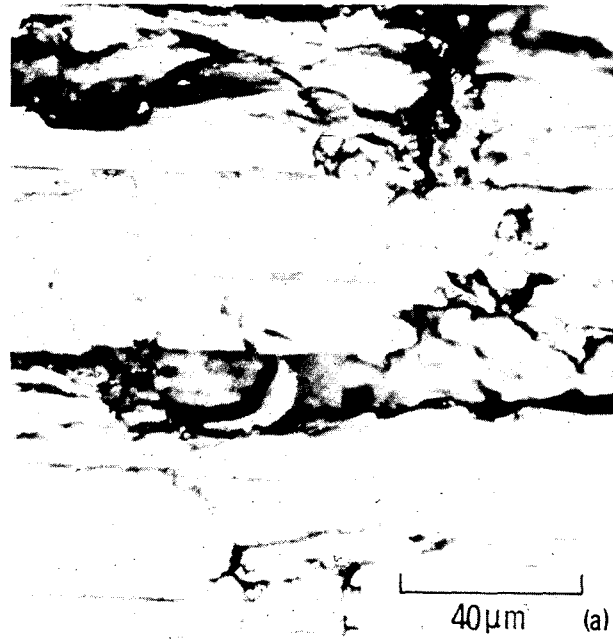
(a) Wear surface.

(b) Wear particles (ref. 9).

Figure 12. – Transition to seizure.
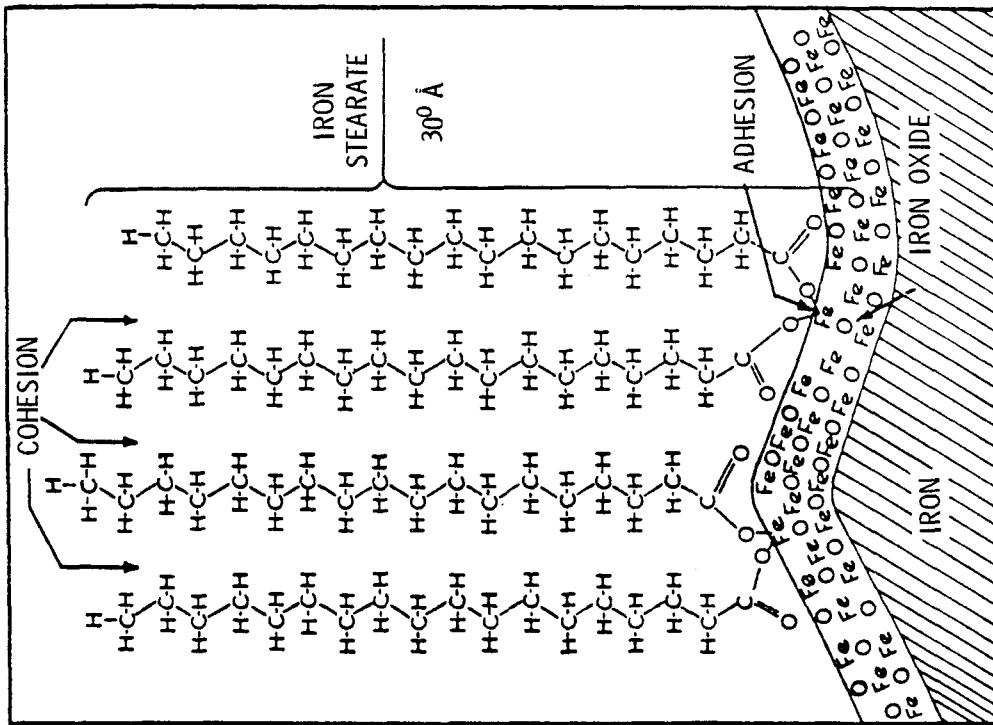
Figure 14. – Chemisorption of stearic acid on an iron surface to form iron stearate (ref. 5).
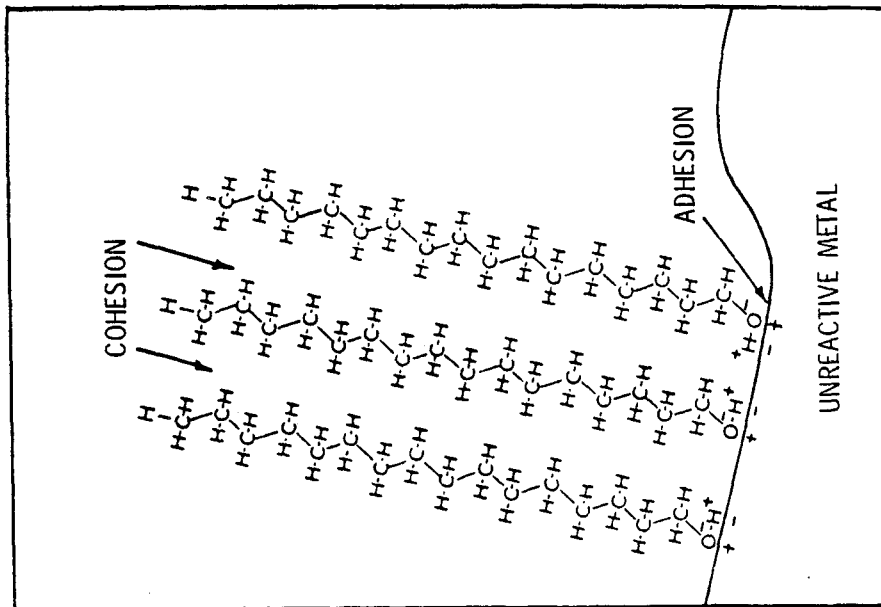


Figure 13. – Physical adsorption hexadecanol (ref. 5).
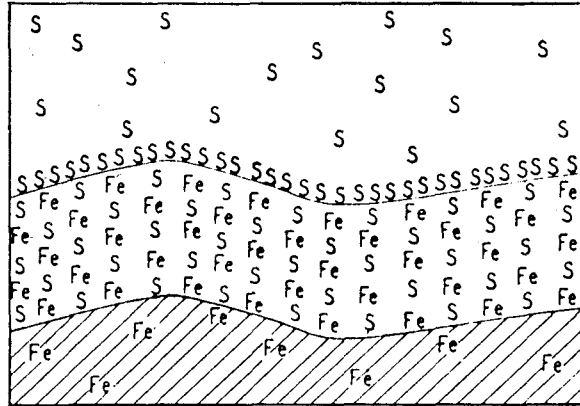
Figure 15. - Inorganic film formed by reaction of sulfur with iron to form iron sulfide (ref. 5).
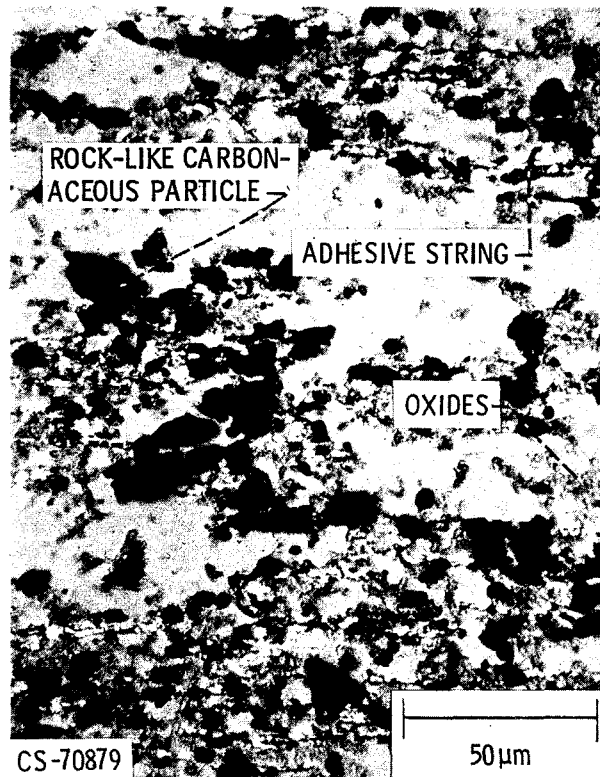


Figure 16. - Photomicrograph of the wear debris generated by a polyphenyl ether at 100° C in dry test atmosphere of 1 percent oxygen and 99 percent nitrogen (by volume)(ref. 15).

Figure 18. – Frictional transition temperatures for several fatty acids on steel as a function of chain length (ref. 18).
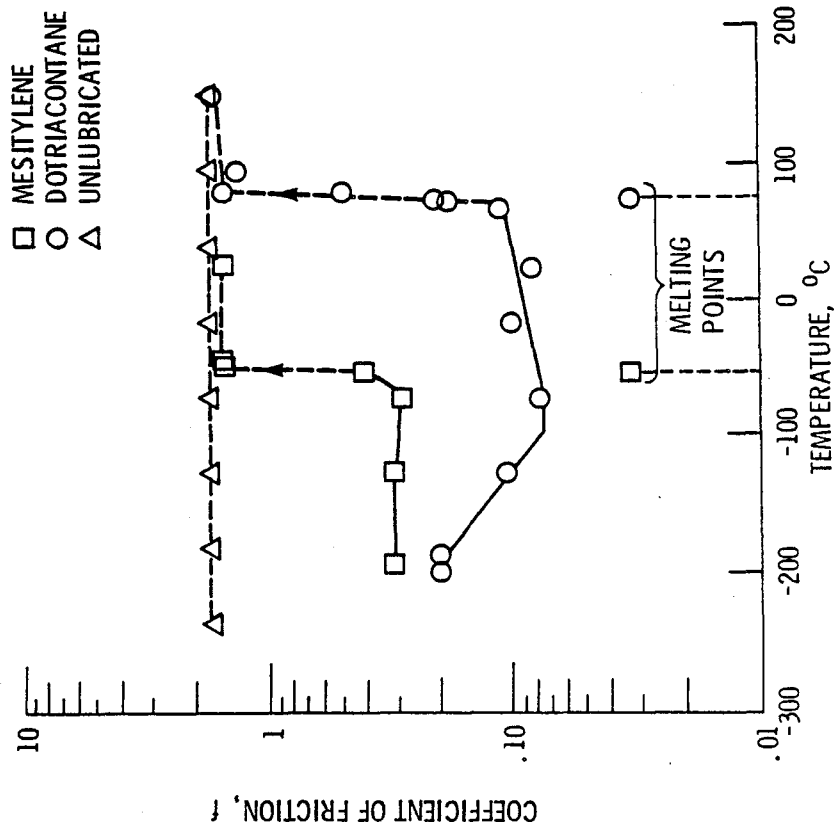


Figure 17. – Friction versus temperature for copper lubricated with hydrocarbons in dry helium (ref. 17).

45
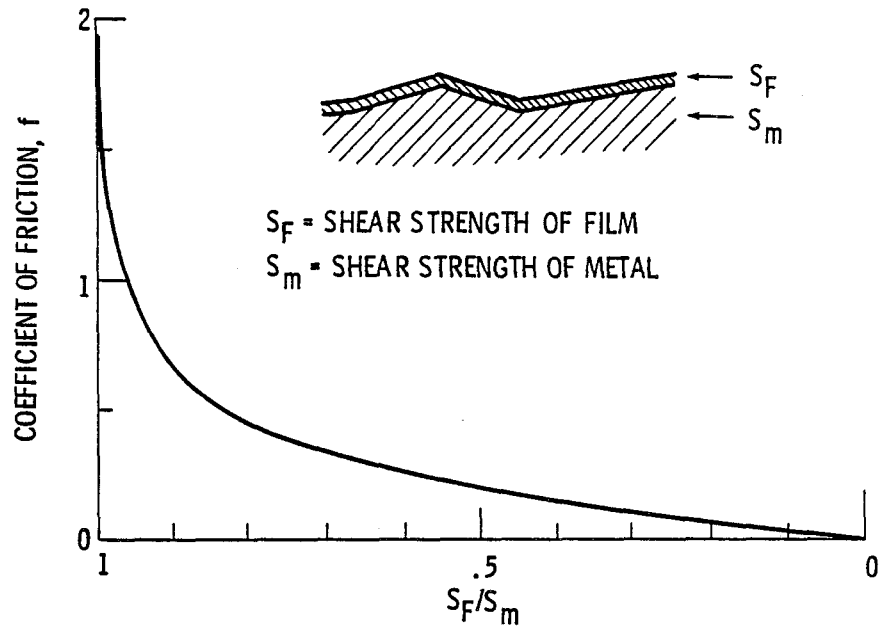
Figure 19. - Friction as a function of the ratio of shear strengths of film and metal (ref. 5).
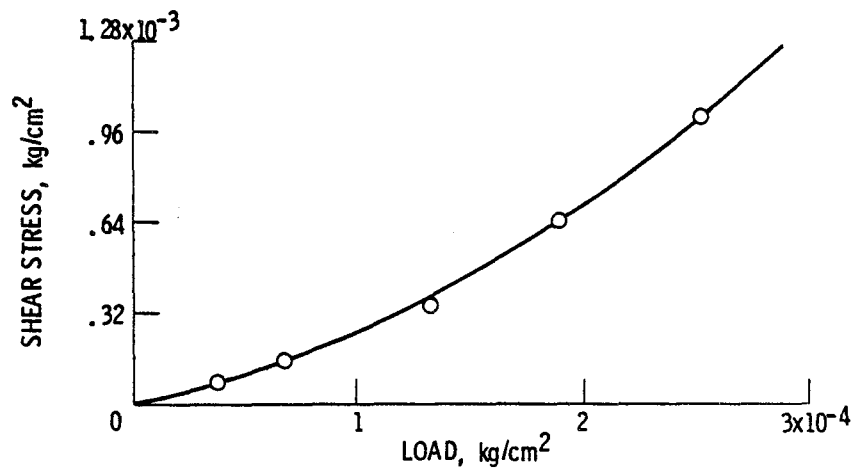


Figure 20. - Shear stress as a function of load for a thin layer of solid stearic acid (ref. 19).
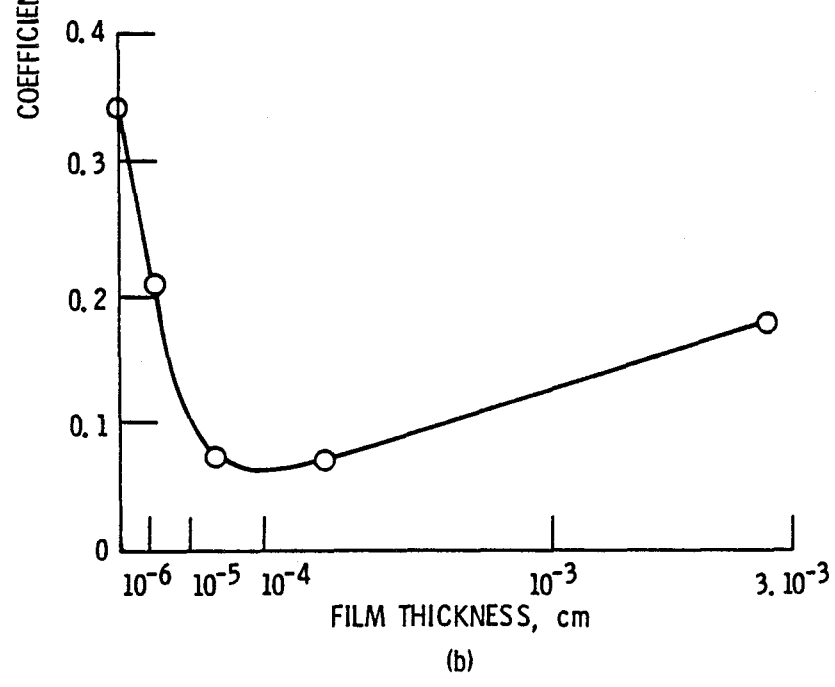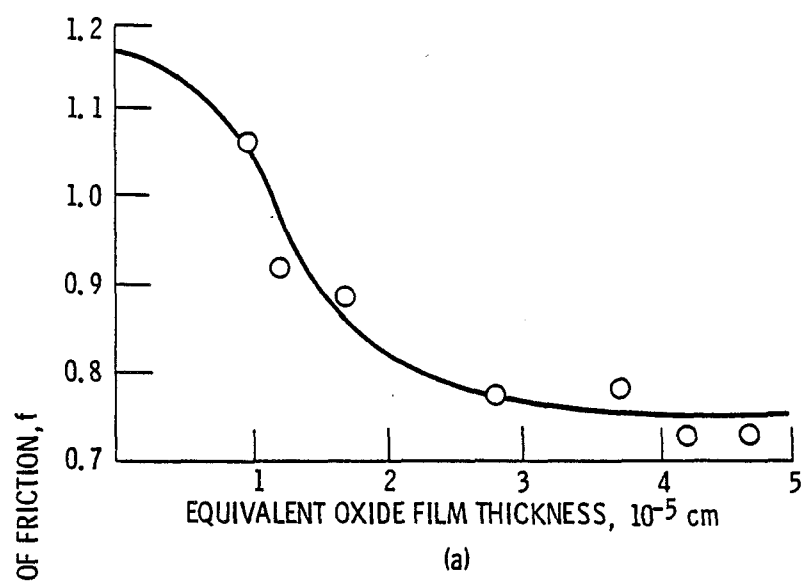
Figure 21. - Relationship between friction and thickness
of surface films: (a) coefficient of friction against oxide
film thickness on copper; (b) coefficient of friction
against thickness of indium film (ref. 21).

47
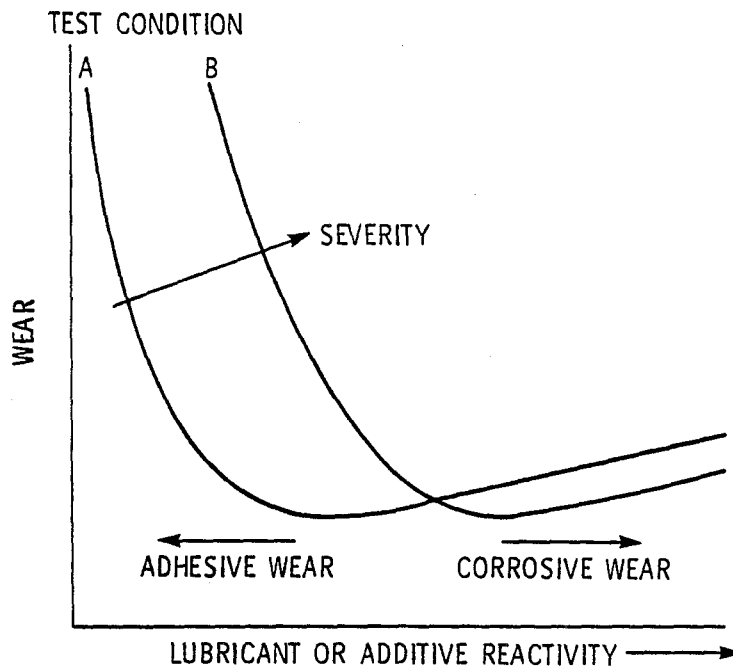
Figure 22. - Relationship between wear and lubricant reactivity (ref. 7).
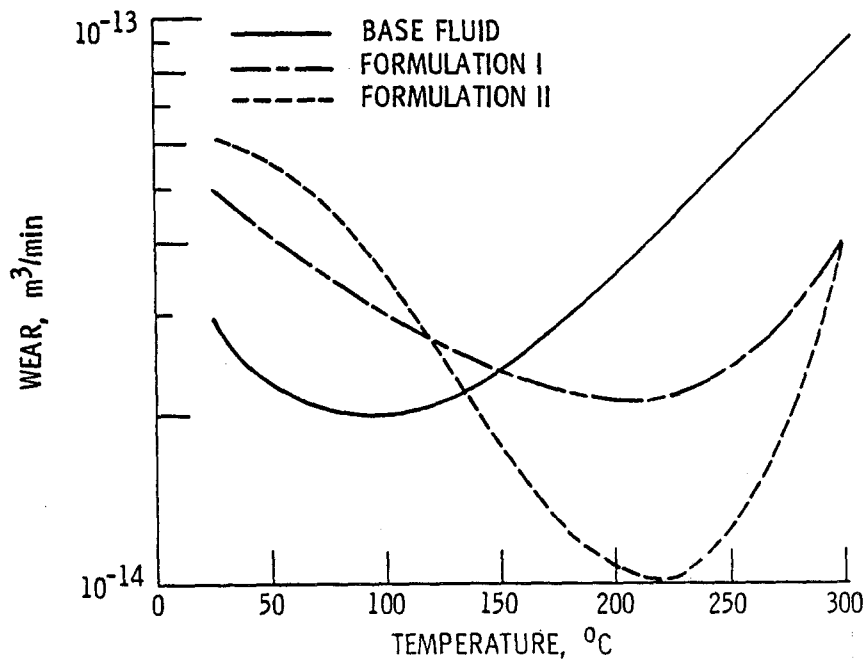


Figure 23. - Wear versus temperature for various C-ether formulations (ref. 22).
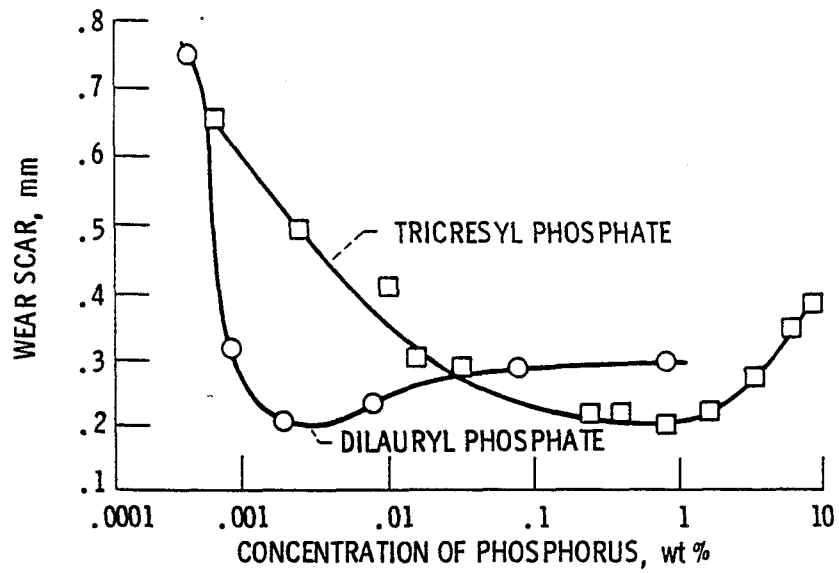
Figure 24. - Wear versus additive concentration from four-ball tests (ref. 7).
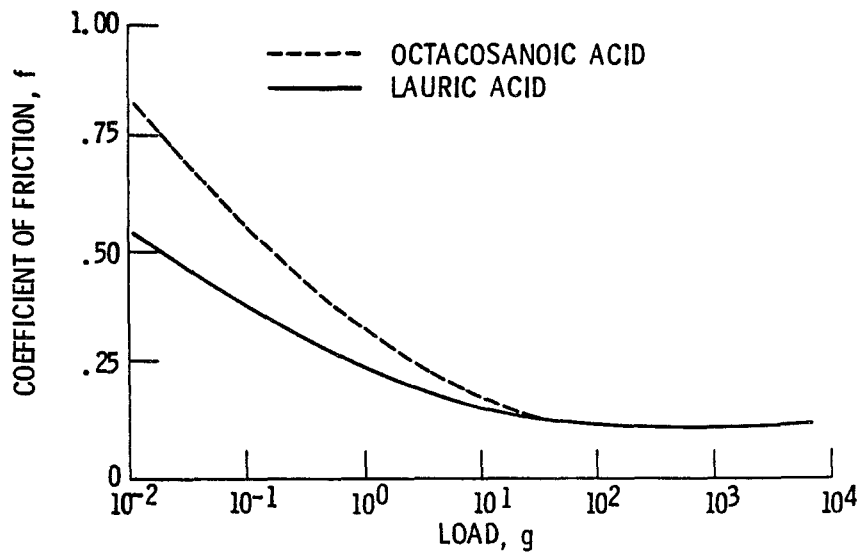


Figure 25. - Friction versus load for copper lubricated with fatty acids (ref. 23).
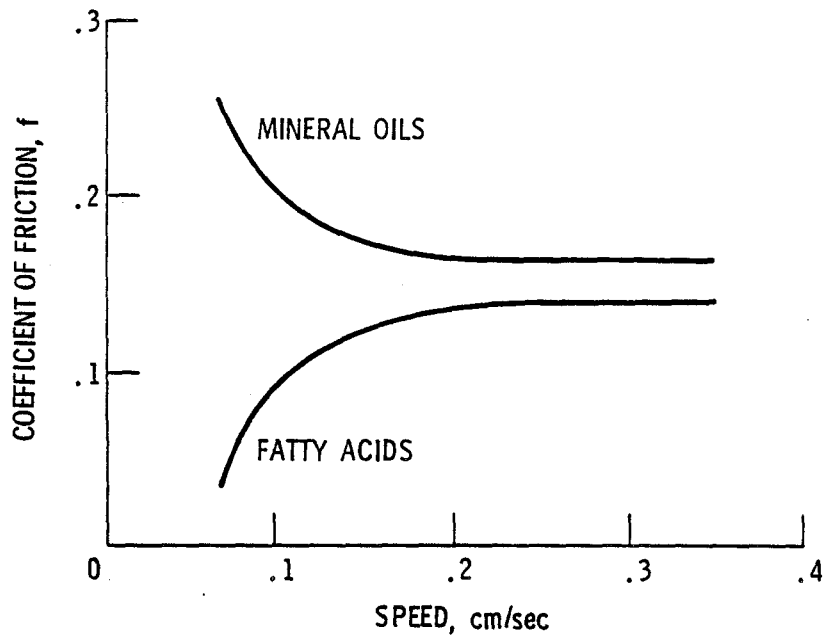
Figure 26. - Friction versus speed (ref. 24).
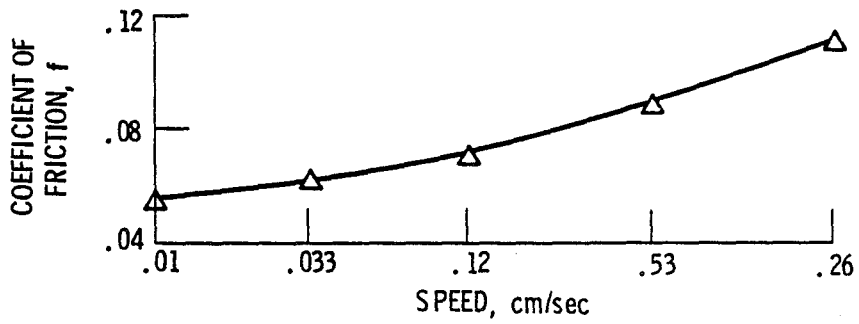


Figure 27. - Friction versus speed for steel/bronze lubricated with oleic acid (ref. 25).
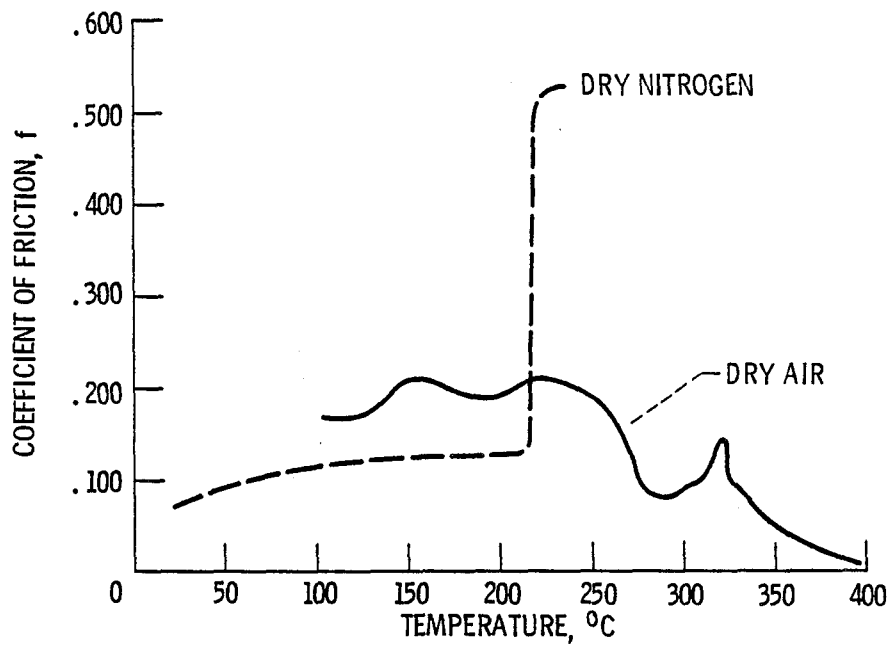
Figure 28. - Friction versus temperature for pure tricresyl phosphate on M-50 steel. (Ref. 26)
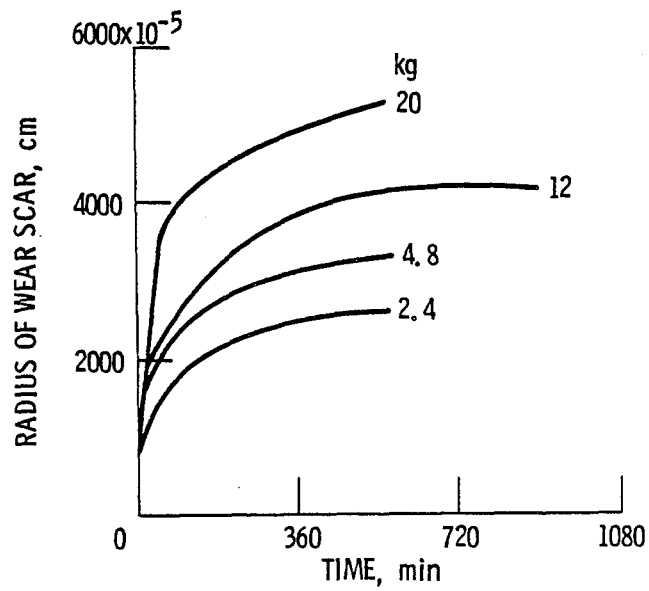


Figure 29. Radius of wear scar as a function of time for several loads. (Ref. 4)
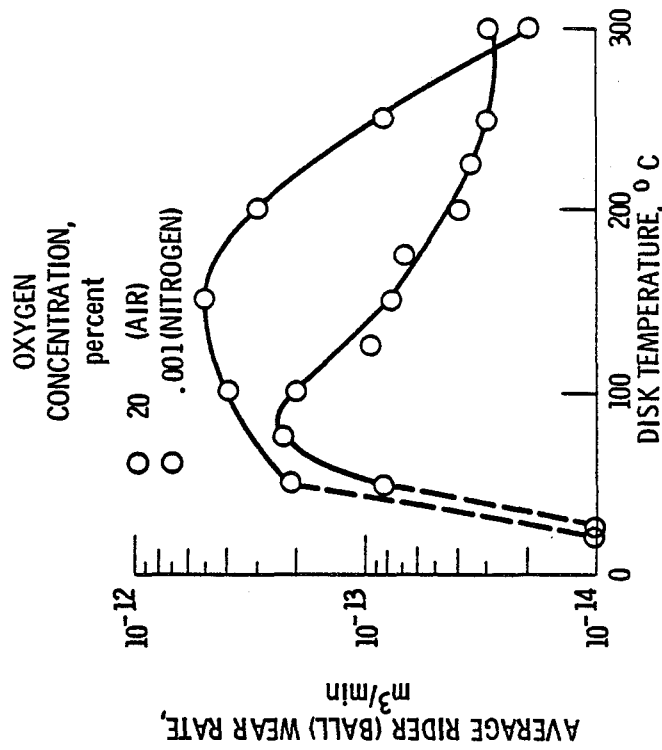
Figure 31. - Average rider (ball) wear as a function of disk temperature with a five-ring polyphenyl ether in atmospheres with two oxygen concentrations. Specimen material, CVM M-50 steel; load, 1 kilogram; sliding speed, 17 meters per minute (100 rpm); test duration, 25 minutes. (Ref. 33)
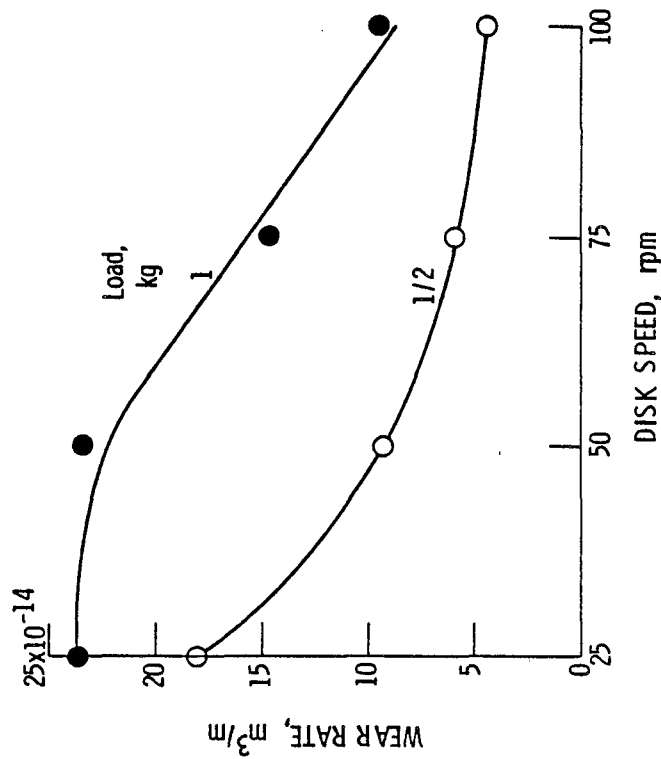


Figure 30. - Effect of disk speed on rider wear rate at two loads with ester-base lubricant. Atmosphere, dry air; disk temperature, 20° C; pure iron rider on M-50 (ref. 28).
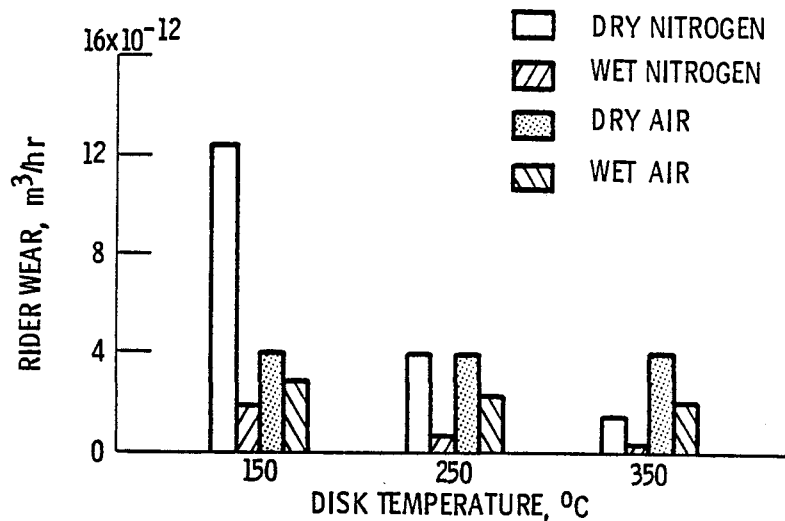
Figure 32. - Rider wear for polyphenyl ether in wet and dry nitrogen and in wet and dry air at disk temperatures of 150°, 250°, and 350° C. (Ref. 27)
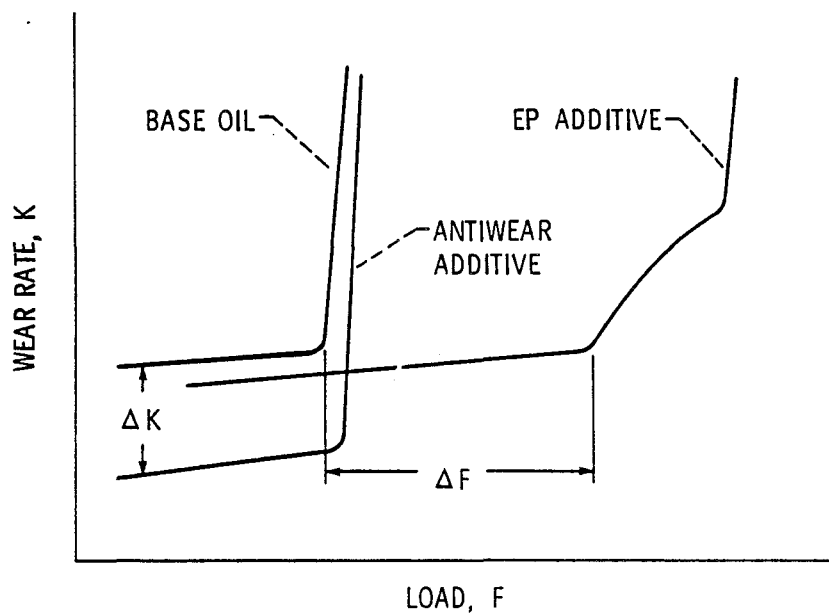


Figure 33. - Wear behavior of boundary-lubrication systems (ref. 34).

# SOLID LUBRICANT MATERIALS FOR HIGH TEMPERATURES - A REVIEW*

Harold E. Sliney
National Aeronautics and Space Administration
Lewis Research Center
Cleveland, Ohio 44135

Solid lubricants that can be used above 300 °C in air are discussed. The scope of the paper includes coatings and self-lubricating composite bearing materials. The lubricants considered are representative dichalcogenides, graphite, graphite fluoride, polyimides, soft oxides, oxidatively stable fluorides, and hard coating materials. A few general design considerations revelant to solid lubrication are interspersed throughout the paper.

## INTRODUCTION

This paper is a review of selected research data which illustrate the tribological properties of materials that are likely to be or are now in use as high-temperature solid lubricants. The term "high temperature" is relative to one's frame of reference; therefore a definition is necessary. For this paper we will somewhat arbitrarily define "high temperature" solid lubricants as those that will not rapidly oxidize or otherwise thermally degrade in air at temperatures to at least 300 °C. Above this temperature most oils, greases, and all but a few organic polymers are not oxidatively stable for any appreciable time.

The scope of this paper includes coatings and self-lubricating composites. The materials considered are representative dichalcogenides, graphite, graphite fluoride, polyimides, soft oxides, oxidatively stable fluorides, and hard coating materials. A few general design considerations relevant to solid lubrication are interspersed throughout the paper.

## LAYER LATTICE SOLID LUBRICANTS

Layer lattice solid lubricants have a hexagonal-layered crystal structure. Their shear properties are anisotropic with preferred planes for easy shear parallel to the basal planes of the crystallites. In some of the compounds such as molybdenum disulfide ($MoS_2$), a low shear strength is intrinsic to the pure material. In others, notably graphite, the presence of absorbed gases or intercalated "impurities" between the basal planes appears to be necessary to develop desirable friction characteristics (ref. 1).

The most common representatives of this class of lubricants are graphite and the dichalcogenides, notably $MoS_2$ and $WS_2$. Since a large volume of literature exists for these materials (e.g., ref. 2), they will not be discussed in detail here except to emphasize the importance of chemical reactivity in determining the suitability of a solid lubricant for a specific application. The maximum useful temperatures for solid lubricants depends strongly on the composition of the ambient atmosphere, the required life at temperature, and factors

---

such as oxygen availability at the lubricated surface (is the coating openly exposed to the atmosphere or shielded within conforming bearing surfaces), airflow rates, lubricant particle size, and the influence of adjuvants and binders.


## The Dichalcogenides

The maximum temperature for lubrication with $MoS_2$ in an air atmosphere is limited by oxidation to about 400 °C under favorable conditions. Some oxidation kinetics data for loosely compacted $MoS_2$ powders of 1-$\mu$m average particle size are given in figure 1(a) (from ref. 3). At a modest airflow rate over the compact, 50 percent of the $MoS_2$ was oxidized to molybdic oxide ($MoO_3$) in 1 hour at 400 °C. At a six times higher airflow rate, the temperature for an oxidation half-life of 1 hour was reduced to 300 °C. Figure 1(b) compares the oxidation kinetics of $MoS_2$ and $WS_2$ at the lower airflow rate. It is interesting that the curves for $MoS_2$ and $WS_2$ intersect, with $MoS_2$ oxidizing more rapidly above about 340 °C. Friction experiments were conducted with a pin-on-disk apparatus using a hemispherically tipped pin in sliding contact with the flat surface of a rotating disk. A comparison of the oxidation data of figure 1 and the friction data of figure 2(b) (from ref. 3) shows that the loss of lubricating ability of $MoS_2$ and $WS_2$ in air coincides with the temperatures at which rapid conversion to the oxides occurs.

Figure 2(a) also shows that both compounds lubricate to much higher temperatures in a nonreactive argon atmosphere. In an inert gas or vacuum the maximum useful temperature is a function of the thermal dissociation rates rather than the oxidation rates of the lubricants. Thermal dissociation rates and the friction coefficients of molybdenum and tungsten disulfides, diselenides, and ditellurides in vacuum have been systematically studied (ref. 4). The major results, summarized in table I, indicate that the disulfides are the most stable, the diselenides are intermediate, and the ditellurides are the least stable. However, thin burnished films of the diselenides with their higher densities evaporate more slowly than the disulfides. Apparently for the very thin, burnished films used in this study, the evaporation rates were the controlling factor in determining the maximum temperature for effective lubrication. A more recent paper described the thermal stability and lubricating characteristics of various bonded $MoS_2$ coatings in vacuum (ref. 5). The limiting temperatures for a significant wear life of these coatings ranged from 600 to 700 °C in agreement with the 650 °C limiting temperature for burnished $MoS_2$ reported in reference 4.


## Graphite

Although $MoS_2$ and $WS_2$ are "intrinsic" solid lubricants that are most effective in a vacuum or a nonreactive gas atmosphere, it has been long known (ref. 6) that graphite, in contrast, is a poor intrinsic lubricant that requires the presence of absorbed vapors such as water or hydrocarbons to develop good lubricating properties. Certain solid adjuvants such as cadmium oxide (CdO) and other oxides or salts are also helpful in improving the lubricating ability of graphite. Figure 3 (from ref. 7) illustrates the remarkable effect of CdO addition on lubrication with graphite powder from room temperature to 540 °C. Without the CdO addition graphite lubricated at room temperature and above

56

425 °C but not at intermediate temperatures. Low friction at room temperature was attributed to the beneficial effect of absorbed moisture. High friction at intermediate temperatures was attributed to desorption of water and possibly other gases. Low friction above 425 °C was attributed to interaction of graphite with oxides of the lubricated metal. Graphite itself begins to oxidize at about 400 °C. Nevertheless it has been reported that graphite can be used as a wire-drawing lubricant for tungsten and molybdenum at temperatures as high as 1100 °C in ambient air conditions (ref. 8). Oxidation of graphite and of the metals occurs rapidly at the drawing temperatures. However, the time at high temperature is so short that effective lubrication is achieved. Therefore high-temperature lubrication must take into account the interaction of the lubricant, the atmosphere, and the surface being lubricated and must further balance reaction rates against the required residence time of the lubricant within the contact.

### Graphite Fluoride

Graphite fluoride $(CF_x)_n$, also referred to as carbon monofluoride (when $x = 1$) is a relatively new solid lubricant that can be loosely described as a layer lattice intercalation compound of graphite. It is prepared by the direct reaction of graphite with fluorine gas at controlled temperature and pressure. It is gray to pure white depending on its stoichiometry. The subscript "x" in $(CF_x)_n$ can vary from about 0.3 to 1.1. For $x \geq 1$, the compound is pure white, electrically nonconductive, and nonwettable by water (hydrophobic). There is some debate about whether $(CF_x)_n$ is a true intercalation compound because the basal planes of the graphite crystallites are distorted to a puckered, non-planar configuration when the compound is formed. However, there is no doubt that the original graphite crystal lattice is the primordial lattice from which the crystal structure of $(CF_x)_n$ is formed. The fluorine-to-carbon bonds are covalent, with the fluorine atoms located between the distorted basal planes. The spacing between the basal planes is expanded from 3.4 Å in graphite to $7.5 \pm 1.5$ Å in $(CF_x)_n$ (ref. 9). The crystal lattice expansion and the distortion of the carbon basal planes are schematically represented and compared with the crystal structure of graphite in figure 4. Although $(CF_x)_n$ is not known to oxidize in air, it decomposes thermally above about 450 °C to form carbon tetrafluoromethane, other low-molecular-weight fluorocarbons, and carbon (ref. 10).

Some early research on the lubricating properties of $(CF_x)_n$ was reported in reference 11. In this study, thin lubricating films of $(CF_x)_n$ were burnished on 440C and 301 stainless steel disks and evaluated in pin-on-disk experiments. Wear life and friction coefficient data for burnished $(CF_x)_n$ and $MoS_2$ films on 440C are compared in figure 5. Film failure was considered to be the time at which the friction coefficient exceeded 0.3. The $(CF_x)_n$ films were the more durable over the entire temperature range shown. Friction coefficients were for the most part well below 0.1 up to the failure temperatures of the coatings, which are indicated by the arrows in figure 5. Failure temperature was 400 °C for $MoS_2$ and 480 °C for $(CF_x)_n$. These failure temperatures correlate well with expectations based on the oxidation kinetics data for $MoS_2$ (fig. 1) and the previously referenced thermal decomposition temperature of $(CF_x)_n$. Similar results were obtained for the lubrication of 301 stainless steel with $(CF_x)_n$, but burnished $MoS_2$ films failed immediately on this alloy. General agreement with these results was obtained with burnished $(CF_x)_n$ by using a flat rub block on a cylinder specimen configuration (ref. 12).

$(CF_x)_n$ exhibits an extreme degree of plasticity within a lubricated contact. It has been observed (ref. 13) that all this ability to readily undergo plastic flow within the contact is a characteristic that all good solid lubricants have in common; nonlubricated solid particles tend to fragment within the contact and, if of sufficient hardness, will embed in one surface and abrade the other. To illustrate the two extremes, compare the plastic behavior of $(CF_x)_n$ shown in figure 6 with the brittle behavior of SiC in figure 7. $MoS_2$ and graphite also readily flow within a moving concentrated contact. The order of plasticity subjectively observed is $(CF_x)_n > MoS_2 >$ graphite.

Various resin binders have been used with $(CF_x)_n$ to achieve longer wear lives and higher load capacities than can be achieved with burnished films. Good results were generally obtained in regard to low friction and wear, but there is some discrepancy in the reported load capacity of the coatings in Falex V-block tests. Reference 14 for example reported a high load capacity for epoxy - phenolic resin - bonder $(CF_x)_n$, but the authors of reference 15 reported, on the basis of their Falex evaluation, that $(CF_x)_n$ is not considered to be suitable for use in heavy load application. Therefore $(CF_x)_n$ coatings may not be the lubricant of choice for highly loaded, concentrated (Hertzian) sliding contacts. However, there are $(CF_x)_n$ coatings that have quite adequate load capacity for lubricating bearings with conformal contacts such as plain spherical bearings or cylindrical bushings. Polyimide-bonded $(CF_x)_n$ in particular has been extensively studied and will be discussed in the next section.


POLYIMIDES

Polyimide Coatings

A few organic polymers are oxidatively stable and also have glass transition temperatures above 300 °C. Examples are polyquinoxilines, polybenzimidazoles, and polyimides. Of these, the polyimides are by far the most readily available and have been the most studied by tribologists. Polyimide coatings have been studied as self-lubricating varnishes (ref. 16) and as resin binders for inorganic solid lubricants (refs. 16 and 17).

The results of pin-on-disk experiments with polyimide varnish coatings on 440C stainless steel are given in figure 8. Wear life and friction characteristics were determined in three different atmospheres: dry argon, dry air, and air containing $10^4$ ppm of water vapor. In all these atmospheres there is a transition in the friction and wear life properties of the polyimide films between 25 and 100 °C. Above the transition temperature polyimide films performed well as solid lubricants. Low friction and long wear lives were obtained even with no solid lubricant additive in the film. At room temperature the polyimide films did not lubricate nearly as well as they did from 100 to 500 °C. This transition in the tribological properties of polyimide has been attributed to second-order relaxation in the molecular bonds of the polymer between 25 and 100 °C (ref. 18).


Polyimide-Bonded Graphite Fluoride Coatings

The effect of adding $(CF_x)_n$ or $MoS_2$ to the polyimide varnish is illustrated in figure 9. The solid lubricant additions clearly improve the wear life and friction at room temperature. In effect, the undesirable friction transition below 100 °C is totally masked by the addition of the solid lubricant pigments.

58

A promising application for polyimide-bonded $(CF_x)_n$ coatings is as a backup lubricant for compliant (foil) gas bearings at temperatures to 350 °C. About 100 °C higher gas temperature capability can be achieved by substituting PI-bonded $(CF_x)_n$ for the more conventional PTFE coatings. Current research by this author shows that these coatings are remarkably durable in start-stop endurance testing of foil bearings.

## Polyimide Composites, Background

Polyimides are also used in heat-cured composite bearing materials. It is shown in references 19 to 21 that polyimide and polyimide compositions containing various powder fillers had interesting possibilities as self-lubricating bearing materials. Polyimide bearing materials with powdered solid lubricant additives such as graphite and $MoS_2$ have found many applications. However, the powdered additives significantly reduce the mechanical strength of the molded polyimide. A polyimide with a compressive strength of 207 MPa (30 000 psi) without additives will typically have about one-half of that compressive strength when 10 to 20 wt % of solid lubricant powder is incorporated into the polymer. However, lubricating properties can be improved with no loss of strength by using graphite fiber, which provides both lubrication and reinforcement.

The potential of graphite-fiber-reinforced polyimide (GFRPI) as a self-lubricating composite material was first demonstrated in accelerated crossed-cylinder wear tests (ref. 22). The performance of GFRPI in oscillating plain spherical bearings was reported in reference 23; in that research chopped graphite fiber reinforcement was used. The fibers were incorporated into the B-staged polyimide and mixed to achieve a random fiber distribution; then the mixture was transfer molded into the bearing and cured under heat and pressure.

GFRPI composite bearing materials fabricated from layers of woven graphite fabric and polyimide have also been reported (e.g., ref. 24). The discussion in this paper is confined to chopped-fiber-reinforced bearing materials.

## Chopped-Fiber-Reinforced Polyimides

Pin-on-disk studies. - The evaluation of chopped-GFRPI composites in a pin-on-disk tribometer is reported in reference 25. In these experiments hemispherically tipped 440C stainless steel pins were slid against the flat surface of rotating GFRPI disks. Two types of graphite fiber and two polyimides were evaluated. The fiber properties are given in table II. The fiber designated type L is a relatively low-strength, low-modulus fiber; the type H fiber has a medium tensile strength and an elastic modulus approximately 10 times higher than the type L fiber. The molecular structures of the two polyimides are given in figure 10. Type A is an addition polyimide and is highly crosslinked. Type C is a condensation polyimide and has a linear, essentially noncrosslinked polymeric structure. Type A polyimides do not produce water vapor as a product of the advanced stage of polymerization (as do type C) and therefore are sometimes considered easier to mold into void-free parts.

Figure 11(a) gives the friction characteristics of the various composites at 25 and 300 °C in air containing $10^4$ ppm of water vapor. At 25 °C the friction coefficient is about 0.2 for all of the composites, but at 300 °C the

59

type AL composite has the lowest friction coefficient (~ 0.05). Profilometer traces (fig. 11(b)) of the wear tracks on the GFRPI disks after 300 000 sliding passes (disk revolutions) showed that the AL composites were also the most wear resistant at both temperatures.

Bearing tests. - Three self-aligning plain spherical bearing designs and cylindrical bushings were tested. The spherical bearing designs shown in figure 12 consisted of (1) a GFRPI spherical element in a steel outer ring; and (2) a steel spherical element and outer ring with a 1.5-mm-thick self-lubricating GFRPI liner transfer molded into the bearing and bonded to the outer ring.

In the first design tested, the spherical element was a molded composite ball of type AL GFRPI (ref. 23). Friction coefficients for various fiber load-ings are shown in figure 13 for temperatures from 25 to 350 °C. Data for a conventional spherical bearing with a glass-fiber-reinforced PTFE liner are shown for comparison. Friction decreased in a regular manner with increasing graphite content. The composite ball with the highest fiber content of 60 wt % gave the lowest friction but failed by brittle fracture at 315 °C and a 35-MPa (5000-psi) radial load. It was concluded that a fiber loading between 45 and 60 percent is about the optimum tradeoff between minimum torque and maximum dynamic load capacity. The standard PTFE-lined bearing had very low friction to 200 °C, but the liner extruded out of the bearing at 250 °C.

When several modifications of the bearing designs shown in figure 12 were compared (refs. 26 and 27), it was found that the design variations had little influence on bearing friction (fig. 14) but had a significant effect on bearing load capacity (fig. 15). It is clear that much higher dynamic load capacity is achieved with a thin (1.5 mm) GFRPI liner between the ball and the outer ring than with a bearing consisting of a GFRPI ball and a metal outer ring. Dynamic load capacities for cylindrical bushings with GFRPI liners are reported in reference 28, and they were about the same as for the lined sphericals. In general, GFRPI-lined oscillating plain bearings for high-load, low-speed appli-cations have dynamic load capacities of about 140 MPa (20 000 psi) from room temperature to 260 °C and about 70 MPa (10 000 psi) at 320 °C. Bearing design changes such as the addition of edge-retention features to prevent the liner from being squeezed out of the bearing at high loads are expected to further improve load capacity.

## UNCONVENTIONAL SOLID LUBRICANTS

### Soft Oxides and Fluorides, Fusion-Bonded Coatings

In a search for even higher temperature solid lubricants much research has been performed on various soft oxides and with fluorides of alkali metals and alkaline earth metals. Oxides are of course obvious candidates for considera-tion when oxidation-resistant compounds are required. The hard oxides, typical of ceramic materials, such as alumina, silica, and the silicates have good wear resistance but generally high friction coefficients. Furthermore unpolished surfaces or wear debris from hard oxides are abrasive to softer, metallic counterface materials.

On the other hand, soft oxides such as lead monoxide (PbO) are relatively nonabrasive and have relatively low friction coefficients, especially at high temperatures, where their shear strengths are reduced to the degree that deformation occurs by plastic flow rather than brittle fracture. Binary and ternary eutectic oxide systems are of interest because the melting-point suppression, which is the primary characteristic of eutectic systems, tends to lower the shear strength relative to the individual oxides. If the second oxide is a vitrifying agent such as $SiO_2$, glaze (glass) formation is promoted at the sliding surface, and this also tends to modify friction by introducing a viscous component of shear. This increases or decreases friction depending on the viscosity of the glaze within the sliding contact. Therefore the friction characteristics of an oxide coating are controlled by a mechanism involving either or both crystalline shear and viscous drag.

Increasing the surface temperature reduces both crystalline shear strength and glass viscosity within the sliding contact and therefore tends to reduce the friction coefficient of oxide surfaces. This is illustrated in figure 16 (ref. 29), which gives the effect of ambient temperature and sliding velocity on the friction coefficients of a stainless steel alloy lubricated with a coating of $PbO-4PbO\cdot SiO_2$. At low sliding velocities the PbO coating lubricated effectively over only a very small temperature range of about 500 to 650 °C. With increasing sliding velocity frictional heating rates increased and low friction was achieved at ever lower ambient temperatures until at 6 m/sec friction coefficients of 0.2 or lower were observed from room temperature to 650 °C. Because of the narrow range of temperatures at which PbO lubricates effectively at low velocities, its use has been limited to high-speed, high-temperature applications such as the lubrication of dies for high-speed wire drawing.

Other studies showed that chemically stable fluorides of some Group I and II metals, such as LiF, $CaF_2$, and $BaF_2$, also lubricate at high temperature but over a broader range of temperatures than PbO. For example, coatings with compositions from the $CaF_2/BaF_2$ binary eutectic system lubricate from about 500 to 950 °C. The tribological properties in air of fused fluoride coating with the composition $62BaF_2-38CaF_2$ are given in figure 17 (ref. 30). Data for uncoated specimens are given for comparison.

The fluorides of the rare earth metals are another group of metal halides that are chemically stable and have shown promise as high-temperature solid lubricants. In an exploratory study of their lubricating properties cerium trifluoride ($CeF_3$) and lanthanum trifluoride ($LaF_3$) were the best solid lubricants among the rare earth fluorides (ref. 31). The individual $CeF_3$ or $LaF_3$ powders lubricated nickel-base super alloys in air to at least 1000 °C. Friction coefficients were 0.3 to 0.4 from room temperature to 500 °C but averaged about 0.2 at higher temperature. These compounds received little further attention in the lubrication literature but definately should be considered where friction coefficients of 0.2 to 0.4 combined with good antiwear characteristics at high temperature are required.

Coatings of oxide and fluoride compositions that melt at a lower temperatures than the substrate metal can be applied by well-known procedures for applying glass or porcelain enamel glazes. In brief, an aqueous slurry of the oxide or fluoride powders is sprayed onto the metal, cured to dryness, then furnace-fired above the melting point of the coating composition. Upon cooling, a fusion-bonded, dense coating is obtained. Good adhesion depends on reasonably matched thermal expansion coefficients and other factors such as the

61

nature of the high-temperature interactions that take place between the melt, the metal, and the atmosphere during firing. Fusion-bonded fluoride coatings can be applied by a similar procedure. However, while oxide coatings are generally fired in air, inert or reducing atmospheres are generally used for fluorides to avoid contamination of the coatings with oxides of the substrate metal.

## Fluoride-Metal Composites

Composite bearing materials in which the solid lubricant is dispersed throughout the structure are advantageous when long lubricant life is required. In some cases a thin, bonded solid lubricant coating is used as an overlay on the self-lubricating composite material. This assures the minimum friction coefficient obtainable by enrichment of the composite surface with lubricant while providing long life because of the underlying, self-lubricating composite material. The friction and wear of a composite consisting of a porous, sintered metal matrix infiltrated with barium fluoride - calcium fluoride eutectic are shown in figure 18 (from ref. 32). Wear life comparisons for composite coatings in air and hydrogen are given in table III. Wear life is herein defined as the number of sliding cycles before the friction coefficient rises above 0.3. It is clear that the composites have longer endurance than the coatings. However, these composites are difficult and time consuming to prepare. The process involves preparing a sintered, porous metal matrix that is then infiltrated with molten fluorides at about 1000 °C, cooled, and finish machined. If an overlay is used, the coating material is next sprayed on from an aqueous slurry and then cured in an argon atmosphere at about 950 °C. Similar compositions can be prepared more conveniently by plasma spraying.

## Fluoride-Metal Composite Coating

Mixed powders of, for example, $CaF_2$ and metal can be deposited by plasma arc spraying to form a composite coating on a wrought metal substrate. Excess coating material is applied, and the coating is then surface ground to the desired thickness (usually 0.010 to 0.020 cm) and a smooth surface finish. Two coatings of this type that have been successfully applied in extreme environments, for example, the space shuttle and the hot section of small jet engines, are designated PS100 and PS101. Their compositions by weight are

PS100:  67 nichrome, 16 1/2 calcium fluoride, 16 1/2 glass
PS101:  30 nichrome, 30 silver, 25 calcium fluoride, 15 glass

The glass in these compositions is a special sodium-free glass that protects the nichrome from oxidation. Its composition is 58 $SiO_2$, 21 BaO, 8 CaO, 13 $K_2O$.

Figure 19 (ref. 33) gives friction coefficients in air for oscillating journal bearings. The cylindrical bores of the bearings were coated with 0.025 cm of PS100 or PS101. A preoxidized, but otherwise uncoated, unlubricated bearing is included for comparison. The oxide film on the preoxidized bearing provided some protection against galling for a time, but the bearing seized at 870 °C. Friction coefficients for the bearing lubricated with PS100 were lower at all temperatures, and effective lubrication was achieved from about 500 to 900 °C. The beneficial effect of silver in reducing low-temperature friction while only

moderately reducing the maximum-temperature capability of the coating system is illustrated by the data for PS101. Friction coefficients of the order of 0.2 were obtained at all temperatures from room temperature to 870 °C.

The friction and wear data for bearings with PS101 lubrication, which were tested in moderate vacuum, cold nitrogen gas, and air, are summarized in table IV. The lowest bearing friction was observed in the $5\times10^{-2}$-torr vacuum, where the friction coefficient was 0.15. Wear rates tended to decrease with test duration. Total diametral bearing wear was $4.5\times10^{-3}$ cm after 5000 oscillating cycles. In cold nitrogen (-107 °C) friction coefficients were typically 0.22 and diametral wear after 5000 journal oscillations was $3.8\times10^{-3}$ cm. As previously discussed, the friction coefficient in air from room temperature to 870 °C was approximately 0.2 over the entire temperature range. Wear rates also were uniformly low over the entire temperature spectrum. These results clearly demonstrate the versatility of PS101 for lubricating plain journal bearings over an exceptionally wide range of temperatures and atmospheric conditions.

In general, the maximum useful temperature in air for a fluoride coating with a superalloy matrix is limited by oxidation of the alloy. Even with a protective glass within the composite structure, the superalloy oxidizes more rapidly in the composite than in the wrought metal state. The oxidation temperature limit is about 900 °C for composites with a nickel superalloy matrix and about 650 °C for cobalt matrix coatings.

## Fluoride-Oxide Composite Coatings

Because of the limitations imposed by oxidation of the metal matrix coatings, completely nonmetallic coatings are of interest. It has been reported that plasma-sprayed coatings of NiO containing about 15 percent $CaF_2$ have good high-temperature wear resistance (ref. 34). This coating is plasma sprayed onto seal bars for regenerators that are used in automotive gas turbine engines to improve thermal efficiency. The coatings must be wear resistant at high temperature while in sliding contact with a porous ceramic regenerator core. The core material is generally lithium-aluminum silicate (LAS), magnesium-aluminum silicate (MAS), or aluminum silicate (AS).

Current preliminary research at Lewis indicates that plasma-sprayed coatings based on zirconium oxide ($ZrO_2$) have attractive tribological properties. Figure 20 gives the friction and wear coefficients of plasma-sprayed $ZrO_2$-$CaF_2$ coatings with and without silver additions. In these experiments the coating was on the cylindrical surface of a rotating disk and placed in sliding contact with two flat nickel-base superalloy rub blocks. Both coating combinations had fairly high wear rates at room temperature, but wear rates were much lower for the $ZrO_2$-$CaF_2$ coating at 650 °C. Silver additions were detrimental and did not have the beneficial effect of improving room-temperature friction and wear that they had on the metal matrix composites. Wear of the uncoated metal shoes that slid against the coatings was low in all cases, indicating that the coatings were not particularly abrasive to the metal rub shoes. Friction coefficients were 0.4 at room temperature and 0.22+0.04 at 650 °C for the $ZrO_2$-$CaF_2$ coating. Higher temperature experiments will demonstrate whether these coatings have a maximum-temperature advantage over the metal matrix plasma-sprayed coatings.

# VACUUM-DEPOSITED COATINGS

Vacuum-deposited coatings used in tribological applications fall into two main composition categories: soft lubricating coatings and very hard, wear-resistant coatings. The methods of application also are in two principal categories: sputtering and ion plating. These techniques have been rapidly adopted by industry especially for aerospace applications (refs. 35 and 36). A very large variety of vacuum-deposited coatings are becoming available; therefore only a few representative examples are discussed here.

## Soft Solid-Lubricant Films (Sputtered)

The most common vacuum-deposited tribological coatings are sputtered dichalcogenides, especially $MoS_2$, and ion-plated soft metals such as gold, silver, and lead. These coatings are often very thin, of the order of 2000 to 5000 Å in thickness. Compounds such as $MoS_2$ are usually applied by sputtering because with proper procedures pure, essentially stoichiometric compounds can be deposited. In contrast, ion plating tends to dissociate chemical compounds. However, ion plating is an appropriate technique for depositing elemental metals because (1) dissociation is obviously not a problem; (2) high ion impact energies can be used to enhance adhesion; (3) excellent throwing power is achieved when coating parts with complex shapes; and (4) rapid deposition rates can be achieved.

The use of sputtering to deposit $MoS_2$ lubricating films was first reported in reference 37. The films were nearly stoichiometric, indicating minimal dissociation of $MoS_2$ by the sputtering procedure used. Figure 21 shows that the coatings, which were only about 2000 Å thick, had good durability in the sliding contact and low friction coefficients of 0.05 to 0.10 in vacuum. Unfortunately durability was much lower in air. For example, 204 size ball bearings with sputtered $MoS_2$ on the cage, balls, and races easily survived 1000 hours of operation in vacuum at 1750 rpm and a 138-N (31-lb) radial load, but when air was admitted into the vacuum chamber, the bearings failed in less than 1 hour (ref. 38). Figure 22 from the same reference shows an abrupt rise in the friction coefficient obtained with sputtered $MoS_2$ as the ambient air pressure was increased above about 300 torr. For air applications the thicker, more conventional bonded $MoS_2$ coatings are usually preferred; the sputter coatings are favored for vacuum applications.

## Soft Metal Lubricant Films (Ion Plated)

The wear lives of ion-plated gold and vapor-deposited gold were compared in reference 39 with the following results. Figure 23 shows that ion-plated gold had nearly twice the wear life of the vapor-deposited film. Furthermore the friction coefficient of ion-plated gold increased gradually, giving adequate indication of impending failure, while the vapor-deposited film failed abruptly without warning. The longer wear life of the ion-plated film was attributed to its superior adherence to the substrate metal.

The use of ion-plated lead films for lubrication of ball bearings in vacuum has been reported (ref. 40). The ion-plated film generated less debris and torque variation than vapor-deposited lead. This was again attributed by the authors to the superior adherence of ion-plated films.

## Sputtered Hard Coatings

Sputtered hard coating are used primarily for wear control. The oxidation temperatures and hardness of some important carbides and nitrides are compared in table V. Coatings of all of the compounds listed are hard enough to be expected to have good wear resistance if adequate bonding to the substrate can be achieved. However, a considerable variation in oxidation resistance exists. Chromium carbide, boron carbide, silicon nitride, and silicon carbide are oxidatively stable to at least 1000 °C; but tungsten and titanium carbides oxidize during long-duration exposure to air at temperatures above about 540 °C. Tungsten carbide tends to oxidize more rapidly than titanium carbide because its oxides are volatile at high temperature and their sublimation tends to accelerate the oxidation. Titanium nitride is another promising hard coating material, but it too will convert to the oxide above 550 °C. However, some TiC and TiN sputtered coatings have shown surprisingly good resistance to oxide conversion at higher temperatures than those listed in table V. Oxidation occurs, but the rate is very low, probably because of high coating density and the passivating nature of the initially formed oxide film, which protects the coating against catastrophic oxidation.

Sputtered chromium oxide ($Cr_2O_3$) is an interesting antiwear coating. In start/stop tests, an optimized, sputtered coating of $Cr_2O_3$ on nickel-chromium foil bearings has shown outstanding endurance over a wide temperature range (ref. 41). For example, the coating did not wear out after 9000 start/stop rubs against a journal coated with chromium carbide at temperatures from room ambient to 650 °C (ref. 42).

Great care is required in the sputtering process because reactive gases in the sputtering chamber can react with the sputtered material to alter its composition. This effect can be an annoyance, or it can be used to advantage in a process known as reactive sputtering in which controlled contaminants are intentionally introduced into the vacuum chamber to obtain the desired coating composition. It has been shown in reference 41, for example, that a controlled mixture of TiC and TiN can be codeposited by using a TiC target in combination with a partial pressure of nitrogen in the sputtering chamber.

## CONCLUDING REMARKS

Solid lubricants for use above 300 °C were discussed. The more conventional layer lattice solid lubricants such as $MoS_2$ and graphite in the form of powders or bonded coatings are serviceable in air to 350 to 400 °C under proper conditions and can be used to much higher temperatures for short durations as, for example, in some metalworking processes. The high-temperature polyimides have about the same upper temperature limitations as $MoS_2$ and graphite and are conveniently used in the form of graphite-fiber-reinforced, self-lubricating composites. For higher temperatures some soft oxides and fluorides provide lubrication to as high as 900 °C. They are currently used as fused coatings (0.001 to 0.002 cm thick) on metal substrates or as the lubricating component of metal matrix composites. The composites are prepared by powder metallurgy methods or by plasma arc spraying. For wear control sputtered hard coatings of some selected carbides, nitrides, and oxides are serviceable to 1000 °C if adequate adhesion to the substrate is maintained at all temperatures required by the application. Thin, sputtered $MoS_2$ films, typically of 2000 to 5000 Å

thickness, are very effective in vacuum but of limited durability in reactive atmospheres such as air. Ion-plated films of soft metals such as gold and lead are effective lubricants particularly for solid-lubricated rolling contact bearings.

<div align="center">REFERENCES</div>

1. Bryant, P.J., Gutshall, P.L., and Taylor, L.H., A study of mechanisms of graphite friction and wear, Wear, Vol. 7 (1964) 118-126.

2. Winer, W.O., Molybdenum disulfide as a lubricant, a review of the fundamental knowledge, Wear, Vol. 10 (1965) 422-452.

3. Sliney, H.E., High temperature solid lubricants, Mechanical engineering, Vol. 96, No. 2 (1974) 18-22.

4. Brainard, W.A., The thermal stability and friction of the disulfides and ditellurides of molybdenum and tungsten in vacuum. National Aeronautics and Space Administration, NASA TN D-5141 (1969).

5. Matveevsky, R.M., Lazovskaya, O.V., and Popov, S.A., Temperature stability of molybdenum disulfide solid lubricant coatings in vacuum. Proceedings 2nd Int'l Conf. on Solid Lubrication 1978, ASLE SP-6, 41-44.

6. Savage, R.H., Graphite lubrication, J. Appl. Phys., Vol. 19, No. 1 (1948) 1-10.

7. Peterson, M.B. and Johnson, R.L., Friction studies of graphite and mixtures of graphite with several metallic oxides and salts at temperatures to 1000 °F, National Aeronautics and Space Administration, NACA TN-3657 (1956).

8. Daga, R.H., A study of high temperature lubrication by graphite in metal processing, Proceedings 2nd Int'l Conf. on Solid Lubrication 1978, ASLE SP-6, 30-37.

9. Rudorff, W., and Rudorff, G., Structure of carbon monofluoride, Z. Anorg. Chem., Vol. 253 (1947) 281-296.

10. Kuriakose, A.K., and Margrave, J.I., Mass spectrometric studies of the thermal decomposition of polycarbon monofluoride, Inorg. Chem., Vol. 4, No. 11 (1965) 1639-1641.

11. Fusaro, R.L., and Sliney, H.E., Graphite Fluoride $(CF_x)_n$ - A new solid lubricant, ASLE Trans. Vol. 13, No. 1 (1970) 56-65.

12. Play, D., and Godet, M., Study of lubricant properties of carbon monofluoride: $(CF_x)_n$, National Aeronautics and Space Administration, NASA TM-75191, 1975; Translation of Etude des proprietes lubrifiantes de monogluorure de graphite; $(CF_x)_n$, Proceedings Colloques Int. C.N.R.S., No. 233 (1975) 441-450.

13. Sliney, H.E., Dynamics of solid lubrication as observed by optical micro-scopy, ASLE Trans., Vol. 21, No. 2 (1978) 109-117.

14. Gisser, H., Petronio, M., and Shapiro, A., Graphite fluoride as a solid lubricant, Lubr. Eng., Vol. 28, No. 5 (1972) 161-164.

15. McConnell, B.D., Snyder, L.E., and Strang, J.R., Analytical evaluation of graphite fluoride and its lubrication rerformance under heavy load, Lubr. Eng., Vol. 33, No. 4 (1977) 184-190.

16. Fusaro, R.L. and Sliney, H.E., Lubricating characteristics of polyimide bonded graphite fluoride and polyimide thin films, ASLE Trans., Vol. 16, No. 3 (1973) 189-196.

17. Campbell, M. and Hopkins, V., Development of polyimide bonded solid lubricants, Lubr. Eng., Vol. 23, No. 7 (1967) 288-294.

18. Fusaro, R.L., Molecular relaxation, molecular orientation, and the friction characteristics of polyimide films, ASLE Trans., Vol. 20, No. 1 (1977) 1-14.

19. Devine, M.J., and Kroll, Q.E., Aromatic polyimide composition for solid lubrication, Lubr. Eng., Vol. 20, No. 6 (1964) 225-230.

20. Buckley, D.H., Friction and wear of polyimide and filled polyimide compositions in vacuum, National Aeronautics and Space Administration, NASA TN D-3261, 1966.

21. Lewis, R.B., Wear of polyimide resin, Lubr. Eng., Vol. 25, No. 9 (1969) 356-359.

22. Giltrow, J.P. and Lancaster, J.K., Carbon-fiber reinforced polymer as self-lubricating materials, I. Mech. E., 6th Tribology Group Convention, 1968, paper 18, 149-159.

23. Sliney, H.E. and Johnson, R.L., Graphite fiber-polyimide composites for spherical bearings to 340 °C, National Aeronautics and Space Administration, NASA TN D-7078, 1972.

24. Gardos, M.N. and McConnell, B.D., Development of high-load, high-temperature, self-lubricating composites, Parts I - IV, ASLE Preprints. 81-LC-3A-3,4,5, and 6, 1981.

25. Fusaro, R.L. and Sliney, H.E., Friction and wear behavior of graphite fiber reinforced polyimide composites, ASLE Trans., Vol. 21, No. 4 (1978) 337-343.

26. Sliney, H.E. and Jacobson, T.P., Performance of graphite-fiber-reinforced polyimide composites in self-aligning plain bearings to 315 °C., Lubr. Eng., Vol. 31, No. 12 (1975) 609-613.

27. Sliney, H.E., Some load limits and lubricating properties of plain spherical bearings with molded graphite-fiber-reinforced polyimide liners to 320 °C, Lubr. Eng. Vol. 35, No. 9 (1979) 497-502.

28. Williams, F.J., Composite airframe journal bearings, Rockwell International, NA-80-648, National Aeronautics and Space Administration, NASA CR-165249, 1981

29. Sliney, H.E., Effect of sliding velocity on friction properties and endurance life of bonded lead monoxide coatings at temperatures up to 1250 °F, National Advisory Committee for Aeronautics, NACA RM E 58 B11, 1958.

30. Sliney, H.E., Strom, T.N., and Allen, G.P., Fluoride solid lubricants for extreme temperatures and corrosive environments, ASLE Trans., Vol. 8, No. 4 (1965), 307-322.

31. Sliney, H.E., Rare earth fluorides and oxides - An exploratory study of their use as solid lubricants at temperatures to 1800 °F (1000 °C), National Aeronautics and Space Administration, NASA TM D-5301, 1969.

32. Sliney, H.E., Self-lubricating composites of porous nickel and nickel-chromium alloy impregnated with barium fluoride - calcium fluoride eutectic, ASLE Trans., Vol. 9, No. 4 (1966) 336-347.

33. Sliney, H.E., Wide temperature spectrum self-lubricating coatings prepared by plasma spraying, thin solid films, Vol. 64 (1979) 211-217.

34. Moore, G.D. and Ritter, J.E., The friction and wear characteristics of plasma-sprayed NiO-CaF$_2$ in rubbing contact with a ceramic matrix, Lubr. Eng., Vol. 30, No. 12 (1974) 596-604.

35. Christy, R.K. and Barnett, G.C., Sputtered MoS$_2$ lubrication system for spacecraft gimbal bearings, Lubr. Eng., Vol. 34, No. 8 (1978) 437-443.

36. Gardos, M.N., Quality control of sputtered MoS$_2$ films, Lubr. Eng., Vol. 32, No. 9 (1976) 463-480.

37. Spalvins, T. and Przybyszewski, J. S., Deposition of sputtered molybdenum disulfide films and friction characteristics of such films in vacuum, National Aeronautics and Space Administration, NASA TN D-4269, 1967.

38. Spalvins, T., Bearing endurance tests in vacuum for sputtered molybdenum disulfide films, National Aeronautics and Space Administration, NASA TM X-3193, 1975.

39. Spalvins, T., Coatings for wear and lubrication, Proceedings 3rd Int'l. Conf. on Metallurgical Coatings, Elsevier, 1979.

40. Todd, M.J. and Bentall, R.H., Lead film lubrication in vacuum, ASLE SP-6 (1978) 148-157.

41. Bhushan, B., Development of surface coatings for air lubricated bearings to 650 °C, ASLE Trans., Vol. 23, No. 2 (1980) 185-196.

42. Brainard, W.A. and Wheeler, D.R., Use of nitrogen-argon plasma to improve adherence of sputtered titanium carbide coatings on steel, J. Vac. Sci. Technol., Vol. 16, No. 1 (1979) 31-36.

## TABLE II. – TYPICAL GRAPHITE FIBER PROPERTIES

| Property or Characteristic | Type "L" | | Type "H" | |
|---|---|---|---|---|
| | English Units | SI Units | English Units | SI Units |
| Tensile strength | $9.0 \times 10^4$ lb/in$^2$ | $6.2 \times 10^8$ N/m$^2$ | $2.8 \times 10^3$ lb/in$^2$ | $2.0 \times 10^9$ N/m$^2$ |
| Elastic Modulus | $5.0 \times 10^6$ lb/in$^2$ | $3 \times 10^{10}$ N/m$^2$ | $5.7 \times 10^7$ lb/in$^2$ | $3.9 \times 10^{11}$ N/m$^2$ |
| Length | 0.25 in. | $6.4 \times 10^{-3}$ m | 0.25 in. | $6.4 \times 10^{-3}$ m |
| Diameter | $3.3 \times 10^{-4}$ in. | $8.4 \times 10^{-6}$ m | $2.6 \times 10^{-4}$ in. | $6.6 \times 10^{-6}$ m |
| Specific gravity | 1.4 | 1.4 | 1.4 | 1.4 |

## TABLE I. – RESULTS OF THERMAL STABILITY AND FRICTIONAL EXPERIMENTS IN VACUUM OF $10^{-9}$ to $10^{-6}$ TORR

| Compound | Probable onset of thermal dissociation as detected by TGA, °C | Dissociation products first detected by mass spectrometry, °C | Maximum temperature at which burnished films provided effective lubrication, °C |
|---|---|---|---|
| $MoS_2$ | 930 | 1090 | 650 |
| $WS_2$ | 870 | 1040 | 730 |
| $MoSe_2$ | 760 | 980 | 760 |
| $WSe_2$ | 700 | 930 | 760 |
| $MoTe_2$ | 700 | 700 | 540 |
| $WTe_2$ | 700 | 700 | (a) |

[a]Friction coefficient greater than 0.2 at all temperatures.

## TABLE III. – COMPARATIVE WEAR LIFE OF FLUORIDE COMPOSITES AND COATINGS IN AIR AND HYDROGEN

| Specimen temperature | Cycles at which friction coefficient increased to 0.30[a] | | | |
|---|---|---|---|---|
| | Air | | Hydrogen | |
| | Composites | Coatings | Composites | Coatings |
| 25· | (b) | (c) | [d]1 560 000 | (c) |
| 260 | 2 750 000 | 115 000 | [d]1 499 000 | (c) |
| 540 | 1 105 000 | 389 000 | [d]1 610 000 | 275 000 |
| 650 | 1 370 000 | (c) | [d]1 370 000 | (c) |
| 816 | 850 000 | (c) | 570 000 | (c) |

[a]Based on single runs.
[b]Low wear rate but friction coefficient of 0.30 to 0.35.
[c]No test.
[d]Experiments terminated before failure. (Friction coefficient did not increase to 0.3 during number of cycles indicated.)

TABLE IV. - PERFORMANCE SUMMARY FOR OSCILLATING PLAIN

SLIDING BEARINGS SELF-LUBRICATED WITH A PLASMA-

SPRAYED COATING IN VARIOUS ATMOSPHERES

[PS101 Coating: 30 Ag, 30 NiCr, 25 CaF$_2$, 15 glass; 0.025 cm
(0.010 in.) thick; 3.5×10$^7$ N/m$^2$ (5000 psi) unit load, ±15°
oscillation at 1 hertz.]

| Bearing temperature | | Ambient atmosphere | Typical friction coefficient | Increase in radial clearance | |
|---|---|---|---|---|---|
| | | | | cm ×10$^3$ (milliinches) | |
| °C | °F | | | After 100 cycles | After 5000 cycles |
| Room | Room | Vacuum 5×10$^{-2}$ torr | 0.15 | 1.3 (0.5) | 4.5 (1.8) |
| -107 | -160 | Nitrogen | .22 | 0.3 (0.1) | 3.8 (1.5) |
| Room | Room | Air 760 torr | .24 | .5 (0.2) | 7.0 (2.8) |
| 540 | 1000 | ↓ | .19 | .5 (0.2) | 6.0 (2.4) |
| 650 | 1200 | | .21 | .3 (0.1) | 2.5 (1.0) |
| 870 | 1600 | ↓ | .23 | .3 (0.1) | 2.5 (1.0) |

TABLE V. - BULK PROPERTIES OF SOME HARD COAT MATERIALS[a]

| Material | Microhardness, kg/mm$^2$ | Oxidation temperature[b], °C |
|---|---|---|
| B$_4$C | 4200 | 1090 |
| TiC | 3200 | 540 |
| SiC | 2900 | 1650 |
| Cr$_3$C4 | 2650 | 1370 |
| WC | 2050 | 540 |
| Si$_3$N4 | 2000 | 1400 |
| TiN | 1950 | 540 |
| Cr$_2$O3 | [c]1800 | ---- |

[a]Data from: Engineering Properties of Ceramic Materials,
Battelle Memorial Institute, Published by American
Ceramic Society, Columbus, Ohio, 1966.
[b]Temperature for appreciable detrimental oxidation (passi-
vating oxide films form at lower temperatures).
[c]Estimated conversion from published Moh hardness of 9.
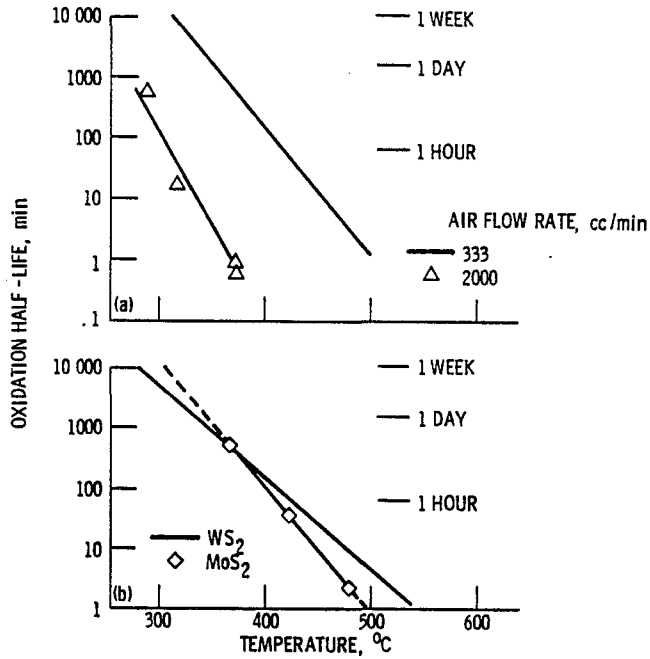
(a) Oxidation characteristics of $MoS_2$ at two air flow rates.

(b) Comparative oxidation of $WS_2$ and $MoS_2$ air flow rate, 1/3 L/min.

Figure 1. - Oxidation kinetics of $MoS_2$ and $WS_2$ average particle size: 1 μ, compact density; 50 %.



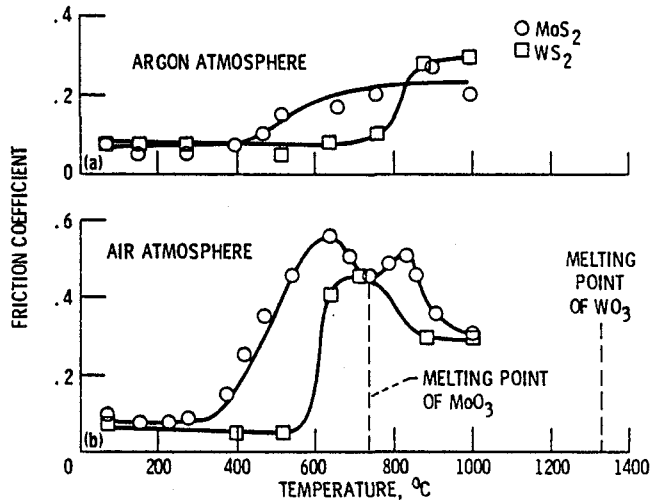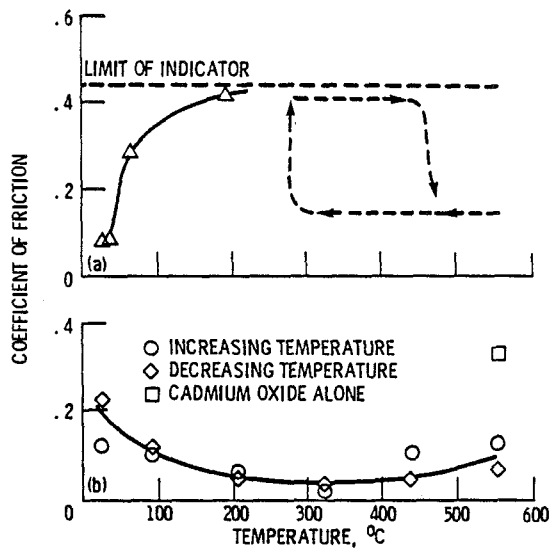Figure 2. - Friction characteristics of $MoS_2$ and $WS_2$ in argon and in air.

(a) Graphite alone.

(b) Cadmium oxide - graphite mixture.

Figure 3. - Effect of oxide adjuvant on lubrication with graphite.
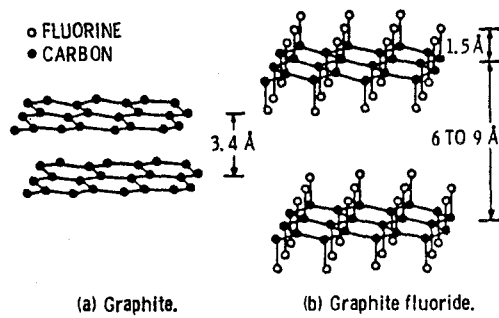


(a) Graphite.

(b) Graphite fluoride.

Figure 4. - Structure of graphite and proposed structure of graphite fluoride illustrating the expansion of the carbon layer planes due to the intercalation of fluorine atoms.
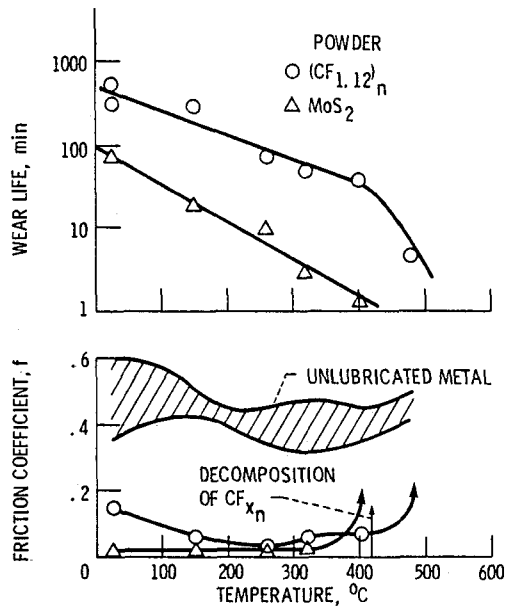
Figure 5. - Effect of temperature on wear life and friction coefficient of graphite fluoride $((CF_{1.12})_n)$ and molybdenum disulfide powders burnished on sandblasted 440-C stainless-steel disks. Riders, 440-C stainless steel; linear sliding speed, 1.6 m/s; load, 500 g; atmosphere, dry air (moisture content, 20 ppm).



(a) FIRST PARTICLES ENTERING CONTACT.

(b) PROGRESSIVE FILM FORMATION.

(c) PROGRESSIVE FILM FORMATION.

(d) COMPLETE FILM FORMATION AFTER ONLY 10 mm OF SLIDING.
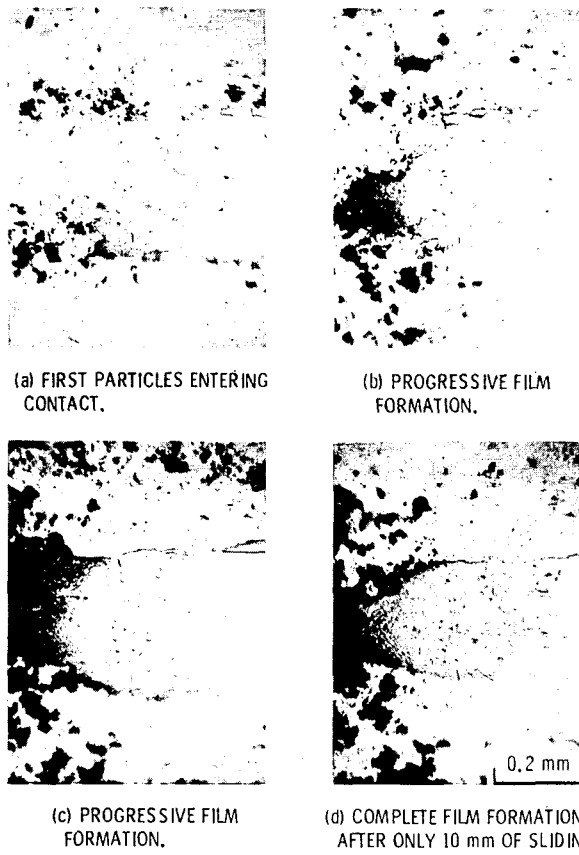
Figure 6. - Behavior of graphite fluoride in initially unlubricated contact. Load, 13.2 N (3 lb); original magnification, X150.

73

(a) SiC PARTICLE ENTERING CONTACT.

(b) PARTICLE PART WAY THROUGH CONTACT.

(c) PARTICLE AT CONTACT EXIT.

(d) CONTACT AFTER 10 DISK REVOLUTIONS.
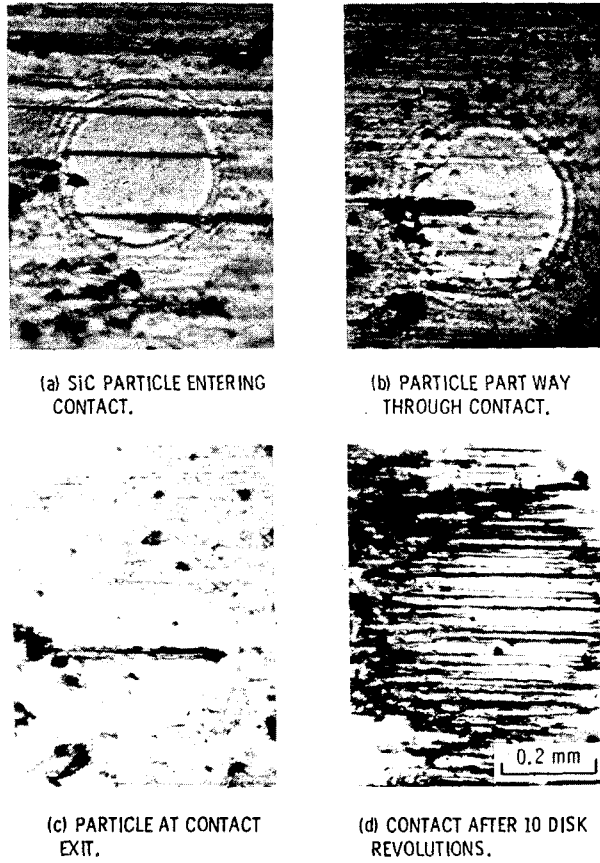
Figure 7. – Abrasive action of silicon carbide particles. Load, 13.2 N (3 lb); original magnification, X150.
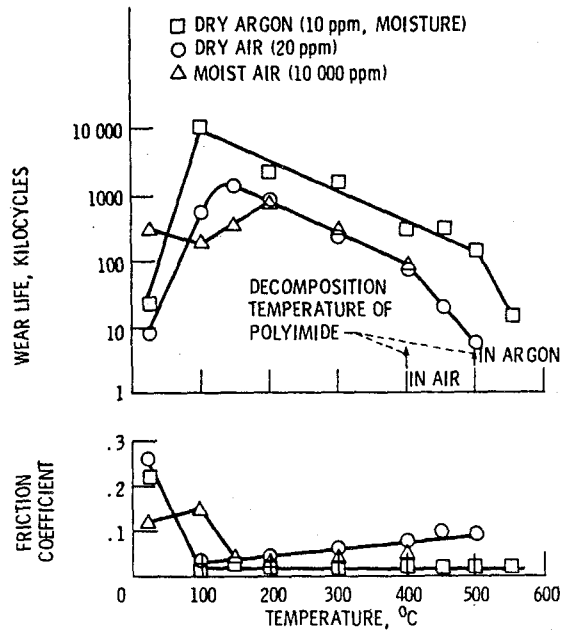


Figure 8. – Friction coefficient and wear life as a function of temperature for thin films of polyimide run in atmospheres of dry argon, dry air, and moist air. Load, 1 kg; velocity, 3 m/sec.

74
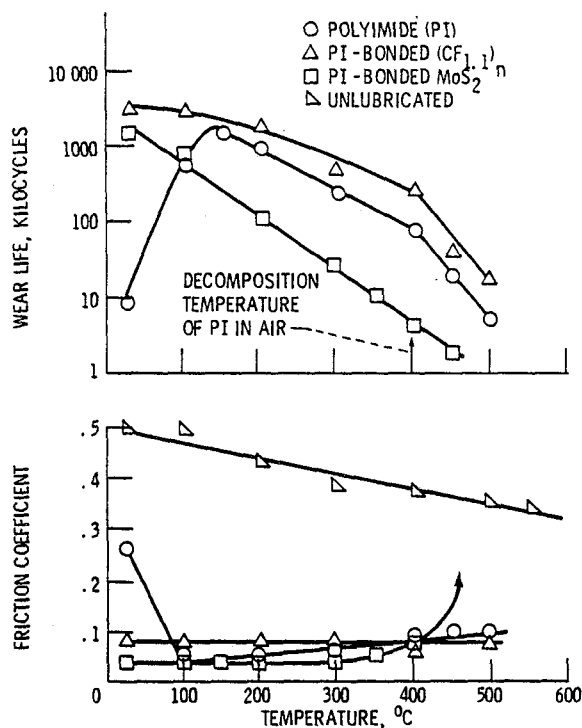
Figure 9. – Friction coefficient and wear life as a function of temperature for three solid lubricant films run in dry air (moisture content, 20 ppm). Load, 1 kg; velocity, 3 m/sec.
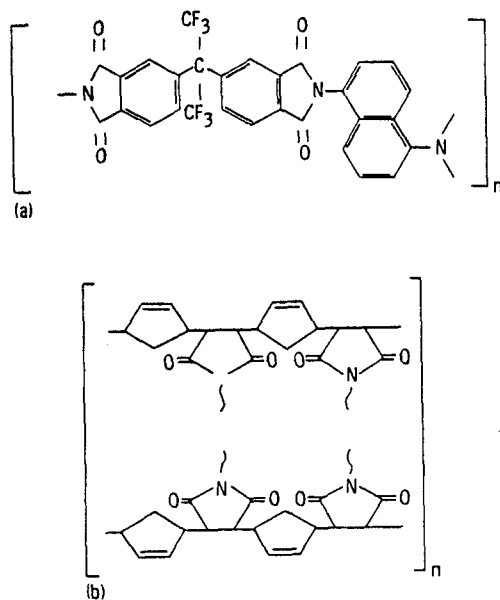


(a) Condensation-type of polyimide polymer (type "C").

(b) Addition-type of polyimide polymer (type "A").

Figure 10. – Two major types of polyimide structures.

(a) Friction coefficients.

TYPE OF
COMPOSITE



"CH"

"CL"

"AL"

$2x10^{-3}$ cm

$1x10^{-1}$ cm

25° C

300° C

(b) Surface profiles of wear tracks after 300 000 cycles of sliding.
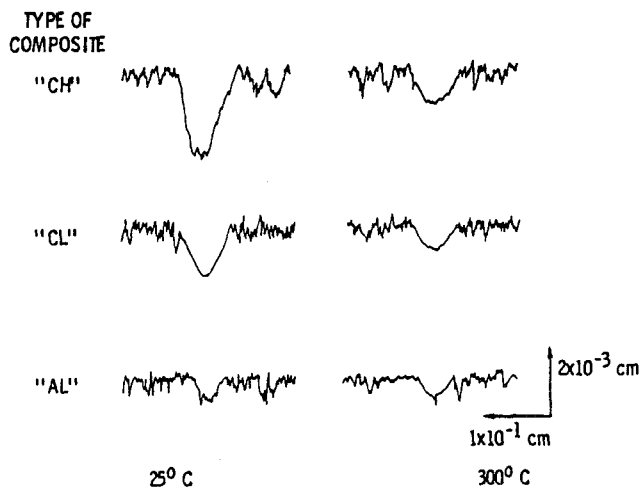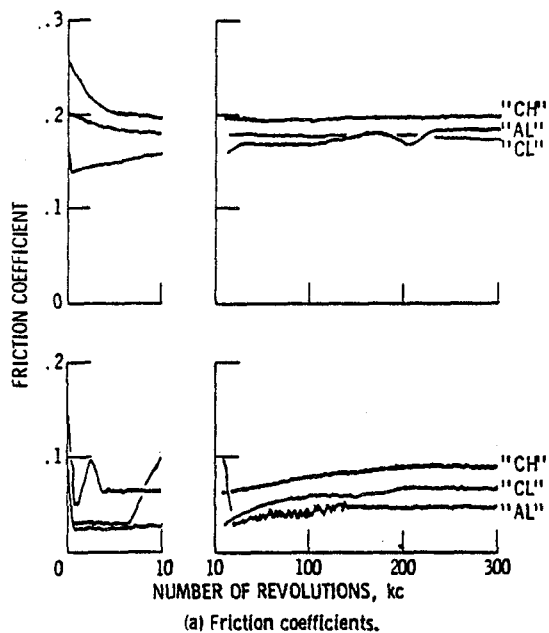
Figure 11. - Friction and wear of graphite fiber reinforced polymide composites in moist air atmospheres (10 000 ppm $H_2O$).



440C-HT SPLIT
OUTER RING

BONDED 440C-HT INSERT

SNAP RING GROOVE

GRAPHITE FIBER REINFORCED
POLYIMIDE BALL

GRAPHITE FIBER REINFORCED
POLYIMIDE LINER

440C-HT BALL

440C-HT OUTER RING
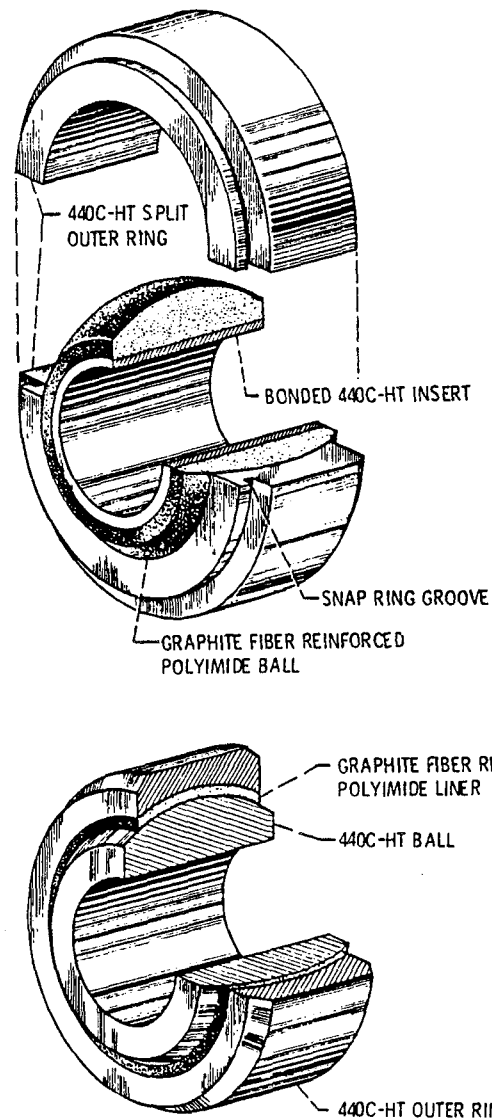
Figure 12. - Test bearings employing graphite fiber reinforced polyimide.
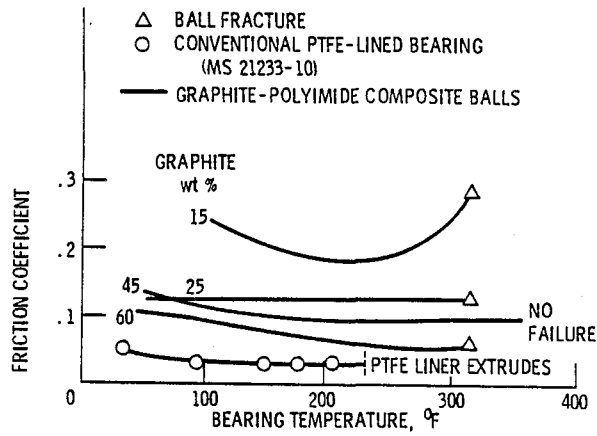
Figure 13. - Summary of friction of spherical bearings with polyimide - graphite-fiber composites of various fiber contents. Stellite 6B journal; radial unit load, $3.5 \times 10^7$ N/m² (5000 psi); journal oscillation in cylindrical bore at 1 Hz, ±15°.
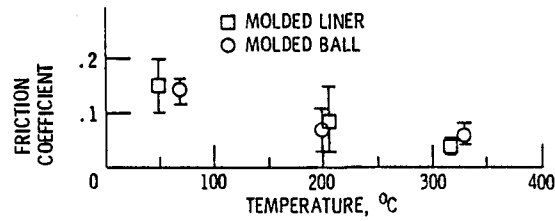


Figure 14. - Friction-temperature characteristics of two bearing designs lubricated with GFRPI composite.
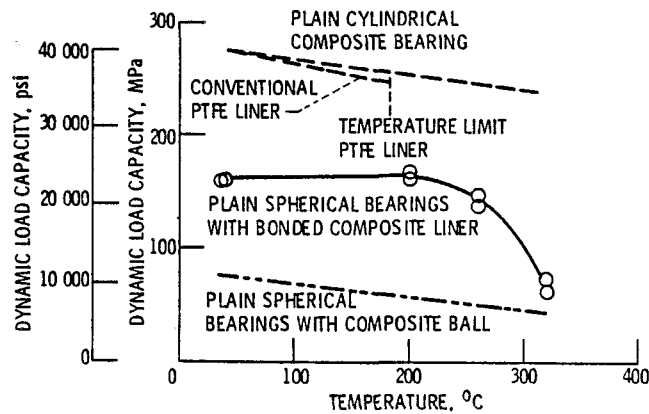


Figure 15. - Dynamic unit load capacities of three bearing designs self lubricated with GFRPI composite.
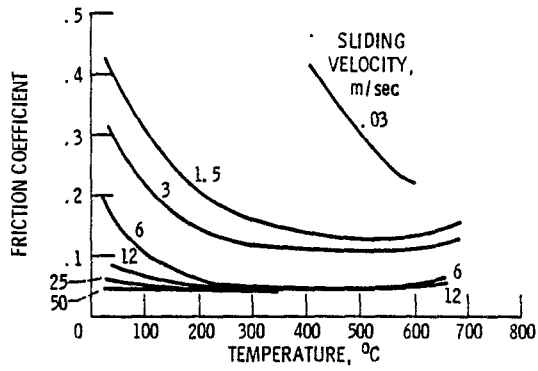
Figure 16. - Effect of sliding velocity and temperature on friction properties of bonded PbO-SiO$_2$. 0.003 cm thick; load, 1000 g.
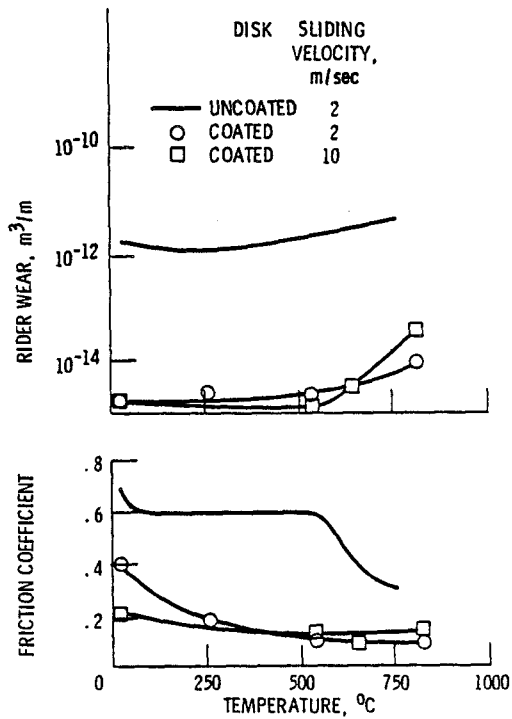


Figure 17. - Lubricating properties of 0.003 cm thick fused fluoride coating composition in air. Load, 500 g.
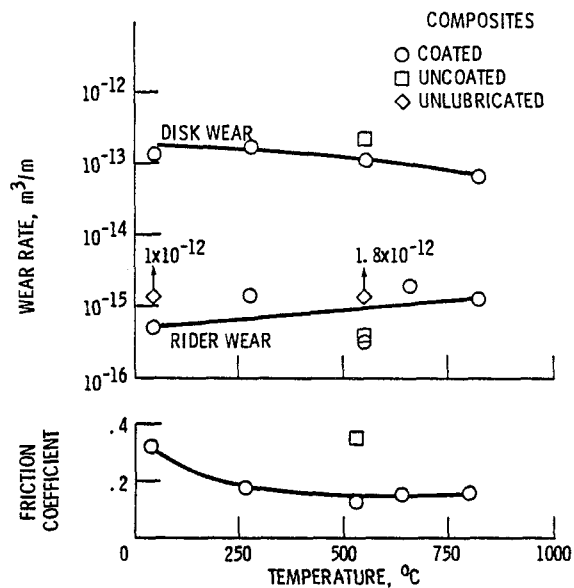
Figure 18. - Friction and wear of fluoride-Inconel composite disks and cast Inconel riders in air. (35 vol % $BaF_2$-$CaF_2$ eutectic, 65 vol % sintered Inconel; 500-g load, 10 m/sec.)
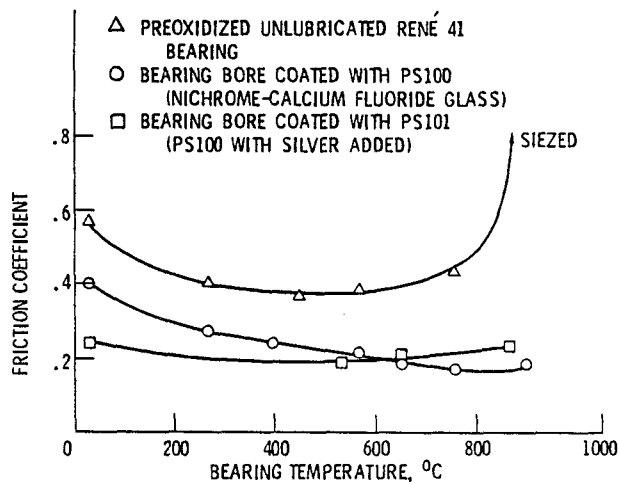


Figure 19. - Bearing friction.
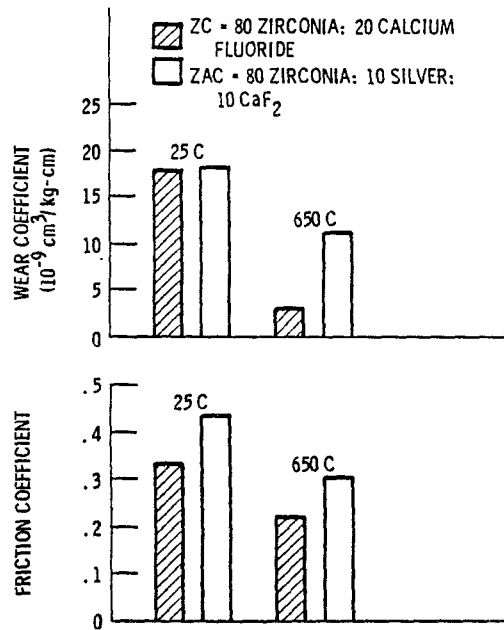
Figure 20. - Wear and friction of plasma - sprayed coatings of zirconia and calcium fluoride, with and without silver. Double rub shoe tests with 22.7 kg per Inconel shoe against coated disk at 0.3 m/sec (150 rpm).



(a) Specimen, niobium.

(b) Specimen, nickel-chrome alloy.
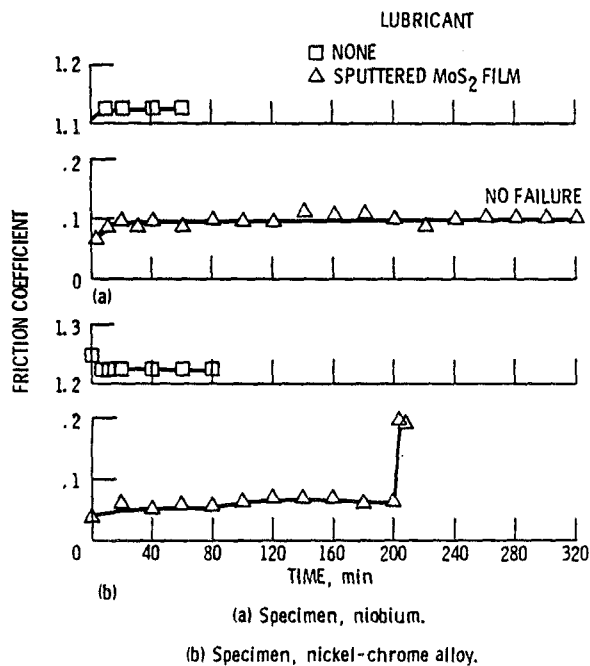
Figure 21. - Average friction coefficients of niobium sliding on two different specimens coated with sputtered molybdenum disulfide in vacuum ($10^{-11}$ torr or $1.33 \times 10^{-9}$ N/m$^2$). Load, 250 g; speed, $2.54 \times 10^{-2}$ m/sec; ambient temperature.
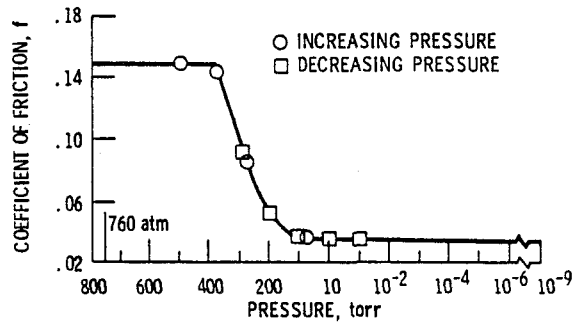
Figure 22. - Effect of pressure on coefficient of sliding friction for sputtered MoS$_2$. Load, 250 g; speed, 0.11 m/sec; substrate/rider, Ni/Ni; room temperature.
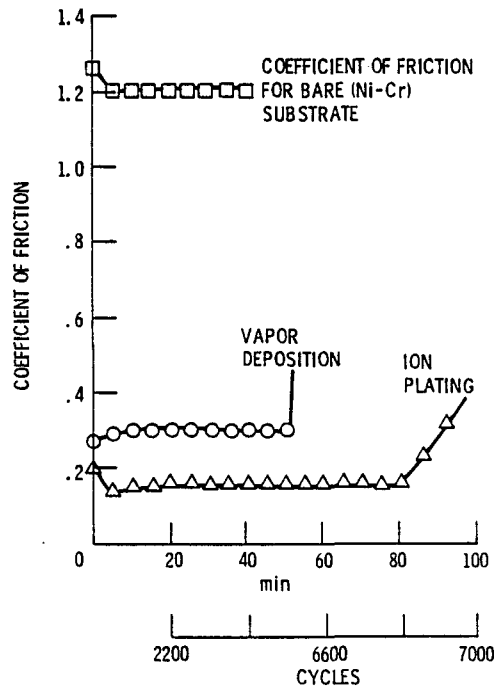


Figure 23. - Coefficient of friction of niobium sliding on (Ni-Cr) alloy with gold deposited by vapor deposition, and ion plating about 2000 Å thick (load, 250 g; speed, 1.52 m/min; ambient temperature 10$^{-11}$ torr).

# Mechanical Components

Bearings
Gears
Traction Drives

# DESIGN AND LUBRICATION OF HIGH-SPEED ROLLING-ELEMENT BEARINGS*

Erwin V. Zaretsky
National Aeronautics and Space Administration
Lewis Research Center
Cleveland, Ohio 44135

The speed capability of rolling-element bearings has increased from speeds of less than two million DN to speeds of three million DN. The life and relia-bility of these bearings have also increased where they are equal to, or greater than, those of bearings with limited speed capability. However, high-speed bearings are not "off-the-shelf" bearings which can be readily ordered from a manufacturer's catalog. Design parameters must be carefully chosen and optimized based upon sophisticated bearing computer programs. Material and lubricant selection must be integrated into the bearing design. Bearing thermal management must be implemented through proper lubrication and cooling. Parameters which can be used to design, specify, and lubricate high-speed bearings are presented and discussed.

## INTRODUCTION

In the early years of the aircraft turbojet engine, engine life and reliability were generally limited by rolling-element bearing technology. Bearing life in a jet engine environment was limited to approximately 300 hr MTBR (mean time between removal). Research and development activities by the major U.S. engine manufacturers, bearing companies and government laboratories over the past three decades have resulted in extending bearing lives in engine operation to approximately 30 000 hr MTBR. At the same time bearing speed capability has also been vastly increased (fig. 1). Bearing speeds of 3 mil-lion DN and lives 100 times catalog rating have been demonstrated for specially designed rolling-element bearings using material, lubrication and manufacturing technologies which are now commercially available.

Bearings used in commercial turbomachinery operating at higher speeds demand the same design and lubrication considerations as those found in advanced airbreathing aircraft engines. Besides the effect of higher stress at the contact of the rolling element and the outer race due to centrifugal force at higher speeds, heat generation and power loss within the bearings are major problems. Thermal analysis of the internal geometry of the bearing with regard to fits and clearances becomes important. Shaft and housing tolerances on the fit and expansion of the bearing rings are a consideration. Cooling of the bearing through lubrication must be efficiently performed. Material and lubricant type must be selected to both assume compatibility with each other and with the higher temperatures found in high-speed bearings. Current lubri-cants are limited to bearing temperatures of 425 °F and materials to tempera-tures above 600 °F.

In designing a bearing for these higher speeds a balance must be main-tained among attaining the required life, incurring surface damage by skidding

---

of the rolling elements, inner-ring fracture due to resulting hoop stresses and fretting problems due to improper fits at operating conditions. Shaft deflections from shaft loading and rotor dynamics can exceed the bearing design limitations. When a tolerance of 100 millionth (0.0001) of an inch is critical to bearing operation and performance these deflections become an important design consideration.

The design of a high-speed rolling-element bearing is a rather sophisticated process. Contrary to the implication of many engineering design texts, it is not possible to select a high-speed bearing from a manufacturer's catalog considering only the external dimensions of the bearing and the applied load and speed. These bearings must be designed for the high-speed application and conversely, the application must be designed for the bearings. Sophisticated bearing computer analysis must be employed for this purpose. It becomes the objective of this paper to review the design and lubrication methods currently used in high-speed, rolling-element bearing design and lubrication as well as material and lubricant selection. While there may be other design methods and analysis employed for this purpose, the methods presented have been established in laboratory experiments and field service to achieve the desired performance results.

## COMPUTER ANALYSIS

There are several comprehensive computer programs that are capable of predicting rolling-element bearing operating and performance characteristics. These programs generally accept input data: bearing internal geometry (such as sizes, clearance, and contact angles), bearing material and lubricant properties, and bearing operating conditions (load, speed, and ambient temperature). The programs then solve several sets of equations that characterize rolling-element bearings. The output produced typically consists of rolling-element loads and Hertz stresses, operating contact angles, component speeds, heat generation, local temperatures, bearing fatigue life, and power loss. The critical assumptions currently necessary in the use of these programs are the form of the lubricant traction model and the lubricant volume percent (the assumed volume percent of the bearing cavity occupied by the lubricant). Two of these programs titled "Shaberth" and "Cybean" are available from COSMIC, 112 Barrow Hall, University of Georgia, Athens, GA 30602, or SKF Industries, Inc., 1100 First Ave., King of Prussia, PA 19406.

The Shaberth program simulates the thermal-mechanical performance of a flexible shaft supported by as many as five rolling-element bearings comprising combinations of ball, cylindrical and tapered roller bearings. Cybean analyses a single cylindrical roller bearing. Both programs are capable of calculating the thermal and kinematic performance of high-speed bearings, and Cybean includes a roller skew prediction for misaligned conditions. Figure 2 illustrates the modal system for thermal routines in Cybean. The correlation between predicted and experimental results with these two programs is very good. However, the proper use of these programs requires an engineer knowledgeable in bearing technology.

## MATERIAL SELECTION

A commonly accepted minimum hardness for rolling-element bearing components at operating temperature is Rockwell C58. At hardnesses below this

value brinelling of the bearing races can occur at stress levels normally experienced. Bearing life is also a function of material hardness. Since hardness decreases with temperature, conventional bearing materials, such as AISI 52100 can be used only to temperatures of about 250 °F. The M-series steels such as AISI M-50 can retain a minimum hardness of Rockwell C58 to approximately 700 °F. Because of its life potential and hardness retention, the AISI M-50 material is the choice material for high-speed ball and roller bearings. The nominal room temperature material hardness of the rolling elements and the races should be Rockwell 63. The hardness difference ($\Delta H$) of the rolling elements minus the races should be zero. This material in its through hardened state can be used to speeds of approximately 2.3 million DN. At higher speeds with the occurrence of a spall in the inner race, hoop stresses due to centrifugal force and press fits can cause the inner ring to fracture causing catastrophic failure of the bearing and probable secondary failure of the rotor system. Clearly this failure mode is unacceptable. As a result, bearing speeds using through hardened steels must be limited speeds of less than 2.3 million DN.

A solution to this problem is the use of carburized or surface hardened steels wherein the material core remains in a soft ductile state and fracture resistant. E.N. Bamberger at the General Electric Company, devised a modified AISI M-50 material which can be carburized. This material is designated M-50 Nil. With the M-50 Nil material, bearing speeds of 3 million DN can be achieved without fear of inner-ring fracture.

Retained austenite content of the AISI M-50 material should be kept at 3 percent or less. This should minimize dimensional growth because of the retained austenite transforming into martensite.

Rolling-element bearing reliability and load capability increases significantly when nonmetallic inclusions, entrapped gases, and trace elements are eliminated or reduced. Improvements in steel making processing, namely double melting in a vacuum, can achieve this. Vacuum-induction melted, vacuum-arc remelted (VIM-VAR) AISI M-50 steel achieves the aforesaid results with significant improvement in bearing life and reliability over single-vacuum melted (VIM) steel. VIM-VAR AISI M-50 and VIM-VAR M-50 Nil are commercially available and should be specified for high-speed bearing application.

For angular-contact ball bearings, the bearing races should be forged to assure parallel grain flow in the ball-race contact. Research has shown that improvement in life of rolling-element bearings occurs with parallel grain flow. For cylindrical roller bearings and deep groove ball bearings, the preferential grain flow already exists without the need for forging.

In recent years the use of ceramic rolling elements has been proposed for high-speed bearing applications because of their lighter weight resulting in lower centrifugal force at the outer-race contact. What has not been considered is that the modulus of elasticity (Young's modulus) and/or Poisson's ratio of these materials are higher than steel such that, even considering the reduction in centrifugal force, the contact stresses at the inner and outer races are greater than with steel rolling elements. This would result in lower lives than with an all steel bearing. Unless there are conditions where the environment is noncompatible with steel, ceramic materials are not recommended for high-speed bearing application.

# BEARING DESIGN

Angular-Contact Ball Bearings - Angular-contact ball bearings can be designed and operated for speeds of 3 million DN with acceptable life and reliability. Based upon experience, a nominal contact angle of 24° and race comformities of 54 and 52 percent at the inner and outer races, respectively, can be used as starting parameters in the design. These parameters can be varied in the design processes to optimize fatigue life and minimize power loss and temperature differences between the inner and outer races. The nominal contact angle β will change with load and speed as shown in fig. 3. As speed is increased, the contact angle at the outer race will decrease while the contact angle at the inner race will increase. The bearing designer or user must determine whether at full operating speed and load the ball will ride on the shoulder of the inner race. Should this occur, bearing life can be significantly shortened. The differences in temperature between the inner and outer races will affect the internal bearing clearances and, thus, bearing performance and life. Should the inner-race temperature increase at a greater rate than that of the outer race, the bearing may lock up.

For high-speed applications with bore sizes greater than 75 mm, the cage design should be a one-piece inner-land riding type. Experience has indicated that the cage should be made out of an iron base alloy (AMS 6415) heat treated to a Rockwell C hardness range of 28 to 35 and having a 0.005-cm (0.002 in) maximum thickness of silver plate (AMS 2410). The cage should be balanced within 3 gm-cm (0.042 oz-in). For bore sizes less than 75 mm, single-land, outer-race riding cages may be the preferred design.

The tolerance grade of the bearings should be ABEC-5 or better. However, the ABEC specification does not consider surface finish or waviness. Waviness of the raceway should be 100 μin or less. Surface finishes of the races should be 2 μin or better and 1 μin for the balls. With honing, surface finishes of 1 μin can be obtained for the raceways. However, not all precision bearing manufacturers can attain this finish.

Roller Bearings - High-speed roller bearings present perhaps a greater design challenge than ball bearings. These bearings can be run to speeds of 3 million DN. For these bearings at high speed, surface distress caused by roller skidding or skewing is the cause of failure. Skidding occurs when the radial load on the bearing is inadequate to develop enough tractive force between the raceways and roller. With insufficient tractive force, true rolling cannot be maintained, and roller sliding or skidding results. Where there is a sufficient lubricant film separating the surfaces no damage to the bearing would be anticipated. However, where the film is marginal, damage can occur.

Skewing of a roller is erratic gyration on a axis not parallel to the axis of the bearing. Skewing results in loading of the roller ends producing excessive end wear, wear of the race flanges or guide channels, and wear of the cage or separator pockets. Should this condition continue for any length of time, cage failure will occur or the roller will wear sufficiently to turn 90° in the direction of rolling and lock up the bearing. Hence, the bearing must be designed to prevent skewing and minimize skidding.

The primary method of eliminating skidding is by increasing the contact stress on the individual rollers. This can be done by reducing both the size

and number of rollers in a bearing. The amount of reduction will be limited by the desired design life of the application.

Another method for increasing the contact stress is shown in fig. 4. In most roller bearings, the maximum number of rollers under load is 20 percent as illustrated in fig. 4(a). Deflecting the bearing outer race by adding a radial preload at two points 90° to the applied load the number of rollers under load can be increased to approximately 60 percent. This is illustrated in fig. 4(b). The design and manufacture of an elliptical outer raceway can accomplish this result.

There have been suggestions to use preloaded hollow rollers to produce a load on all rollers within the bearing. While at first blush this suggestion has merit, experiments have shown that these hollow rollers can fail by flexture fatigue resulting in catastrophic bearing failure.

For most roller bearings, the roller of the bearing is crowned to prevent edge loading of the roller ends and thus premature failure. Typical features of a crowned roller for a high-speed bearing are shown in fig. 5. The length of the roller should not exceed its diameter. The corner radius runout with the diameter of the roller should not exceed 0.001 in total. Concentricity of the crown profile to the diameter should be within 25 millionth of an inch. Roller ends should be square within 0.0001 in. Surface finishes on the rollers are usually 2 to 5 $\mu$in and on the raceway 4 to 6 $\mu$in.

Referring to fig. 6, a relatively large crown drop is necessary to accommodate a large misalignment and prevent skewing. This misalignment is caused by improper assembly or shaft bending under load. However, increasing crown drop beyond 0.007 in will not greatly affect skewing.

Unbalance of the roller will cause roller-gyration skewing. Where the roller is not dynamically balanced then roller-gyration skewing may be caused by (a) excessive corner radius runout with the roller diameter; (b) a crown profile skewed to axis of the roller and (c) lack of squareness of the ends of the roller to the diameter.

Cage design considerations should be similar to those of the ball bearings. Clearance of the roller in the cage pocket should be approximately 5 percent of the roller diameter to permit the roller to move within the pocket without excessive wear. Speed variations cause this roller movement.

Channel-to-roller clearances must be small to maintain good guidance of the roller. Total clearance should be approximately 0.0010 to 0.0015 in. This clearance is sufficient to allow for lubrication of the roller end - flange contact and provides for adequate guidance.

Frederick T. Schuller of the NASA Lewis Research Center has developed a three piece inner-race roller bearing (fig. 7). This concept allows the flanges and races to be manufactured from different materials where required and to be machined with super finishes on the raceway and the roller-flange contacts on the order of 1 to 2 $\mu$in RMS. The concept eliminates stress concentrations at lubricant holes in the raceway surfaces at higher speeds found in conventional designs. It also allows for modified configurations of the flange and roller (fig. 8). This bearing design has been successfully run

to speeds of 3 million DN. While the bearing is not commercially available, it can be specially ordered from precision bearing manufacturers.

Tapered-Roller Bearing - Tapered-roller bearings have been restricted to lower speed applications than have been ball and cylindrical roller bearings. The speed limitation is primarily due to the cone-rib/roller-end contact which requires very careful lubrication and cooling consideration at higher speeds. The speed of tapered roller bearings is limited to approximately 0.5 million DN (a cone-rib tangential velocity of approximately 700 ft/min) unless special attention is given to lubricating and designing this cone-rib/roller-end contact. At higher speeds centrifugal effects starve this critical contact of lubricant.

A computer optimized design of a tapered roller bearing capable of speeds to 2.4 million DN is given in table 1. Tapered roller bearings must use case carburized steels. For higher speed applications materials such as CBS-1000 M and CBS 600 should be considered. To date, M-50 Nil has not been used for tapered roller bearings.

There is a caveat for using tapered-roller bearings at higher speeds. Should there be lubricant starvation to the bearing, the bearing will fail in an extremely short time period. This time is usually less than the time to shut down the system without secondary damage. The problem is currently being worked on. However, no state-of-the-art solution to a commercial user is available.

## LUBRICATION METHODS

Jet Lubrication - Where speeds are too high for grease or simple splash lubrication, jet lubrication is used to both lubricate and control bearing temperatures by removing generated heat. In jet lubrication the placement and number of nozzles, jet velocity, lubricant flow rates, and removal of lubricant from the bearing and immediate vicinity are all very important for satisfactory operation.

The placement of jets should take advantage of any natural pumping ability of the bearings. This is illustrated in fig. 9 for a ball bearing with relieved races and for a tapered-roller bearing. Centrifugal forces aid in moving the oil through the bearing to cool and lubricate the elements.

Directing jets in the radial gaps between the races and the cage is beneficial. The design of the cage and the lubrication of its surfaces sliding on the shoulders of the races greatly affects the high-speed performance. The cage has been typically the first element to fail in a high-speed bearing with improper lubrication.

It has been shown that with proper bearing cage design, nozzle placement, jet velocities, and adequate scavenging of the lubricant, jet lubrication can be successfully used for small-bore ball bearings at speeds to 3 million DN. For large ball bearings, speeds to 2.5 million DN are attainable. For large tapered-roller bearings, jet lubrication was successfully demonstrated to 1.8 million DN, although a high lubricant flow rate of 0.0151 $m^3$/min (4 gpm) and a relatively low oil-inlet temperature of 170 °F were required.

Under-Race Lubrication - A more effective and efficient means of lubricating rolling-element bearings is under-race lubrication. Conventional jet lubrication fails to adequately cool and lubricate the inner-race contact as the lubricant is thrown centrifugally outward. Unfortunately, increased flow rates add to heat generated from oil churning. An under-race lubrication system used in turbofan engines for ball and cylindrical roller bearings is shown in fig. 10. Lubricant is directed under the inner race and centrifugally forced out through a plurality of holes in the race to cool and lubricate the bearing. Some lubricant may pass completely under the bearing for cooling only as shown in fig. 10(a). Lubricant supply holes are usually provided for the cage-land and the roller-flange contacts (fig. 11).

Proper "Bearing Thermal Management" is a requirement for successful high-speed bearing operation. This can be further achieved by outer-race cooling with under-race lubrication (fig. 12). By control of lubricant flow to the outer- and inner-races internal clearances of the bearing are maintained and controlled over a range of loads and operating speeds to 3 million DN (fig. 12(a)). For the tapered-roller bearing (fig. 12(b)), by supplying lubricant to the cone-rib/cage contact as well as the cone-rib/roller-end, contact speeds of 2.4 million DN can be reached.

## LUBRICANT SELECTION

The criteria for a liquid lubricant to function in a rolling-element bearing are that (a) it be thermally and oxidatively stable at the maximum bearing operating temperature, and (b) it form an elastohydrodynamic (EHD) film between the rolling surfaces. The EHD film, which is generally dependent on lubricant base stock and viscosity, is 5 to 100 $\mu$in thick at high temperatures. When a sufficiently thick EHD film is present, rolling-element bearings will not usually fail from surface distress. Instead, they fail from rolling-element fatigue which usually manifests itself, in the early stages, as a shallow spall with a diameter about the same as the contact width.

A requirement for long-term high-temperature bearing operation is that the EHD film thickness, h, divided by the composite surface roughness, $(\sigma_1^2 + \sigma_2^2)^{1/2}$, equal 1-1/2 or greater, where $\sigma_1$ and $\sigma_2$ are the surface finishes of the raceway and rolling elements, respectively. The EHD film thickness is a function of several lubricant and bearing operating variables. However, as a general rule, the minimum viscosity required of a lubricant is 1 cSt at operating temperature. This same research indicated that the ester based lubricants (table 2) meeting the MIL-L-23699 specification could provide the necessary lubrication requirements to 425 °F in an air environment. While other base stock lubricants could give satisfactory operation to 600 °F, they were precluded from further consideration because of their cost and/or commercial availability. Further, at temperatures above approximately 450 °F a low oxygen environment would be required to minimize lubricant oxidation for most lubricant types.

## CONCLUSION

The speed capability of rolling-element bearings has increased from speeds of less than 2 million DN to speeds of 3 million DN. The life and reliability of these bearings have also increased where they are equal to, or greater than,

those of bearings with limited speed capability. However, high-speed bearings are not "off-the-shelf" bearings which can be readily ordered from a manufacturer's catalog. Design parameters must be carefully chosen and optimized based upon sophisticated bearing computer programs. Material and lubricant selection must be integrated into the bearing design. Bearing thermal management must be implemented through proper lubrication and cooling.

## BIBLIOGRAPHY

Bamberger, E.N., Averbach, B.E., and Pearson, P.K., Improved Fracture Toughness Bearings, AFWAL-TR-84-2103, Jan. 1985.

Bamberger, E.N., Zaretsky, E.V., and Signer, H., Endurance and Failure Characteristic of Main-Shaft Jet Engine Bearing at $3 \times 10^6$ DN, J. Lubr. Technol., Vol. 98, No. 4, Oct. 1976, pp. 580-585.

Bamberger, E.N. et al., Life Adjustment Factors for Ball and Roller Bearings - An Engineering Design Guide, ASME, N.Y., 1971.

Fischer, G.K., ed., Advanced Power Transmission Technology, NASA CP-2210, 1983, pp. 193-269.

Greby, D.F., What Turbine Technology is Teaching us About High-Speed Roller Bearings, Mach. Des., Vol. 42, No. 11, Apr. 20, 1970, pp. 229-234.

Hamrock, B.J., and Anderson, W.J., Rolling-Element Bearings, NASA RP-1105, 1983.

Harris, T.A., Rolling Bearing Analysis, 2nd ed., John Wiley & Sons, N.Y., 1984.

Parker, R.J., Pinel, S.I., and Signer, H.R., Performance of Computer-Optimized Tapered-Roller Bearings to 2.4 Million DN, J. Lubr. Technol., Vol. 103, No. 1, Jan. 1981, pp. 13-20.

Schuller, F.T., Operating Characteristics of a Three-Piece-Inner-Ring Large-Bore Roller Bearing to Speeds of 3 Million DN, NASA TP-2355, 1984.

Zaretsky, E.V., Schuller, F.T., and Coe, H.H., Lubrication and Performance of High-Speed Rolling-Element Bearings, ASLE Preprint 85-AM-3F-2, May 1985.

TABLE 1. - COMPUTER OMTIMIZED DESIGN FOR
HIGH-SPEED TAPERED-ROLLER BEARING

| | |
|---|---|
| Cup half angle . . . . . . . . . . . . . | 15°53' |
| Roller half angle . . . . . . . . . . | 1°35' |
| Roller large end diameter, mm (in) . . | 18.29 |
| | (0.720) |
| Number of rollers . . . . . . . . . . | 23 |
| Total roller length, mm (in) . . . . . | 34.18 |
| | (1.3456) |
| Pitch diameter, mm (in) . . . . . . . | 155.1 |
| | (6.105) |
| Bearing outside diameter, mm (in) . . | 190.5 |
| | (7.500) |
| Roller crown radius, mm (in) . . . . | $25.4 \times 10^3$ |
| | (1000) |
| Roller spherical end radius, percent of apex length . . . . . . . . | 80 |

TABLE 2. - PROPERTIES OF TETRAESTER LUBRICANT

| | |
|---|---|
| Additives . . . . . . . . . . . . . | Antiwear, oxidation inhibitor, antifoam |
| Kinematic viscosity, cS, at: | |
|   311 K (100 °F) . . . . . . . . . . . . . . . . | 28.5 |
|   372 K (210 °F) . . . . . . . . . . . . . . . . | 5.22 |
|   477 K (400 °F) . . . . . . . . . . . . . . . . | 1.31 |
| Flash point, K (°F) . . . . . . . . . . . . | 533 (500) |
| Autoignition temperature, K (°F) . . . . . | 694 (800) |
| Pour point, K (°F) . . . . . . . . . . . . | 214 (-75) |
| Volatility (6.5 h at 477 K (400 °F)), wt % . . . . . . . . . . . . . . . . | 3.2 |
| Specific heat at 477 K (400 °F), J/(kg)(K)(Btu/(lb)(°F)) . . . . . . . | 2340 (0.54) |
| Thermal conductivity at 477 K (400 °F), J/(m)(s)(K) (Btu/(h)(ft)(°F) . . . . . . . . . . . | 0.13 (0.075) |
| Specific gravity at 477 K (400 °F) . . . . . . | 0.850 |
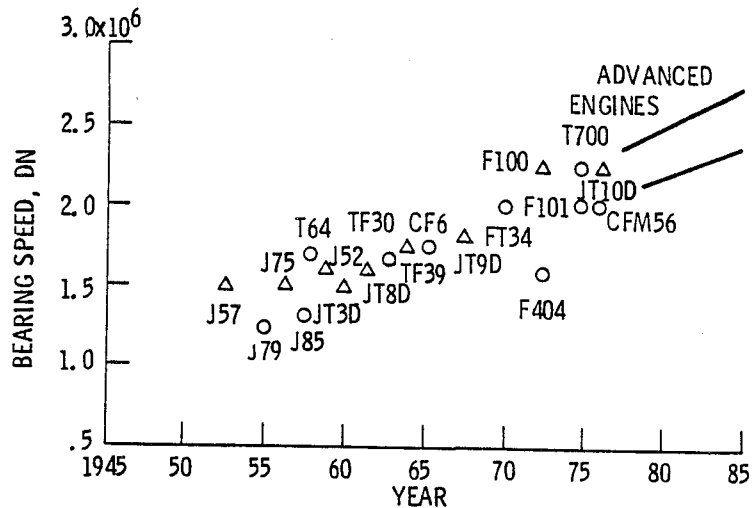
Figure 1. - Increased engine speeds required higher bearing speeds.
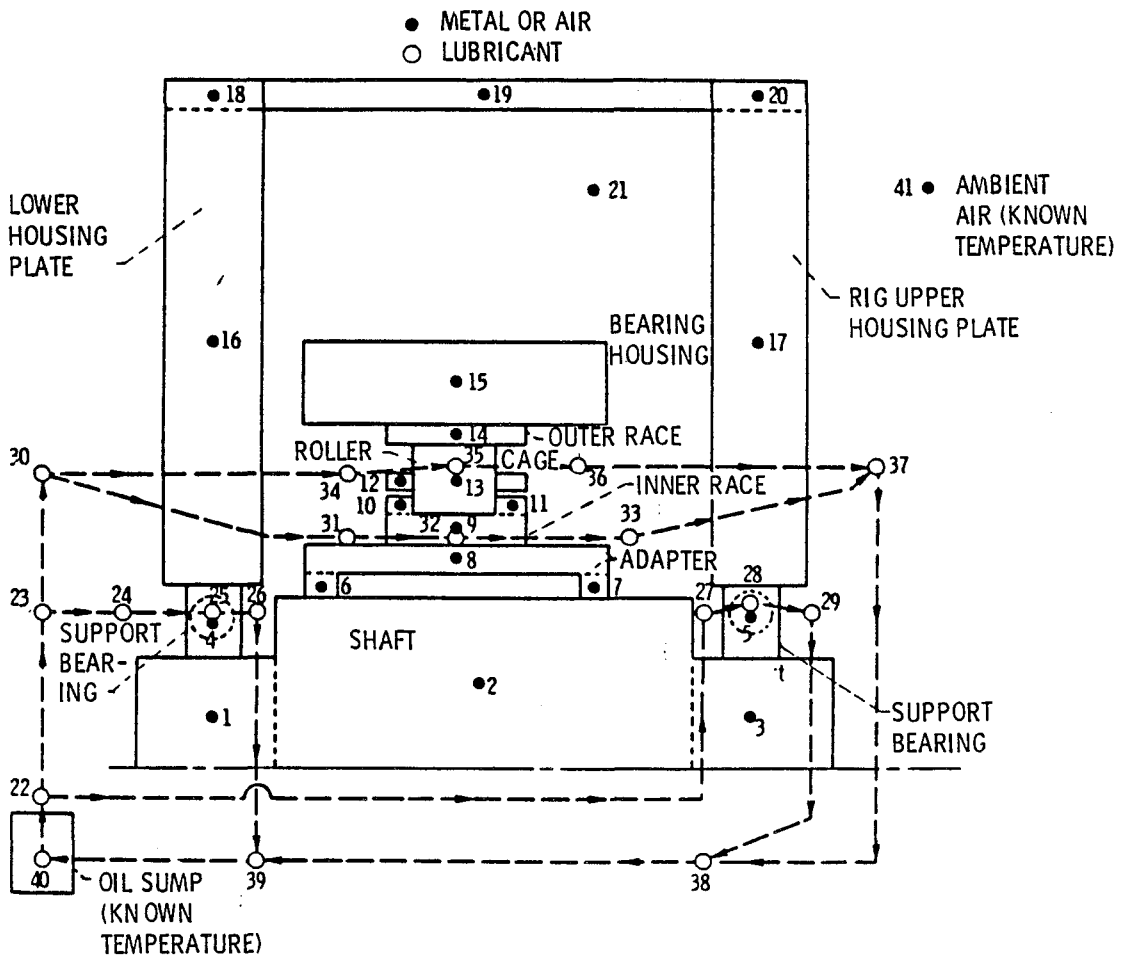


Figure 2. - Nodal system used for thermal routines in Cybean.

94

(a) Free-contact
angle (no load).

(b) Contact angle
when under load.

(c) Contact angles
when under load
and at high speed.
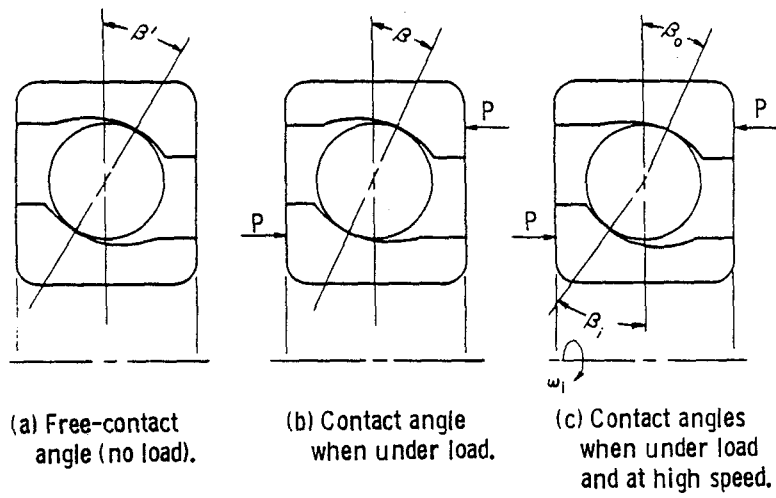
Figure 3. - Changes in contact angle with load and speed.



(a) Radial load.

(b) Radial load and two-point preload.
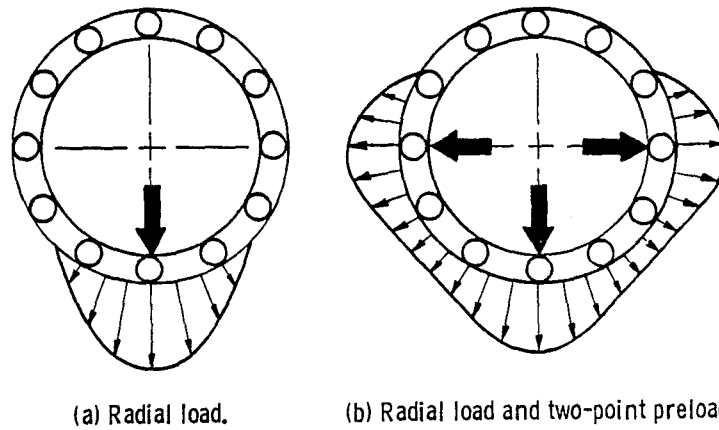
Figure 4. - Roller bearing load distribution for simple radial load and
with two-point preload.
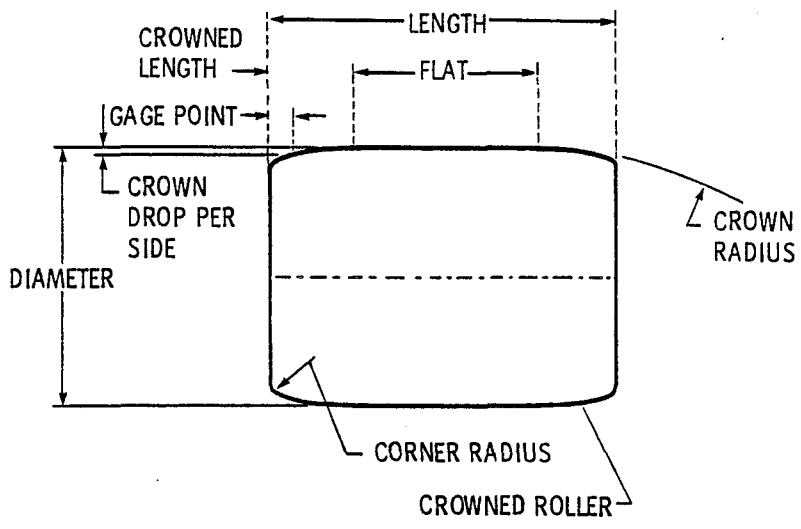
Figure 5. - Crowned roller for high-speed roller bearing application.
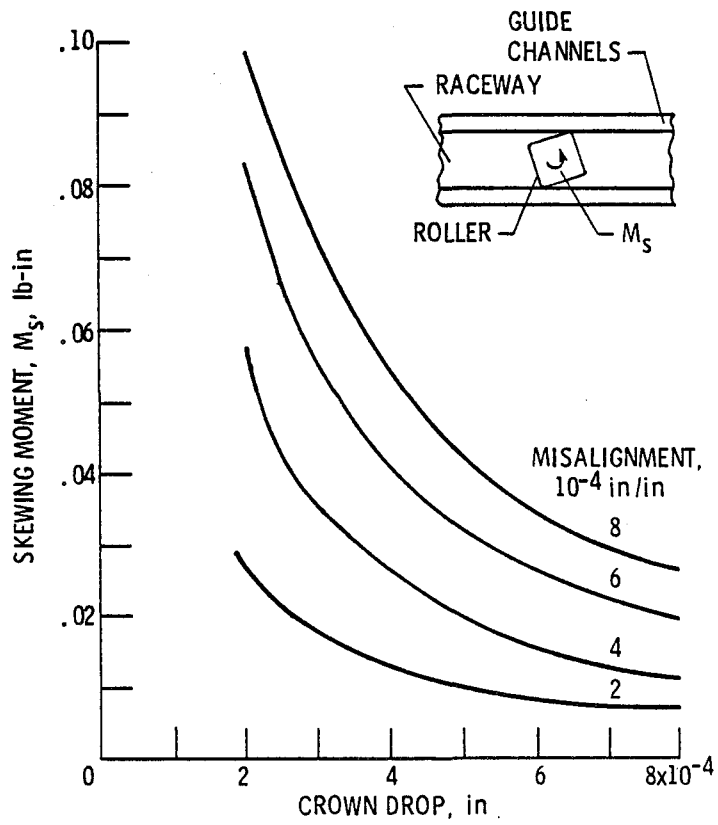


Figure 6. - Effect of crown drop on skewing moment for various amounts of misalignment.

96
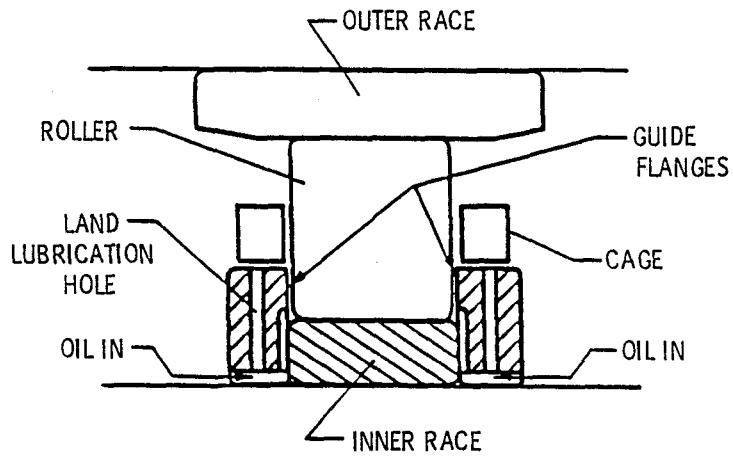
Figure 7. - Three piece inner-race roller bearing.
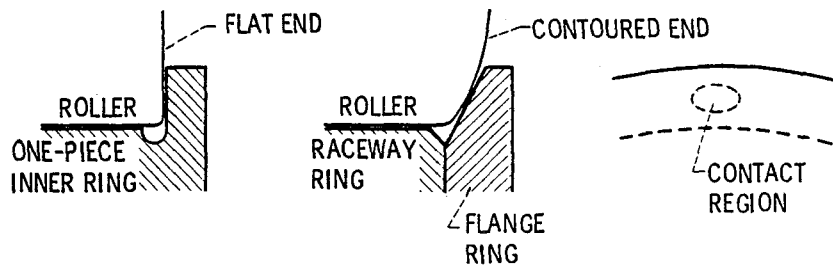


(a) Conventional,
one-piece
inner race

(b) Modified configuration, three-piece inner
race.

Figure 8. - Roller end-contact geometry of one- and three-piece inner-race
bearing.
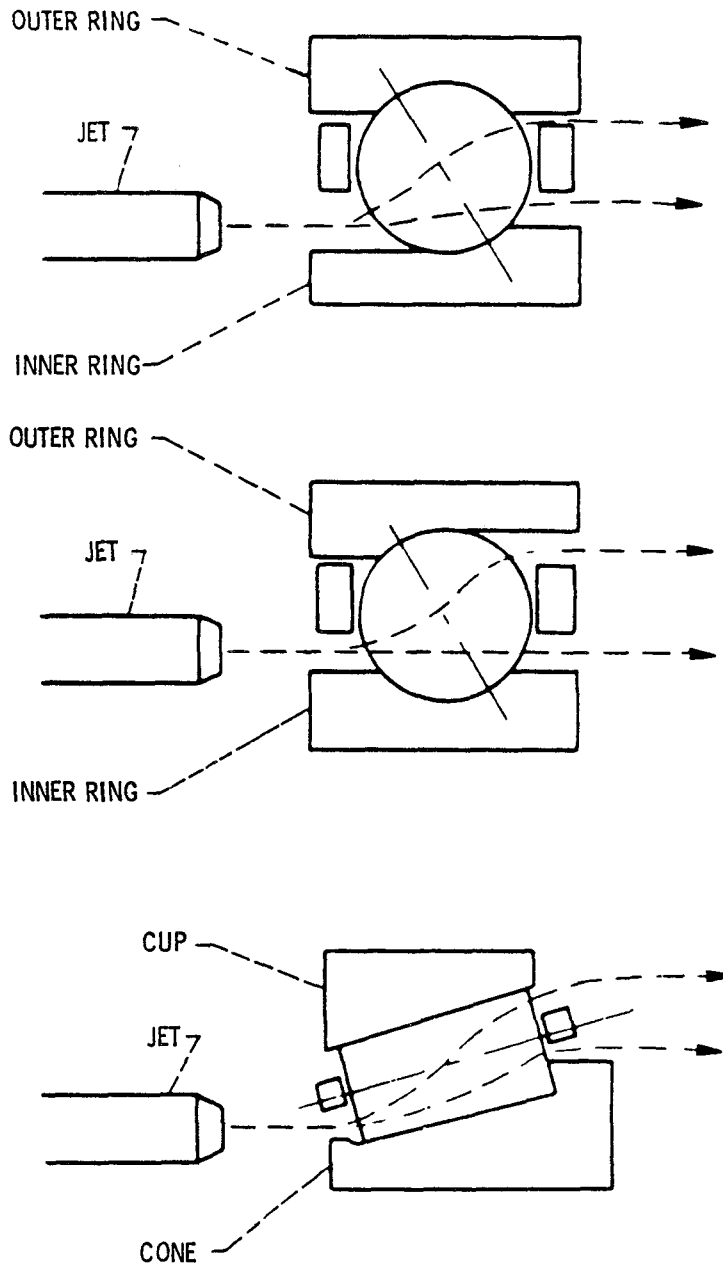
Figure 9. - Placement of jets for ball bearings with relieved
rings and tapered-roller bearings.
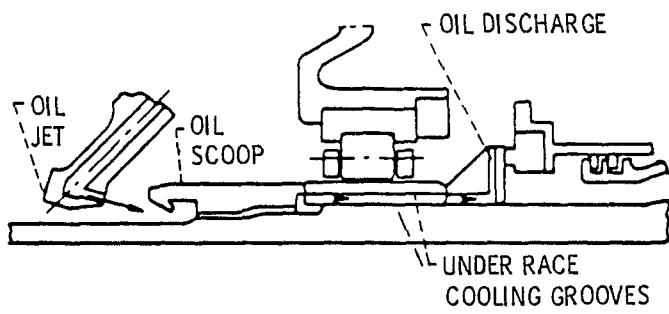
(a) Cylindrical roller bearing.
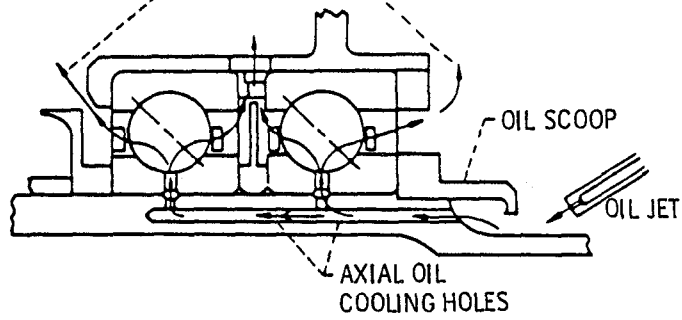
(b) Ball thrust bearing.

Figure 10. - Under-race lubrication system for main shaft bearings on turbofan engine.
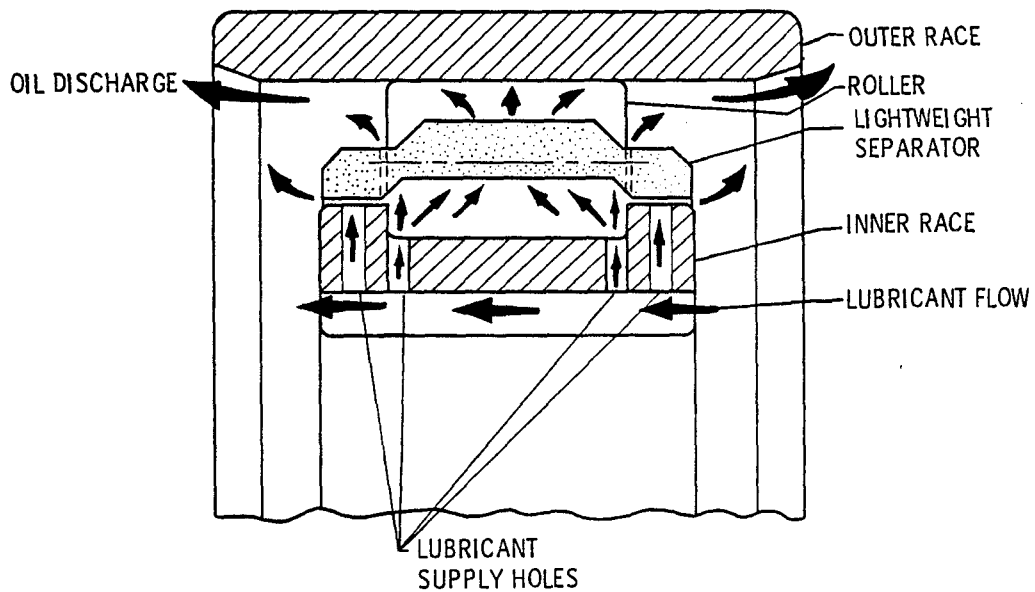


Figure 11. - High-speed roller bearing with under-race lubrication and cooling.

99
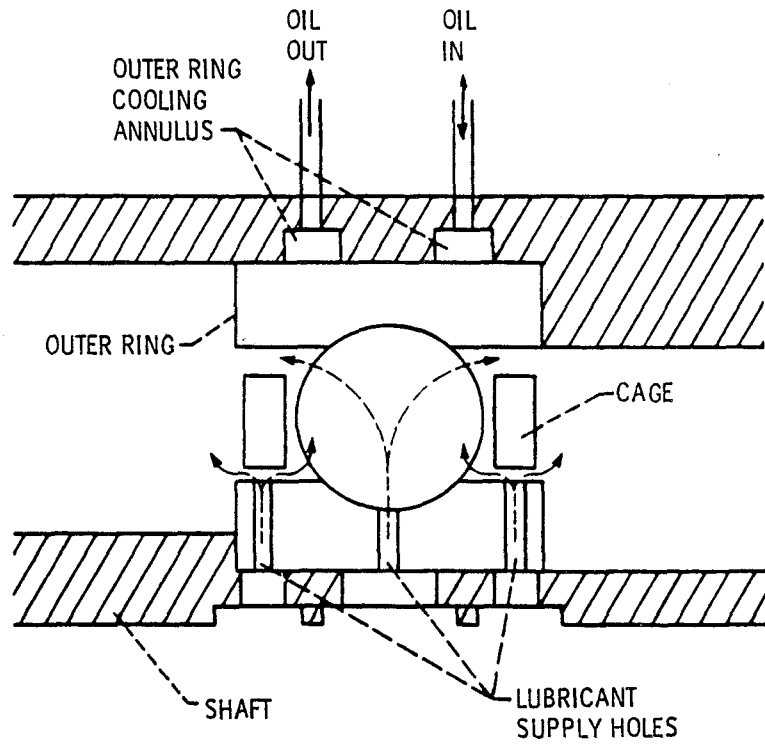
(a) Angular-contact ball bearing.
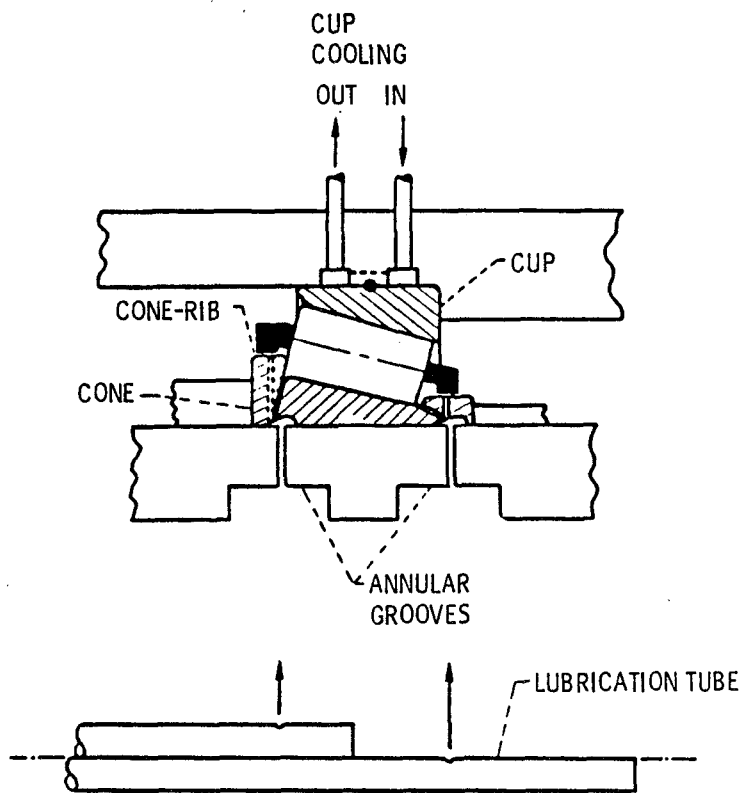


(b) Computer optimized tapered-roller bearing.

Figure 12. - Outer-race cooling with under-race lubrication for high-speed bearings.

100

# LUBRICATION AND COOLING FOR HIGH SPEED GEARS*

Dennis P. Townsend
National Aeronautics and Space Administration
Lewis Research Center
Cleveland, Ohio 44135

The problems and failures occurring with the operation of high speed gears are discussed. The gearing losses associated with high speed gearing such as tooth mesh friction, bearing friction, churning, and windage are discussed with various ways shown to help reduce these losses and thereby improve efficiency.

Several different methods of oil jet lubrication for high speed gearing are given such as into mesh, out of mesh, and radial jet lubrication. The experiments and analytical results for the various methods of oil jet lubrication are shown with the strengths and weaknesses of each method discussed.

The analytical and experimental results of gear lubrication and cooling at various test conditions are presented. These results show the very definite need of improved methods of gear cooling at high speed and high load conditions.

## INTRODUCTION

There are many applications where gears must operate at high speeds >50 m/s (10 000 fpm) and sometimes at high tooth loading. Some of these applications include turbine powered ship propulsion, surface effect ships, turbo-prop, V/STOL aircraft, and geared turbofans. There is very little information available on lubrication and cooling methods, or methods to determine the power losses and lubrication requirements for gears operating at these high power conditions. Many high speed gear sets today are operating at load conditions below those that could be obtained with better cooling methods. Also many gear boxes could operate at better efficiencies with improved lubrication and cooling methods.

There are several methods used for lubrication and cooling gears. Some of these methods include splash lubrication, drip feed, grease, oil mist, and low or moderate pressurized oil jet flow. Some gear boxes are operated with a given lubrication method such as low pressure oil jets with into mesh and/or out of mesh simply because it has worked in the past and no effort has been made to improve the system for better efficiency or higher power rating.

For gears operating at low speeds and low loads the lubrication method is not critical since very little heat is generated. Under these conditions the gears require lubrication but very little cooling. When the heat input to the gear teeth is increased by high speed and high power conditions then the majority of the lubricant must be used for cooling the gear teeth. When inadequate cooling is supplied to the gear teeth several things may happen. The gear teeth can suffer what is called micropitting or grey staining (fig. 1, ref. 1) which is caused by insufficient oil film between the teeth. The gears can have early fatigue spalls (fig. 2, ref. 2) resulting from reduced hardness caused by

a temperature rise of the gear teeth above the gear tempering temperature. The gears can fail by scoring (fig. 3, ref. 3) as a result of a loss of the elasto-hydrodynamic EHD or extreme pressure EP boundary film. The gears can also fail by tooth breakage as a result of reduced strength when the teeth are overheated and lose their hardness. The objective of the work reported herein is to show the gear designer the various lubrication methods that are used in gearing and what can be expected with each method, and to provide the gear designer with methods to reduce gear losses and thereby reduce heating and improve efficiency.

## NOMENCLATURE

$A$     bearing area, $cm^2$ ($in^2$)

$a$     addendum, mm (in)

$B$     backlash, mm (in)

$c_p$     specific heat, cal/g °C (Btu/lb °F)

$c_s$     basic static capacity, N (lb)

$D$     root diameter, mm (in)

$d$     gear diameter, mm (in)

$d_i$     impingement depth, mm (in)

$d_m$     bearing mean diameter, mm (in)

$F$     face width, mm (in)

$F_a$     bearing axial load, N (lb)

$F_\beta$     bearing load, N (lb)

$F_r$     bearing radial load, N (lb)

$F_s$     static equivalent load, N (lb)

$f_0$     friction factor viscosity

$f_1$     friction factor load

$h_1$     bearing clearance, mm (in)

$L_p$     distance from impingement point to center line of gears, mm (in)

$M$     tooth module, mm

$M_b$     bearing friction torque, N-m (lb-in)

$M_1$     bearing load friction torque, N-m (lb-in)

$M_v$     bearing viscous friction torque, N-m (lb-in)

$m_g$     gear ratio

N     speed, rpm

P     power loss, kW

$P_d$     diametrial pitch, 1/in

$\Delta P$     oil jet pressure, N/cm (lb-in)

Q     heat loss, cal/min (Btu/min)

R     pitch radius, mm (in)

r     radius to oil jet impingement, mm (in)

$r_0$     gear outside radius, mm (in)

$S_i$     oil jet offset, mm (in)

$\Delta T$     oil temperature rise, °C (°F)

V     velocity, mm/sec (in/sec)

$V_g$     gear pitch line velocity, m/sec (ft/sec)

$V_j$     oil jet velocity, m/sec (ft/sec)

w     oil flow, g/min (lb/in)

Greek symbols

$\alpha$     bearing contact angle, degrees

$\beta$     oil jet angle, radians

$\gamma$     nondimensional impingement depth = di/whole depth

$\theta_w$     gear rotation angle for oil jet in tooth space, radians

$\lambda$     gearbox space function 1=free space, 0.6-0.7 for large enclosure, 0.5-0.6

       for fitted gear case

$\mu$     viscosity, reyns

$v_0$     lubricant viscosity, centistokes

$\phi$     oil mixture function 1.0=oil free atmosphere

$\phi_g$     gear pressure angle, radians

$\omega_g$     gear rotational speed, radians/sec

There are four main areas of losses in high speed gears. These losses can be controlled for the most part by careful design and construction. The losses consist of bearing losses, tooth friction losses, oil churning losses, and gear windage losses. Bearing losses may account for about half of the losses particularly when fluid film bearings are used. However, when long life is a requirement, the fluid film bearing is the best choice. An approximate method for the friction torque in a fluid film bearing is shown in the following equation from reference 4.

$$M_b = \mu A r V / h \tag{1}$$

Rolling contact bearings have considerably less friction loss when properly lubricated and will generally have a much shorter life than a fluid film bearing. However, rolling element bearings should have sufficient life for many applications. The friction torque for rolling element bearings may be estimated by the following equations from reference 5.

$$M_b = M_1 + M_v$$

The friction torque due to the applied load is

$$F_\beta = 0.9 \, F_a \cot \alpha - 0.1 \, F_r \quad \text{or} \quad F_\beta = F_r \text{ if larger}$$

$$M_1 = f_1 F_\beta d_m \tag{2}$$

where $f_1 = z \, \dfrac{F_s}{C_s}^y$ , $z = 0.001$, $y = 0.33$

for 30 angle contact bearings and $f_1 = 0.0003$ for roller bearings. The viscous friction torque may be estimated by

$$M_v = 1.42 \times 10^{-5} \, f_0 (v_0 N)^{2/3} \, d_m{}^3$$

$$\tag{3}$$

$$M_v = 3.492 \times 10^{-3} \, f_0 \, d_m{}^3 \qquad v_0 N \le 2000$$

for ball bearings $f_0$ values range from 3 to 4. Bearing computer programs have been developed that give more accurate results for bearing torque, (refs. 6 and 7).

The tooth friction loss is probably the lowest loss in the gear system when the gears are adequately lubricated. There is very little that can be done to reduce gear tooth friction loss once adequate lubrication has been provided. Some lubricants will have a little less friction loss than others. Some gears will have more or less tooth friction loss because of the type of design mainly because of the different sliding conditions. For instance, high contact ratio spur gears generally have more sliding and, hence, more losses than standard contact ratio gears. However, since this is a small part of the overall loss, it generally has little effect on the total loss.

Windage losses can account for a large part of the total gear box losses in high speed gears because of the high pitch line velocities. Some of this windage lose can be reduced by careful designs. For instance, it was shown in reference 8 that axial holes in a gear web can significantly increase the windage losses. Also it was shown that placing a shield on the ends of the gear teeth, to prevent the air circulating into the teeth, reduced the windage losses by a large percentage. The windage losses in a gear box with the smooth sides of the box located approximately 1 in from the gear and the inside diameter 0.6 in from the teeth, reduced the windage loss to approximately one-half that for open gears. The pumping loss of the air at the entrance of the mesh accounts for some losses and can be reduced by reducing the pressure in the gear box which also reduces other windage losses. An equation for approximating the windage loss in gears was given in reference 8 as shown in the following equation.

$$P = N^{2.9}(\overset{\text{Sides}}{0.16\ D^{3.9}} + \overset{\text{Periphery}}{D^{2.9}\ F^{0.75}\ M^{1.15}}) \times 10^{-20}\ . \quad \Phi.\lambda \tag{4}$$

Churning losses are caused by the gear striking, pumping, or otherwise moving the lubricant around in the gear box. It is very important in high speed gear boxes to get the lubricant to perform its lubrication and cooling function and then get it out of the way. Shrouds are sometimes used in gear boxes to direct the lubricant oil away from the gears. If too much lubricant is allowed to enter the gear mesh, excessive losses will occur from oil being trapped in the gear teeth and being pumped out of the mesh in the axial direction. In spur gear application this is more critical than helical gears. This is one reason why most gear designers prefer helical gears for high speed gearing. Even with helical gearing, however considerable power loss occurs with too much oil getting into the gear mesh. Some spur gear designs have a groove in the center of the axial length of the gear to reduce pumping losses in the mesh. This is also done in some very wide helical gear applications.

## LUBRICATION AND COOLING METHODS

There are many high to moderately loaded high speed gears operating today with oil jet lubrication using 30 to 50 psig oil pressure to lubricate the gears. This type of low pressure system does not do a good job of cooling the gears in a high speed gear drive and will only allow the gears to operate at a moderate load. In a low pressure oil jet system the oil jet can only penetrate a small distance into the tooth space. This results in cooling of the tips of the gear teeth only. This causes the gear tooth temperature to be higher than that obtained with a better system, such as high pressure radial oil jet. Figure 4(a) is a calculated temperature profile of a gear tooth cooled with low pressure operating at a moderate speed and high load reference 9. When the speed is increased at this load condition and low pressure lubrication, failure of the gears will generally occur. Figure 4(b) shows how the gear tooth temperatures are reduced when the oil jet pressure is increased to obtain good impingement depth.

## OUT OF MESH JET LUBRICATION

A large number of gears are lubricated with low pressure oil jets into mesh or out of mesh or both. In the out of mesh lubrication method the oil

jet has a very modest impingement depth. This is illustrated in figure 5 which shows the analytical results for impingement depth on the pinion using the following equation from reference 10.

$$d_i = r_o - \sqrt{r^2 + L_\beta^2} \tag{5}$$

Figure 6 is a high speed photograph of an oil jet at the out of mesh condition. In order to get the maximum impingement depth for the out of mesh condition care must be exercised to get the proper oil jet location. The analysis indicates that the pinion can be completely missed by a very small change in offset distance from the intersection of the outside diameter of the gear and pinion or from a small change in the jet angle. For maximum impingement depth in most cases the oil jet should be directed at the intersection of the two outside diameters at an angle that will intersect the pitch point of the gear and pinion (ref. 10). For large gear ratios it is probably better to favor the pinion to get a better cooling balance. Reference 11 gives an analytical method for out of mesh jet lubrication for gears with modified center distance and/or addendums. Reference 11 also gives the impingement depth results for various oil jet offsets and oil jet angles. Figure 7 shows the analytical results for the out of mesh jet lubrication for various oil jet angles.

## INTO MESH JET LUBRICATION

Into mesh oil jet lubrication is often used as a means of getting oil to the gear tooth surfaces at a good impingement depth when the oil system is operating at a low pressure. This method is effective because it uses the gear tooth velocity moving with the oil jet velocity as shown in figure 8. References 12 and 13 give equations for the oil jet impingement depth for into mesh lubrication. When the jet velocity is less than the gear velocity, the oil impinges on the backside of the teeth as shown in figure 9. When the jet velocity is greater than the gear velocity, the oil will impinge on the front of the gear tooth. This is shown in figure 8. The optimum impingement depth for into mesh lubrication was shown in references 12 and 13 to occur when the oil jet velocity and gear velocity are equal. The equation for oil jet impingement depth at the opimum velocity is given by the following equation.

$$d_i = 1/P_d = a \qquad V_j = \omega_g \, R \sec \beta \tag{6}$$

When into mesh lubrication is used with high speed gears care must be taken to avoid excessive oil being trapped in the gear teeth. This trapping can cause various problems such as loss of efficiencies, high loads on the teeth, high noise, and even gear failure under some conditions. In many cases the bulk of the cooling oil is supplied to the out of mesh location with only a small percentage for lubrication supplied to the into mesh position reference 14. However, there is usually sufficient oil film remaining on the gear tooth for good lubrication when adequate cooling is provided at the out of mesh location. In some cases where it is difficult to keep the oil out of the into-mesh zone, a circumferential groove will be cut into the center of one of the gears to break up the length of the teeth; thereby, reducing the trapping losses. This groove reduces the axial length required to pump the oil by at least one-half.

When the oil jet is directed radially inward the best impingement depth is obtained. Since gear tooth cooling is a maximum when the oil jet impinges on the face of the tooth, the radial oil jet offers the best method of gear lubrication and cooling. Figure 10 is a high speed photograph of the radial directed oil jet and shows the oil jet penetrating the tooth space just before impingement on the gear tooth flank. The oil pressure here is sufficient to allow the oil jet to impinge on the gear tooth a little more than half way down the working depth of the gear tooth. The maximum cooling is obtained when the oil pressure is sufficient to cause the oil jet to reach an impingement depth equal to the full working depth of the tooth. However adequate cooling can often be obtained with impingement depth just below the pitch line. When radial jet lubrication is used the oil jet should be located near the out of mesh position with the jet directed radially at the center of the gear and pinion. In a speed reducer the pinion will receive cooling on the loaded side of the tooth while the gear will be cooled on the backface of the tooth. When the gear set is a speed increaser, the pinion will receive cooling on the backface of the tooth and the gear on the loaded side. Experiments have shown (ref. 9) that good cooling of the gear or pinion can be obtained when either the loaded flank or unloaded flank of the gear tooth is cooled. Figure 11 shows the effect of oil jet pressure and load on gear tooth temperature using radial oil jet cooling on the back flank of the gear tooth. The temperature was measured on the loaded flank of the gear tooth. This figure very clearly shows that good cooling is obtained when cooling the back flank of the tooth.

The following equations from references 9 and 15 gives the impingement depth on the tooth flank for various speeds and oil jet pressures for a radial directed oil jet.

$$d_1 = \frac{1.5708 + 2\tan\phi + B/2}{P_d \dfrac{N_d}{2977 \ \Delta p} + \tan\phi} \tag{7}$$

The vectorial model used to calculate the radial impingement depth is shown in figure 12. The analysis and experimental results for a radial directed oil jet are shown in figure 13. When the impingement depth for a given gear operating condition is known or desired then the pressure required to obtain that impingement depth is given by the following equation.

$$\Delta p = \frac{d_1 \ P_d \ N_d}{2977 \ \frac{\pi}{2} + \frac{B}{2} + (2 - d_1 P_d)\tan\phi}^2 \tag{8}$$

When the oil jet velocity equals the gear velocity the oil jet will usually impinge to a depth approximately equal to the full working depth and provide very good cooling for the gear teeth. For standard gear tooth geometry the pressure required to obtain this velocity may be approximated by the following equation where V is the m/sec (ft/sec) and $\Delta p$ is in $N/cm^2$ (psi)

$$\Delta p = V_g^2/169 \quad \text{English}$$

$$\Delta p = V_g^2/22.8 \quad \text{Metric} \tag{9}$$

Using the above equation for gear operating at a pitch line velocity of 150 m/s (500 ft/s) the oil jet pressure required for full depth impingement would be approximately 1014 N/cm² (1480 psi). This pressure is much higher than the oil jet pressure used in most high speed gear boxes operating at 150 to 300 m/s (500 to 1000 ft/s). These gear boxes must operate at reduced loads because for the limited cooling available. It should be understood that the oil jet size must be reduced at these high pressures to limit the oil flow to that required for good cooling. Using the minimum orifice size of 1.02 mm (0.04 in) specified by many gear designs would give an oil flow of approximately 1.3 gpm per orifice which may be too much oil for most applications. However if the orifice size is reduced to 0.5 mm (0.02 in) then the oil flow is only 0.33 gpm or 1/4 of that for the larger orifice. In order to limit orifice plugging the oil should be filtered through a 5 or 10 μm filter. It is much better for both the gears and bearings to filter the oil through a 5 μm or better filter. The finer filteration will also improve the gear and bearing life.

## COOLING REQUIREMENTS

This amount of lubricating fluid required for cooling of gears and bearings may be determined by estimating the power loss for gears, bearings etc., and then using an appropriate temperature rise in the oil, the required oil flow can be determined. The following equation can be used to determine the oil flow in a given gear system. Assume 2000 hp is transmitted in a gear set with one mesh and two sets of bearings. The losses per mesh in a well designed spur or helical gearbox should be no more than 0.5 percent with the losses equally divided between the gears and bearings. The oil therefore must absorb 0.005 x 2000 or 10 hp, which is 424.4 Btu/min. Assuming a 50 °F temperature rise, the total oil flow required would be,

$$w = Q/c_p \Delta T = 424.4/0.6 \times 50 = 14.2 \text{ lb/min}$$

(10) with equal flow to the gears and bearings of 7.1 lb/min. If the gear set is less efficient than the above then more oil flow would be required.

## SUMMARY AND CONCLUSIONS

There are several types of losses in gearbox systems that should be evaluated in a high speed gear design. These losses include the gear tooth sliding and friction, the windage of the air flowing around the gears, the churning losses of the oil being pumped or accelerated by the gears and the bearing losses of rolling element or fluid film bearings. Good design practices can reduce the effect of these losses.

The gears may be lubricated by one or more of several methods. For high speed gears the pressure oil jet is definitely required to provide good cooling. Oil jets may be directed into mesh, out of mesh, or in a radial direction at various oil jet pressures. However, for the maximum cooling and lubrication of the gear set the oil jet should be directed radially at the gear and pinion near the out of mesh position. This will provide good cooling and lubrication

an keep the oil from entering into mesh zone where excessive losses may occur.
The conclusions may be summarized as follows.

(1) Gearbox efficiency for high speed gearing can be improved by careful attention to reducing windage and churning losses.

(2) The best method for lubrication and cooling of high speed gearing is a high pressure oil jet at the out of mesh position directed radially at the gear and pinion with sufficient velocity or pressure to impinge on the tooth flank well below the pitch line.

(3) When the above conditions are performed, high speed gears can operate at considerable higher power levels than the majority of high speed gearboxes are operating at today.

## REFERENCES

1. Dudley, Darle W.: Characteristics of Regimes of Gear Lubrication. International Symposium on Gearing and Power Transmissions, Aug. 30-Sept. 3, 1981, Tokyo, Japan, vol. 1, pp. 319-324.

2. Townsend, Dennis P.: The Application of Elastohydrodynamic Lubrication in Gear Tooth Contacts. NASA TM-X-68142, 1972.

3. Townsend, Dennis P.; Baber, Berl B.; and Nagy, Andrew: Evaluation of High Contact Ratio Spur Gears With Profile Modification, NASA TP-1458, 1979.

4. Fuller, Dudley, D.: Theory and Practice of Lubrication for Engineers. Wiley, 1965.

5. Harris, Tedric A.: Rolling Bearing Analysis. Wiley, 1966.

6. Pirvics, Juris; and Klechner, Robert J.: Predication of Ball and Roller Bearing Thermal and Kinematic Performance by Computer Analysis. Advanced Power Transmission Technology, NASA CP-2210, G.K. Fischer, ed., 1983, pp. 185-201.

7. Coe, Harold H.: Predicted and Experimental Performance of Large-Bore High-Speed Ball and Roller Bearings. Advanced Power Transmission Technology, NASA CP-2210, G.K. Fischer, ed., 1983, pp. 203-220.

8. Dawson, F.H.: Windage Loss in Large High-Speed Gears. Proceedings of the Institution of Mechanical Engineers, Part A - Power and Process Engineering, vol. 198A, no. 1, 1984, pp. 51-59.

9. Townsend. D.; and Akin. L.: Analytical and Experimental Spur Gear Tooth Temperature as Affected by Operating Variables. J. Mech. Des., vol. 103, no. 1, Jan. 1981, pp. 219-226.

10. Townsend, D.P.; and Akin, L.S.: Study of Lubricant Jet Flow Phenomena in Spur Gears - Out of Mesh Condition. J. Mech. Des., vol. 100, no. 1., Jan. 1978, pp. 61-68.

11. Akin, L.S.; and Townsend, D.P.: Lubrication Jet Flow Phenomena in Spur and Helical Gears with Modified Center Distances and/or Addendums. For Out-of-Mesh Conditions. Journal of Mechanisms, Transmissions, and Automation in Design, vol. 107 no. 1, Mar. 1985, pp. 24-30.

12. Akin, L.S.; and Townsend, D.P.: Into Mesh Lubrication of Spur Gears with Arbitrary Offset Oil Jet. Part I - For Jet Velocity Less Than or Equal To Gear Velocity. Journal of Mechanisms, Transmissions and Automation in Design, vol. 105, no. 4., Dec. 1983, pp. 713-178.

13. Akin. L.S.; and Townsend, D.P.: "Into Mesh Lubrication of Spur Gears with Arbitrary Offset Oil Jet. Part II - For Jet Velocities Equal to or Greater Than Gear Velocity. Jounral of Mechanisms, Transmissions and Automation in Design, vol. 105, no. 4., Dec. 1983, pp. 719-724.

14. Tucker, A.I.: Bevel Gears at 203 m/s (40,000 FPM). ASME Paper 77-DET-178, Sept. 1977.

15. Akin. L.S.; Townsend, D.P., and Mross, J.J.: Study of Lubricant Jet Flow Phenomena in Spur Gears. J. Lubr. Technol., vol. 97, no. 2, Apr. 1975, pp. 283-288.
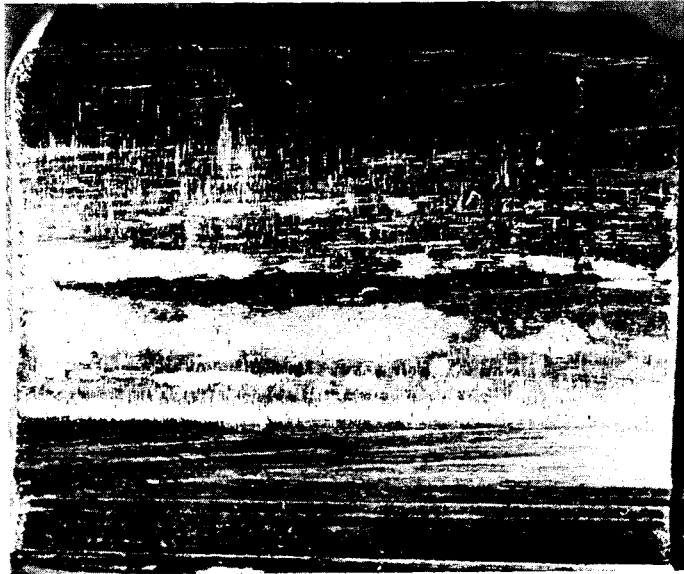
(a) Spur, 60 HRC.
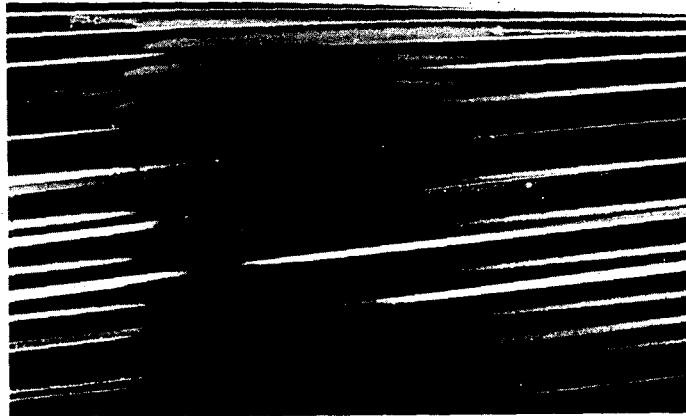


(b) Helical, 60 HRC.

Figure 1. - Examples of micro pitting.
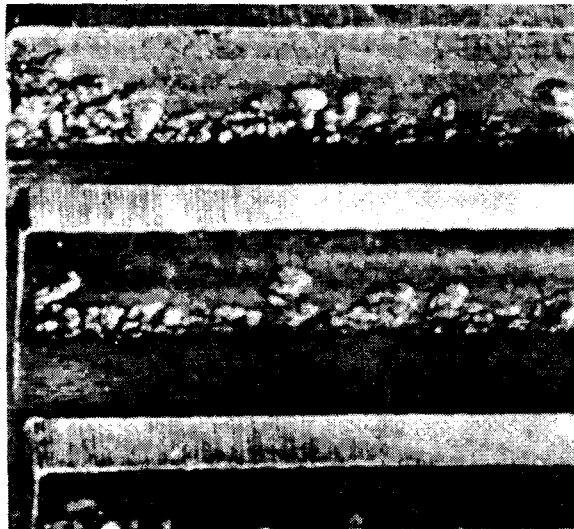
Figure 2. - Destructive pitting: Heavy pitting has taken place, predominantly in the dedendum region (ref. 2).
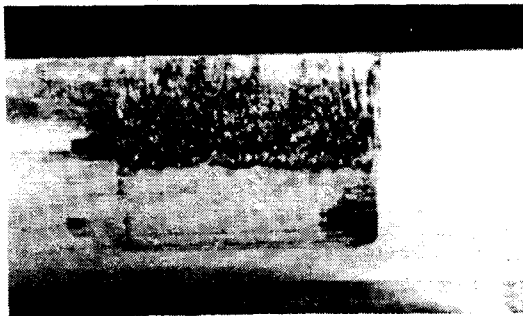


(a) Standard gear.
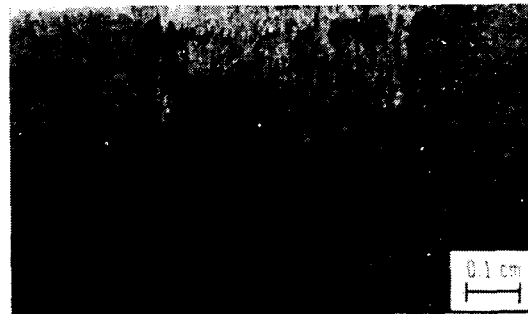


(b) New-tooth-form gear.

Figure 3. - Typical scoring failures.
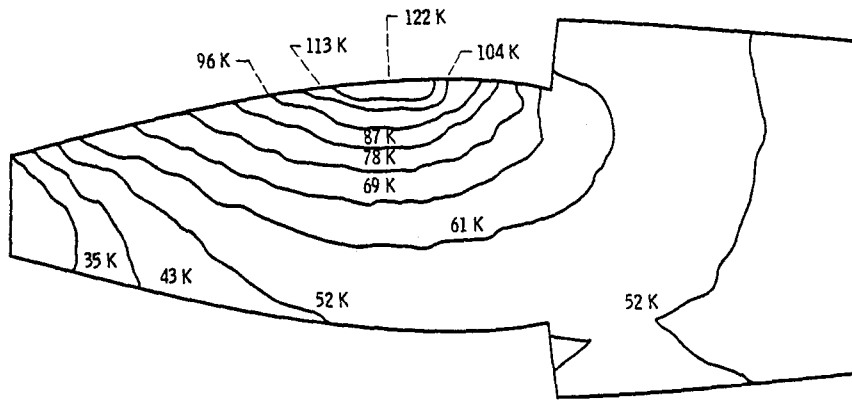
(a) Zero impingement depth.
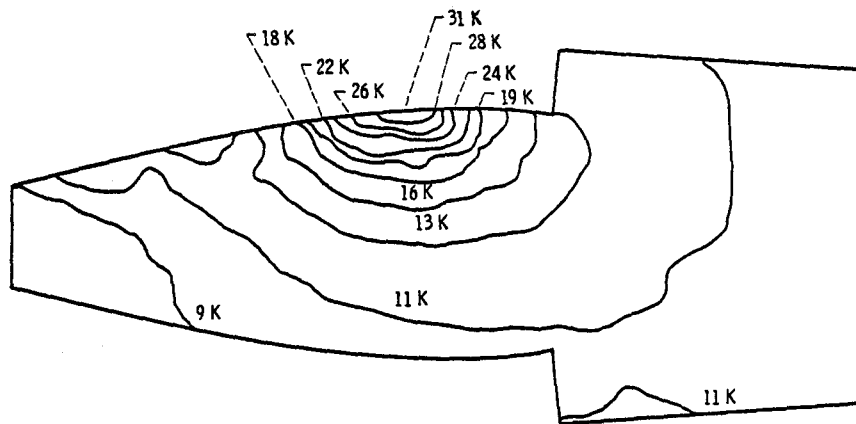


(b) 87.5 percent Impingement depth.

Figure 4. - Calculated gear tooth temperatures speed 10 000 rpm, load 5903 N/cm (3373 lb/in).
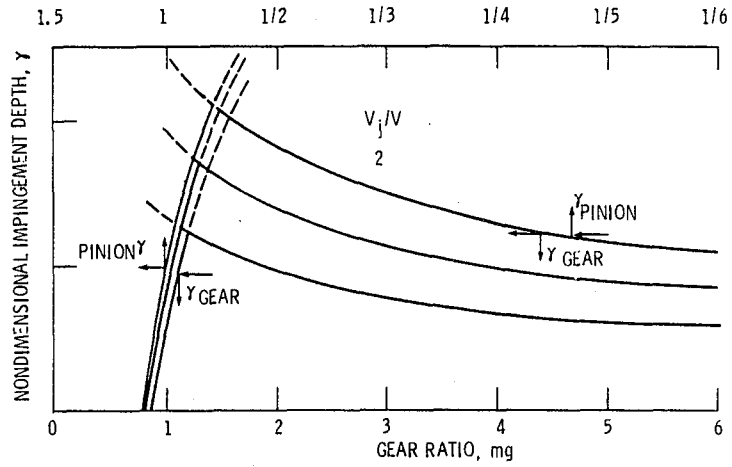
Figure 5. - Gear ratio vs nondimensional impingement depth speed 3600 rpm jet pressure 17x10$^4$ N/m$^2$ (25 psi) 28 pinion teeth.



(a) Oil jet clearing pinion teeth.
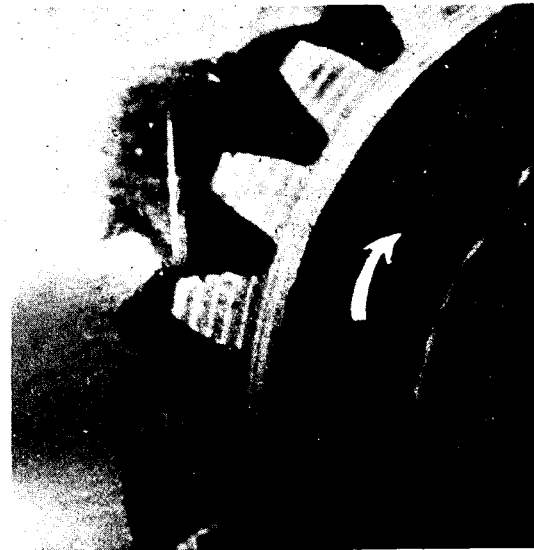
(b) Oil jet clearing gear teeth.

Figure 6. - Oil jet impingement depth, out of mesh. Speed, 3600 rpm; jet pressure, 8.3x10$^4$ N/m$^2$ (12 psi).
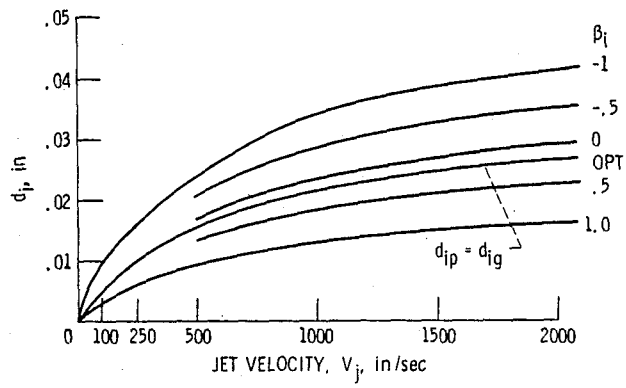
Figure 7. - Effect of $\beta_i$ on impingement depth, $S_i = 1.0$, 21/35 gear ratio.



Figure 8. - Into mesh lubrication for $V_j > V_g$.

Figure 9. - Into mesh lubrication for $V_j > V_g$.
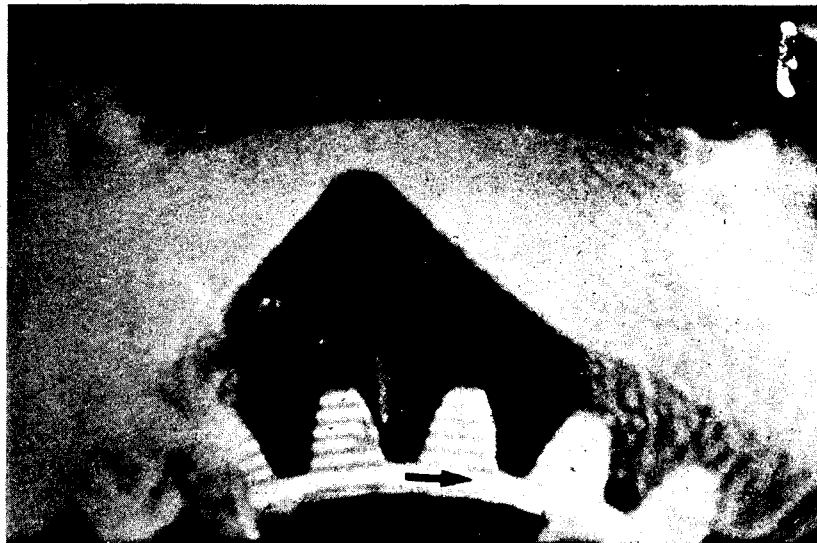


Figure 10. - Radial jet lubrication 5000 RPM oil jet pressure $21 N/cm^2$ 30 PSI.
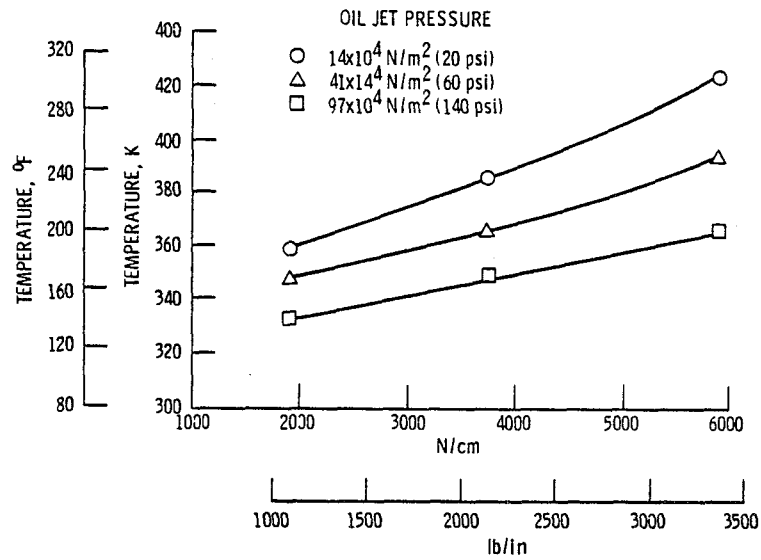
Figure 11. - I.R. microscope measurement of gear average surface temperature vs load for three oil jet pressures, speed 7500 rpm, oil jet diameter 0.04 cm (0.016 in) inlet oil temperature 308 K (95 °F).
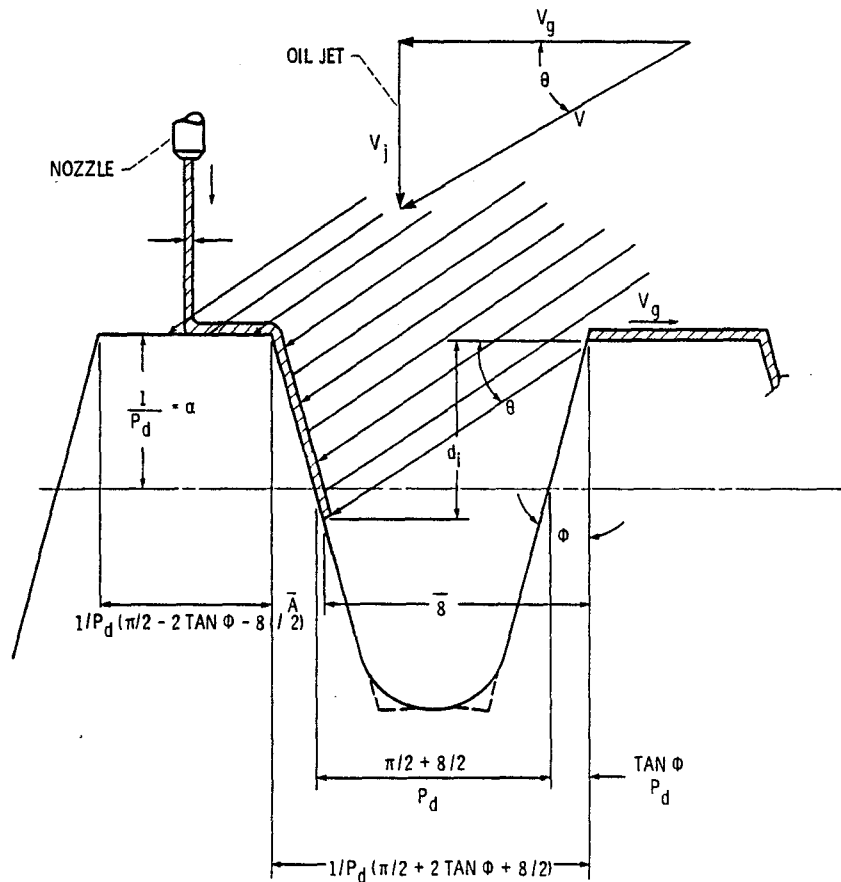


Figure 12. - Vectorial model for penetration depth.

117
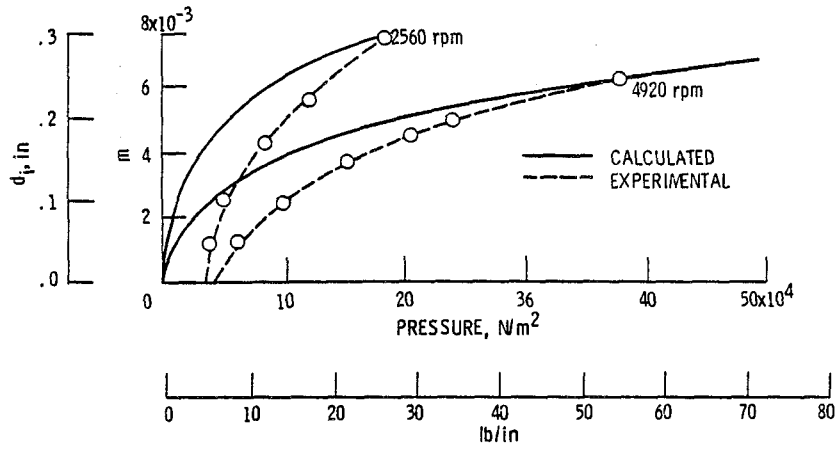
Figure 13. - Calculated and experimental impingement depth vs oil jet pressure at 4920 and 2560 rpm.

# A Historical Perspective of Traction Drives and Related Technology*

Stuart H. Loewenthal
National Aeronautics and Space Administration
Lewis Research Center
Cleveland, Ohio 44135

Traction or friction drives are perhaps the simplest of all rotary mechanisms and yet relatively little is known and even less has been written about them. In its simplest form a traction drive is just two smooth, unequal sized wheels in driving contact. Their simplicity suggests that their existence predates that of the gear drive. As speed regulators, oil-lubricated traction drives have been in industrial service for more than 50 years; yet the concept of transmitting power via traction remains unfamiliar and even alien to many. Indeed, traction drives are commonplace in our daily existence. Our car tires engaged against the road surface or a locomotive's driving wheels against the rail are but two common examples.

Many applications may be found in equipment where simple and economical solutions to speed regulations are required, such as phonograph drives, self-propelled lawnmowers, and even the amusement park ride driven by a rubber tire. Of course, in these examples, simple dry contact is involved. However, this same principle can be harnessed in the construction of an oil-lubricated transmission containing all steel components.

Traction drives can be constructed to give a single, fixed-speed ratio, like a gearbox or, unlike a gearbox, a speed ratio that can be continuously varied. This latter arrangement is of extreme interest to drive-train configurators since it provides them with an essentially "infinite" number of shift points to optimize the performance of their drive system.

Because power transfer occurs between smooth rolling-bodies, generally across a thin, tenacious lubricant film, traction drives possess certain performance characteristics not found in other power transmissions. Traction drives can be designed to smoothly and continuously vary the speed ratio with efficiencies approaching those of the best gear drives. Unlike transmissions with gear teeth, which, even when perfectly machined, generate torsional oscillations as the load transfers between teeth, power transfer through traction is inherently smooth and quiet without any "backlash." Film trapped between the rollers, tends to protect against wear and to dampen torsional vibrations. The operating speed of some traction drives is limited only by the burst strength of the roller material and the available traction in the contact. In many cases traction drives can be designed to be as small as or smaller than their nontraction-drive counterparts. When manufactured in sufficient quantity, costs can also be quite competitive because of the similarities in manufacturing traction-drive components and ordinary mass-produced ball and roller bearings.

Although traction drives have been available for some time (refs. 1 to 7), it is perhaps within the past 15 years or so that they have been considered serious competitors of conventional mechanical power transmissions in some of the more demanding applications. The earlier drives, particularly those targeted for automotive applications, had their share of durability problems above nominal power levels and, as a consequence, relatively few succeeded in the market place. The underlying reason for this was that certain critical pieces of technology were generally lacking. Designs were based on mostly trial and error. No uniform failure theories were available to establish service life or reliability ratings. The drive materials of the day were crude by today's standards. In short, traction drives were in their technical infancy.

Prompted by the search for more efficient automotive transmissions and bolstered by advancements made in rolling-element bearing technology, interest in traction drives has been renewed. Today's analytical tools, materials, and traction fluids are far superior to those available only 10 years ago. This has lead to the re-emergence of traction drives and the technology related to their design.

It is the intent of this review to trace the evolution of traction-drive technology, in a limited sense, from its early development to the efforts underway today. The reader will appreciate that no attempt has been made to comprehensively document the history of traction drives but rather to
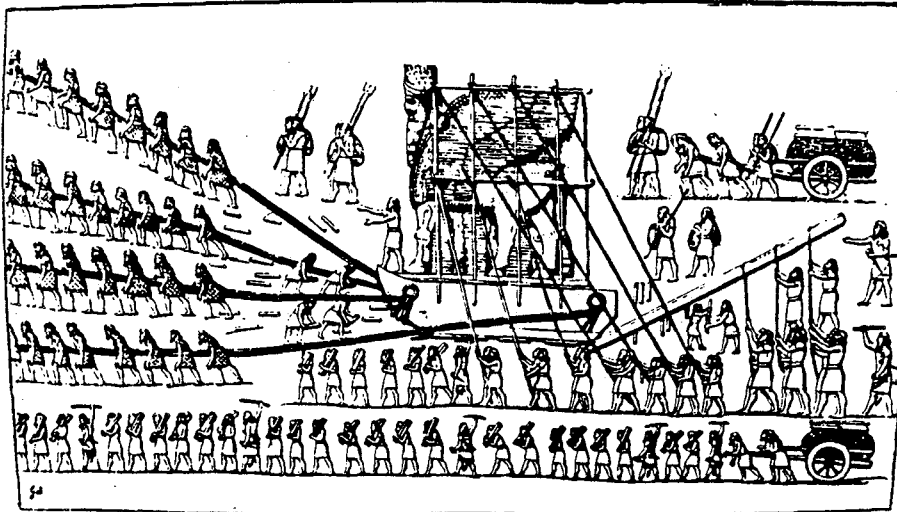
Figure 1. - Assyrians positioning stone figure using log rollers and "human traction," circa 700 B.C. (ref. 8).

assemble, in a single place, a collection of source material on this broad subject for the benefit of those unfamiliar with these interesting devices.

## Early History

Since the development of machines there has been a need for transmissions to effectively match the speed of the power source to that of the driven device. In early human history, the power sources were either human or animal and in "direct" drive with the load. This is vividly illustrated in figure 1 (ref. 8). This scene (ca. 700 B.C.) depicts Assyrians positioning a stone figure with the aid of log rollers and "human traction." Traction as an assistance to motion is a natural part of the human experience. Also depicted are humans pulling wheeled-carts. It is clear that the ancients had knowledge of both the roller and the wheel. Thus, the ingredients to develop simple traction wheel mechanisms were available to them.

The existence of mechanical drive systems may even predate this by hundreds of years, according to Dudley (ref. 9). He speculates that gear devices might have been used in clocks, temple devices, and water-lifting machines as far back as 1000 B.C. by the ancient Greek, Egyptian, and Babylonian civilizations. Unfortunately, there is no tangible evidence to support this view. Drachmann (ref. 10) maintains that the origins of the toothed gear wheel are often erroneously associated with a passage in a book by Aristotle. The passage was, in fact, not due to Aristotle but to his school (ca. 280 B.C.), and there is no explicit mention of teeth on the wheels. These wheels may just as well have been smooth disks in *frictional contact* according to Drachmann. Although there seems to be no evidence in the literature or artifacts to establish when friction wheels were first used, it is reasonable to assume that before man went to the trouble of cutting notches in smooth wheels, he probably used them as they were to transmit rotary motion. Pins or cogs might have been added to the wheel to overcome dimensional variations due to the crude, out-of-round wheels of the day or when the driving load simply became too large to be sustained by frictional contact. It is ironic that these very cogs, though now more sophisticated than in earlier times, are often the source of many power transmission problems. Although the writer's limited efforts failed to uncover tangible examples of friction drives before the modern era, the likelihood of their use in primitive rotary machinery is too great to dismiss.

One of the earliest known examples of a friction drive[1] is that patented by C. W. Hunt in 1877 (fig. 2; ref. 11). This drive had a single, spoked transfer wheel, which was probably covered with

---

[1]The term "friction drive" is normally used to refer to a drive that is nonlubricated, while "traction drive" refers to one with oil-wetted components. The friction terminology may have evolved from the fact that these drives intentionally used at least
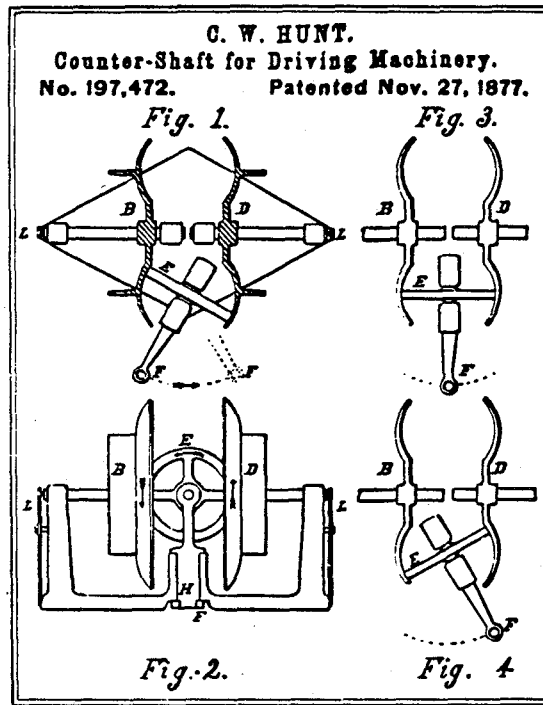
Figure 2. - Hunt's 1877 toroidal friction drive (ref. 11).
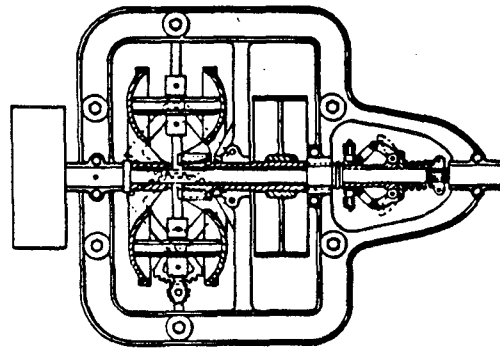


Figure 3. - 1899 Hoffman toroidal friction drive for belt-driven machinery
(ref. 12).

leather, running against a pair of toroidally shaped metal disks. Judging by the pulley flanges attached to the toroidal disks, the drive was intended to regulate the speed of belt-driven machinery such as that commonly found in factories at the turn of the century. By tilting transfer wheel E, the effective rolling radii of toroids B and D could be altered and, hence, their relative speeds.

A similar drive was devised by W. D. Hoffman as shown in an 1899 British patent application (fig. 3 from ref. 12). The toroidal drive arrangement apparently has found great favor with traction-drive designers through the years. Work continues on this configuration even today, more than 100 years later!

one roller that was covered with a high friction material such as leather, rubber, fiber or even wood. This not withstanding, the term "friction" is somewhat of a misnomer since it is still the traction force responsible for positive motion of the driven element.

**═══THE═══**

# Gearless Transmission

"The Only Direct Drive Friction Transmission"

Does Away Entirely With the Use of Gears Gives an Unlimited Number of Speeds

The Ideal Transmission for Both Pleasure and Commercial Vehicles.
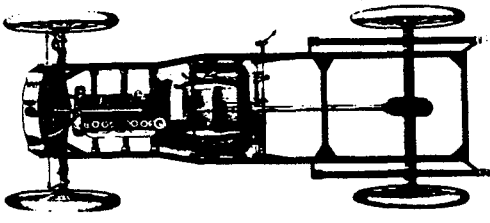
Giving a BROAD RANGE OF SPEEDS FORWARD OR REVERSE, DIRECT DRIVE ON HIGH SPEED. Single Lever Control, ELIMINATING ENTIRELY All of the Difficulties Encountered in the Present Forms of Transmission Employing Gears with their Attendant Troubles.

Built in TWO Sizes For Light and Heavy Cars.

Can Be Used With Either Shaft or Chain Drive.

Write For Catalogue and Prices To-day.

Thoroughly Tested During the Past Two Years.

Showing Transmission Installed in Car

We Furnish the Transmission As Shown Herewith to Include Fly-wheel and Direct Clutch. The Frame is of Steel. Bearings, Balls and Rollers. Material and Workmanship of Highest Grade.

Friction Surfaces only in use on Intermediate Speeds Forward and Reverse.

Showing Transmission in Reverse Speed

Write for Catalogue

Side Friction Wheels Do Not Rotate on Direct Drive. Central Friction Wheel is Driven on Intermediate Speeds by Both Side Wheels From Flywheel. Note The Direct Clutch in Hub of the Flywheel.

Puts Less Strain on the Running Gear of a Car Than Any Other Transmission.

## GEARLESS TRANSMISSION CO., Rochester, N. Y.

Figure 4. - An early automotive friction drive, circa 1906, (ref. 17).

Friction drives also found use on several types of wood-working machinery dating back before the 1870's. The 1876 edition of Knight's American Mechanical Dictionary (ref. 1) describes a deal-frame machine for slitting pine-timber which employed a friction disk drive for regulating the feed motion. In another source (ref. 2), a wood panel-planer is.described whose feed rolls are driven by friction wheels. Appleton's Cyclopedia of Applied Mechanics, published in 1880 (ref. 3), reports of frictional gearing being used on wood-working machinery in which one wheel was made of iron and the other, typically the driver, of wood or iron covered with wood. For driving light machinery, wooden wheels of basswood, cottenwood, or even white pine reportedly gave good results. For heavy work, where from 30 to 45 kW was transmitted by simple contact, soft maple was preferred. Appleton's Cyclopedia also discusses bevel frictional gearing in which the bevel-gear is a smooth-faced iron cone being driven by a bevel pinion, with a wooden rim. This rim comprises several layers of hardwood followed by soft maple bolted on to a flanged-hub made of iron.

## Automotive Transmissions

It was not until the introduction of the horseless carriage at the end of the 19th century that the goal of developing a continuously variable transmission (CVT) for the automobile sparked considerable friction drive activity. Although the potential performance benefits associated with a CVT for other types of machinery had been recognized before, the safety, simplicity, and reliability

122

of the gearset offered greater appeal. It was good enough to select roughly the right speed ratio and to up-size the powerplant slightly, if needed, to drive the load. It quickly became apparent to the designers of early automobiles that a highly flexible transmission was badly needed to compensate for the lack of flexibility of the early gasoline engines. These engines had a tendency to run well only at one speed. As noted by P. M. Heldt in an unusually comprehensive review of the development of the automatic transmission (ref. 13), the chief objection to early sliding-gear transmission, apart from their lack of flexibility, was the difficulty in gear shifting. The gearboxes used on many of the early vintage cars, such as 1890 Panhard, were adopted from the clash gears used in factory equipment (ref. 14). Gear changing was not merely difficult but potentially damaging to the gear teeth. According to Hodges and Wise (ref. 15), "the best technique with those early cars was to slip the clutch gently and bang the gears home as quickly as possible, in the hope that you might catch the cogs unawares." (Although Prentice and Shiels patented the synchromesh principle back in 1904, it wasn't until the late 1920's that General Motors developed the syncromesh gearshift for production. Syncromesh allowed almost any driver to shift from one speed to the next without clashing the gears (ref. 16).) In view of the limitations and inconveniences associated with gear changing, it is not surprising that the inventors of the day looked for a simple means of continuously and, hopefully, automatically varying the speed ratio between the engine and the wheels.

Mechanical ratchet, hydraulic, and electro-mechanical drives were all tried, but friction drives, because of their simplicity, were the first automobile transmissions to provide infinite ratio selection. The earliest of these was the rubber V-belt drives that appeared on the 1886 Benz and Daimler cars, the first massproduced gasoline-engine-powered vehicles. Friction disk drives, similar in construction to the gearless transmission illustrated in a 1906 advertisement (fig. 4 from ref. 17), were used as regular equipment on a number of early motor cars. These included the 1906 Cartercar, 1907 Lambert, 1909 Sears Motor Buggy, and 1914 Metz Speedster. An early advertisement for the Lambert appears in figure 5.

The Cartercar (fig. 6) had an extremely simple friction drive consisting of a metal disk, driven by the engine crankshaft, in traction contact with a large, fiber-covered spoked wheel mounted on a transverse countershaft. The countershaft, in turn, was connected to the rear axle by an ordinary chain drive. To vary speed ratio, a driver operated lever (fig. 6) was used to radially position the



Figure 5. - An early advertisement for a friction-drive car (ref. 17).
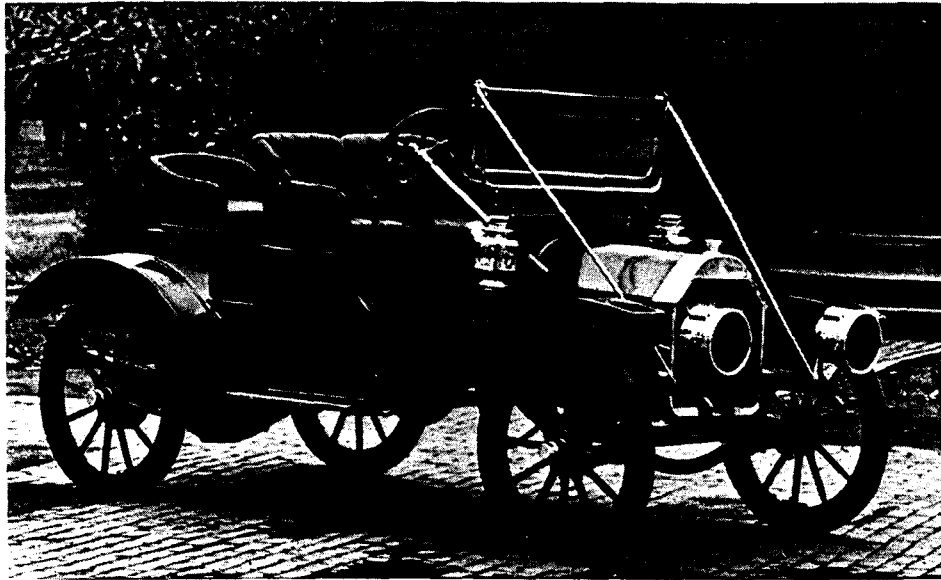
Figure 6. - 1909 Cartercar equipped with a friction, continuously varible transmission (CVT). (Courtesy of the Henry Ford Museum, Dearborn, Michigan.)

output follower wheel across the face of the metal disk—turntable fashion. Neutral was achieved when the follower wheel was centered. By moving the follower wheel past center, reverse rotation would occur to allow the vehicle to back up. The smoothness and ease of operation of the Cartercar transmission made it quite popular. It is not well-known that Mr. W. C. Durant, founder and first president of General Motors Company, acquired the Cartercar Company in 1908 because of his expectation that friction drives would soon be universally used in automobiles (refs. 16 and 18). In 1910 the Cartercar Company even produced a Model "T" truck, equipped with their friction drive. Despite its catchy slogan, "No clutch to slip—no gears to strip . . . a thousand silent speeds and only one control lever, that's a Cartercar," the Cartercar Company's commercial success was shortlived.

From 1909 until 1912, Sears marketed a two-cylinder, 14-horsepower "Motor Buggy," also equipped with a friction drive (ref. 19). "Absolute simplicity, its positiveness under the most severe conditions and its unequalled flexibility," boasted one of the Sear's ads. However, by about 1915, cars equipped with friction drives had virtually disappeared (ref. 19), presumably due, in part, to the need for frequent renewal of the friction material.

Despite the limited success of these earlier attempts, the goal of designing an automotive transmission that smoothly and automatically shifted was not lost. In the late 1920's the Buick Division of General Motors was given the task of developing a continuously variable, oil-lubricated, steel-on-steel traction drive. This transmission was similar in design to the Hayes double toroidal traction drive, patented in 1929. The Hayes Self-Selector Transmission (ref. 20), although originally developed here, was later offered as an option on the 1935 British Austin Sixteen (ref. 21).

The General Motors toroidal drive, later called the toric transmission, is illustrated in figure 7. The geometry of the drive is remarkably similar to the 1877 Hunt drive, with the addition of a second toroidal cavity and a ball differential to balance loading between the two cavities. An extensive test program was conducted on this drive. Seventeen road-test vehicles equipped with the toric drive accumulated over 300 000 miles of road testing (ref. 18). A 20-percent improvement in highway fuel mileage was reported. In 1932 General Motors decided to produce this type of transmission (ref. 16); however, no cars equipped with the toric drive were ever sold to the public. The reasons for halting production were never really made clear. Some say that there were unresolved discrepancies in service-life data obtained during road tests and that obtained from laboratory bench testers. Others believe that the availability of premium quality bearing steel, needed in large amounts to make each drive, was simply not great enough at the time to meet expected production requirements. Whatever the reasons, Alfred P. Sloan, Jr., then president of General Motors, turned the transmission down for production in the belief that it would simply be too expensive to make (ref. 16).

124
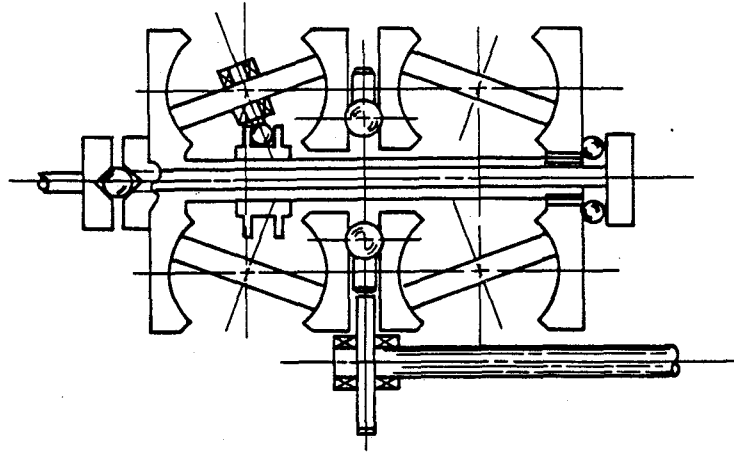
Figure 7. - General Motor's Toric transmission (ca. 1928).

Work on various types of automatic transmissions, beginning in the early 1920's finally lead to the production of the 1937 Oldsmobile semiautomatic, self-shifting transmission. This transmission still required the use of a clutch pedal for stopping and starting. The hydramatic soon followed. It was the first mass-produced, fully automatic transmission—first appearing on the 1940 Oldsmobile (ref. 16). However, the old toric drive was not completely forgotten, it reappeared briefly in the 1960's on General Motor's experimental gas turbine RTX bus.

General Motor's New Departure Bearing Division produced an industrial counterpart to the toric drive. By 1935 when production was halted, over 1600 units of the "Transitorque" traction CVT had been marketed (ref. 20). The drive's design is credited to Richard T. Erban, an early traction-drive pioneer, who briefly worked for General Motors during this period (ref. 4).

In England, after several years of analyzing the Hayes Self-Selector drive, Perbury Engineering, Ltd., retrofitted a modified, scrapped Hayes transmission into Hillman Minx sedan in 1958 (ref. 21). Fuel savings were reported to be 20 to 25 percent but the concept really never caught on with any of the several dozen companies or so that had previously expressed interest in the drive (ref. 21).

In the United States in 1959, Charles Kraus installed a modified version of a toroidal CVT into an American Motors Nash Rambler (ref. 4). This unit had a semitoroidal roller geometry similar to that patented in 1932 by Jacob Arter for industrial service. The Arter drive is still commercially produced in Switerzerland. In 1962 Mr. Kraus joined Curtis-Wright Corporation and headed up a program supported by the Army Tank-Automotive Center to retrofit this semitoroidal traction drive to an Army Jeep. A drive malfunction was encountered after approximately 17 000 miles of road testing (ref. 22). Design improvements were made on a second test drive but this unit also experienced operational problems that caused a halt to the program. In 1973 Tracor, Inc., demonstrated a Ford Pinto equipped with an improved version of the Kraus drive lubricated with Monsanto's new traction fluid. Although operational characteristics were established, expected fuel economy improvements were largely negated by the hydraulic losses in the thrust bearings used to clamp the toroids together (ref. 23). More recent toroidal drive designs partially overcame this problem by mounting two toroidal drive cavities back-to-back along a common shaft, thereby eliminating these troublesome thrust bearings.

**Industrial Traction Drives**

Starting with the 1877 Hunt drive, adjustable-speed traction drives have been in industrial service for more than 100 years. The bulk of these drives has been performing a speed matching function for light-duty equipment, such as drill presses. Typical uses are listed in table I.

A sample of representative traction-drive configurations appears in figure 8 (ref. 4). According to Carson (ref. 24), more than 100 United States patents on adjustable-speed traction drives are on file. Out of these, perhaps a dozen or so basic geometries are in production. Some of these drives are shown in figure 8. Of those commercially available, few are rated greater than 10-kW power capacity.

TABLE I. - TYPICAL APPLICATIONS FOR TRACTION DRIVES

| |
|---|
| Marine propulsion drives |
| Earthmoving equipment |
| Textile machinery |
| Farm equipment, agramachinery |
| Rubber machinery |
| Propeller drives |
| Forest products and paper machinery |
| Crane drives |
| Construction equipment |
| Pump drives |
| Locomotive and railroad machinery |
| Machine tools |
| Outdoor tools and recreation vehicles |
| Oil field drives and offshore rigs |
| Household appliances |
| Auto transmissions |
| Air conditioning systems |
| Steel mill drives |
| Mining and ore processing machinery |

The "ball and cone" geometry was commercially introduced in the 1940's by Jean Kopp in Switzerland. The Kopp Variator is said to be the most widely used traction drive, with more than 250 000 units sold around the world through 1975 (ref. 24). A more recent cone-roller variator developed by Kopp extends the variator's power rating to 75 kW in a 582-kg package.

The wheel and single-disk drive typify the Cartercar and Sears Motor Buggy transmission. Because heavy contact loads must be directly reacted by the support bearings, the torque capacity of this geometry is greatly restricted. The cone and ring with reducer drive, produced by Graham in 1935, is one of the earliest traction drives developed in the United States, Graham drives are available for ratio ranges to 10:1 and power levels to about 4 kW. The disk-to-disk drive, also known as the Beier disk drive, was one of the earliest (1949) industrial traction drives capable of handling high powers, with current power ratings to 164 kW. The drive components are imported from Japan, assembled, and marketed in the United States by Sumitomo Machinery Company. With the possible exception of the toroidal geometry, the commercial CVT's of figure 8 are generally too large and complex or have insufficient power capacity to be suitable for advanced automotive applications without substantial modifications. An early review of the basic types of adjustable-speed traction drives can be found in reference 25. Reference 26 gives descriptive information on 24 types of variable speed traction drives that were commercially available in 1963.

**Early Drive Limitations**

As we have seen, the earliest traction drives generally used leather, wood, rubber, or fiber covered friction wheels running against metal disks. As these soft friction materials aged, they lost flexibility and wore rapidly. The driving surfaces generally had to be renewed or replaced at frequent intervals, depending on the rate of usage. Despite this, friction drives found use in early steam tractors, factory machinery, wood-working tools, and in several vintage cars (ref. 20). These simple, smooth, low-cost speed changers are still in use today for light-duty applications ranging from hand tools, washing machines, and record players to amusement park rides and cement mixers. In these modern drives more durable rubber and reinforced plastic materials have been substituted for the leather and fiber wheels of yesteryear. However, the thermal capacity and wear characteristics of these softer materials still basically set the useful power capacity of this class of transmission. For applications needing a low-cost speed changer, adjustable-speed friction drives are good choices. Sizing criteria and typical design information for friction drives can be found in reference 27.

Oil-lubricated traction drives having hardened steel roller contacts appeared in the early 1920's. Carson (ref. 11) credits Erban in Austria with the development of the first metal-to-metal, oil-lubricated drive in 1922. The 1923, Arter drive is another example. The presence of hardened steel

126
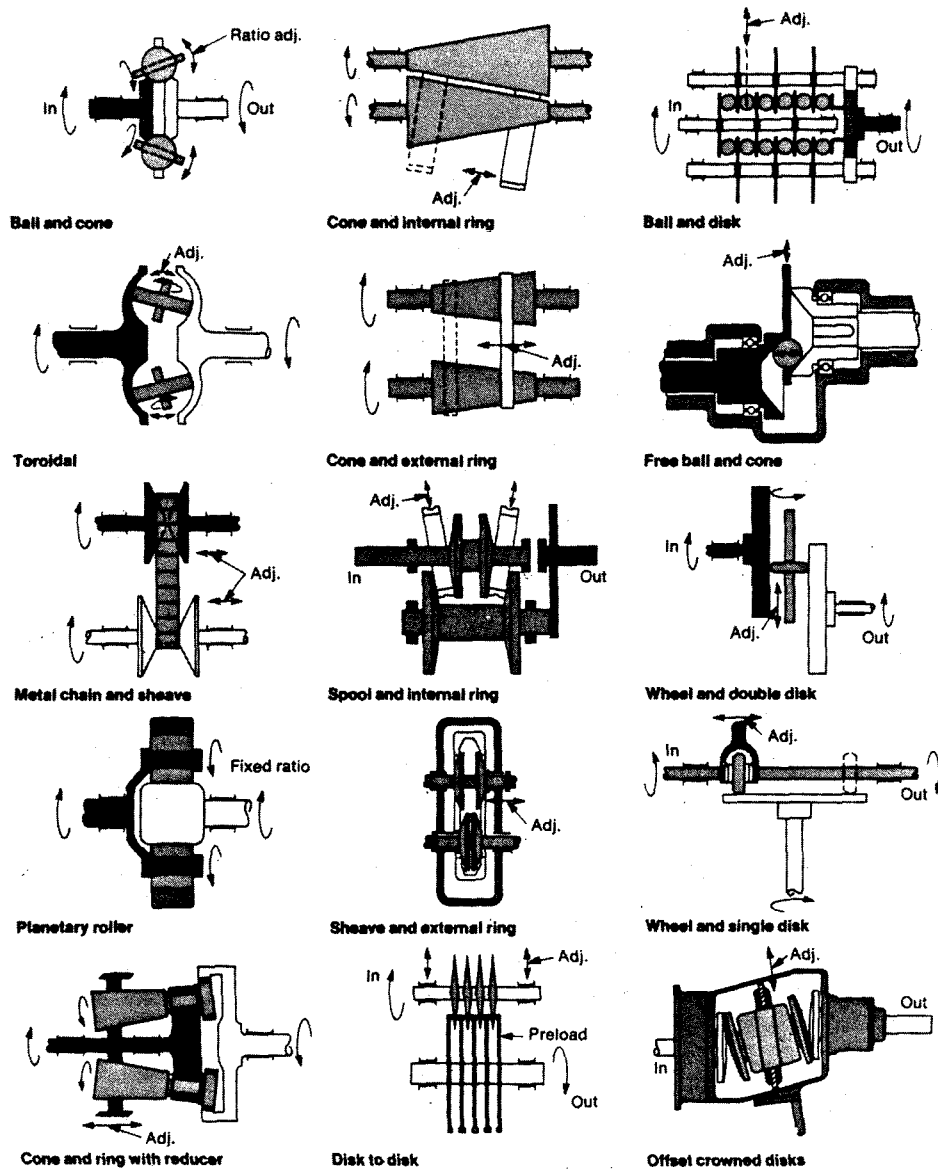
Figure 8 - Typical industrial traction-drive geometries. (Courtesy of Design Engineering (ref. 4).)

rollers in these drives significantly increased the allowable operating contact stresses. The purpose of the oil was to protect the contact surfaces from wear while providing cooling. However, the relatively low coefficient of traction of the oil meant that these drives had to carry unusually high-contact loads to inhibit slip. High loading generally leads to early pitting, unless the torque rating of the drive was appropriately restricted. Even though the early traction drives tended to be bulky, their relatively high efficiency and smoothness of operation still made them attractive for many applications.

The very early friction drives were also vulnerable to slip damage in the event of an overtorque, since the normal load to prevent slip was set during assembly and did not change. To overcome this problem and to prevent the drive contact from being overloaded during periods of low power, Erban, while in Germany, patented in 1921 a mechanism to automatically regulate the contact normal load in porportion to the transmitted torque (ref. 20). Keeping the contact pressures low at light torques not only extended fatigue life but helped to reduce unnecessary power loss. Automatic loading mechanisms of this type have become regular features of almost all successful traction drives.

# Advancements in Technology

Traction drive technology made relatively little progress for the first half of this century except for the occassional introduction of a new geometric variation. Designs were largely predicated on laboratory or field experience and very little of this information was reported in the open technical literature.

Because of the great similarity in the contact operating condition, traction-drive technology benefitted greatly from the wave of technical advancements made for rolling-element bearings. Major advancements in bearing design occurred in the late 1940's with Grubin's work in elastohydrodynamic lubrication (ref. 28) and Lundberg-Palmgren's analysis of rolling-element fatigue life (ref. 29). In fact, the lubrication principles, operating conditions, and failure mechanisms of traction-drive contacts and bearing contacts are so similar that the design fundamentals are virtually interchangeable. The same may be said for gear contact design criteria as well.

In view of the durability shortcomings of earlier traction drives, much of the recent research has centered on improving the power capacity and reliability of these devices without sacrificing their inherent simplicity or high mechanical efficiency. Although work has been performed on many fronts, research efforts to date can be loosely categorized under one of several areas: (1) modeling the tractive behavior of the lubricant within the contact and its attendant power losses; (2) predicting the useful torque that can be passed between rollers without surface distress or that amount corresponding to a given fatigue life; (3) determining and improving the durability characteristics of traction-drive materials, primarily bearing-grade steels; (4) developing lubricants that produce higher traction forces in the contact without sacrificing conventional lubricant qualities; and (5) developing drive arrangements that maximize durability, torque capacity, and ratio capability and minimize size, weight, power loss, and complexity.

## Traction Phenomena

A basic understanding of how power is transferred between traction-drive rollers is helpful in reviewing the contribution made in this area. Figure 9 shows a simple, lubricated, roller pair in traction contact. A sufficiently large normal load $N$ is imposed on the rollers to transmit the tangential traction force $T$. The amount of normal load required to transmit a given traction force without destructive gross slip is dictated by the available traction coefficient, $\mu$, which is the ratio of $T$ to $N$. Since contact fatigue life is inversely related to the third power of normal load, it is extremely desirable to make use of lubricants that produce high values of $\mu$. The search for lubricants having high traction capabilities will be discussed later.

The rollers, as illustrated in the enlarged view of the contact appearing in figure 9, are not in direct contact but are, in fact, separated by a highly compressed, extremely thin lubricant film. Because of the presence of high pressures in the contact, the lubrication process is accompanied by some elastic deformation of the contact surface. Accordingly, this process is referred to as elastohydrodynamic (EHD) lubrication. Ertel (ref. 30) and later Grubin (ref. 28) were among the first to identify this phenomenon, which also occurs for other oil-lubricated, rolling-element machine elements such as bearings and gears. The importance of the EHD film in traction contacts lies in its ability to reduce and/or eliminate wear while acting as the principal torque transferring medium. An excellent accounting of the role of EHD lubrication traction is given by Martin (ref. 31).

## Traction Curve

The technological properties of the lubricant in the contact, particularly its traction characteristics, is fundamental to the design of traction drives. Figure 10 shows a typical traction-versus-slip curve for a traction fluid. This type of curve is typically generated with a twin-disk traction tester (refs. 32 to 35). Imposing a traction force across a lubricated disk contact which is rotating at an average surface velocity $U$ gives rise to a differential surface velocity $\Delta U$. Three distinct regions can generally be identified on a traction curve. In the linear region the traction coefficient increases linearly with slip. In the non-Newtonian regions it increases in a nonlinear fashion, reaches a maximum, and then begins to decrease. Finally, the curve shows a gradual decay with slip in the thermal region due to internal heating within the oil film. It is the linear region of the traction curve that is of the greatest interest to traction-drive designers. The design traction coefficient, which
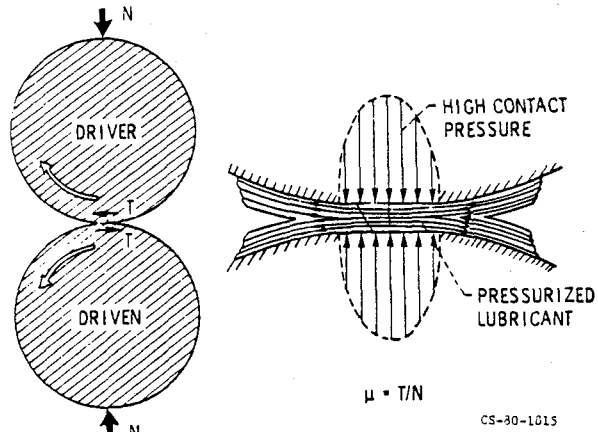
Figure 9. - Power transfer through traction.
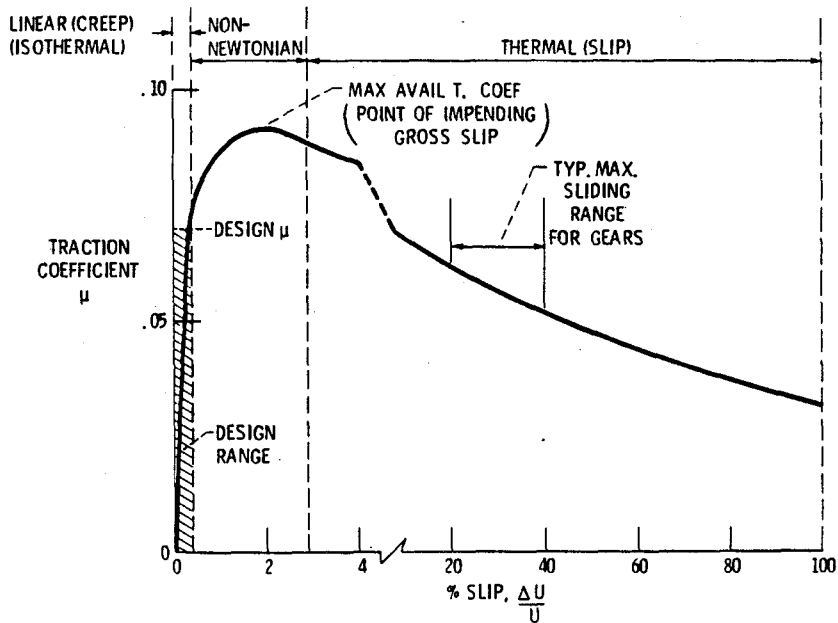


Figure 10. - Typical traction curve showing design range for traction drives.

dictates how much normal load is needed to transmit a given traction force, is always chosen to be less than (by, generally, 20 to 30 percent) the peak available traction coefficient to provide a safety margin against slip. Traction drives are generally equipped with a torque-sensitive loading mechanism that adjusts the normal contact load in proportion to the transmitted torque. Such mechanisms insure that the contact will always have sufficient load to prevent slip without needlessly overloading the contact under light loads.

## Traction Coefficient

Perhaps the single most important factor affecting the torque capacity, life, and size of a traction drive is the maximum value of the available traction coefficient. It is this parameter that determines the necessary contact load. Since the fatigue life of a contact is inversely proportional to the cube of contact load, a 50-percent improvement in the traction coefficient would, for example, mean a 240-percent life increase for a given drive under a given set of operating conditions.

129

## Solidification Behavior

In a typical traction-drive contact, severe transient operating conditions are imposed on the lubricant. The lubricant is swept into the contact, exposed to contact pressures, which are 10 000 times atmospheric or greater, and returned to ambient conditions, all in a few milliseconds. Clark, et al. (ref. 32), in 1951 were the first to experimentally observe that, under these high pressures and shear rates, the lubricant exhibits shearing properties of a plastic solid and will, in fact, yield at some critical shear stress. Although it had been known from static high-pressure viscometry experiments that an oil's viscosity would increase dramatically with increasing pressure and eventually solidify under high enough pressure, this was really the first time that this effect was observed to occur under the highly transient conditions of a traction contact. This solidification phenomenon was later also observed by experimentors Smith (ref. 33), Plint (ref. 34), and Johnson and Cameron (ref. 35), among others. Indeed, one can see a striking similarity in the shear-stress–shear-strain rate curves of a traction fluid and the tensile-stress–strain curves of a typical thermoplastic (fig. 11). It is also clear from figure 17 that temperature has a similar adverse effect on the limiting shear strength (maximum traction coefficient) of the traction fluid and the yield strength of the thermoplastic. Furthermore, both materials exhibit either viscous or elastic behavior depending on the rate of straining. Plastics will flow like a liquid if stretched slowly enough but will show elastic resiliancy if pulled suddenly. An EHD film in the traction contact shows similar visco-elastic behavior.

## Effects of Operating Conditions

Whether the lubricant exhibits viscous behavior or acts as an elastic solid depends on a number of factors. Contact pressure, temperature, shear rates, and lubricant composition all play important roles. Knowledge of the rheological characteristics of the lubricant as it passes through the contact is essential to predicting the performance of the contact, particularly in the absence of specific experimental data.

Visco-elastic lubricant behavior has been a subject pursued by a large number of investigators. Among them were Crook (ref. 36) and Dyson (ref. 37), who were among the first to call attention to such behavior, Johnson and Roberts (ref. 38), who experimentally demonstrated the transition from predominantly viscous to predominantly elastic response, and Trachman and Cheng (ref. 39), who used a compressional visco-elasticity model to numerical solve for the traction curve.

Based on the work of these investigators and on the comprehensive traction model advanced by Johnson and Tevaarwerk (ref. 40), one can assume that for most traction-drive contacts the maximum available traction coefficient is directly related to the shear yield strength of the solidified lubricant film.

From a large body of traction data generated on a twin-disk tester (refs. 41 to 44), it was found that an increase in contact pressure is beneficial to the available traction coefficient but that an increase in surface velocity, temperature, contact ellipticity ratio, misalinement, or spin (circumferential slip) have a negative effect. Figure 12 shows the typical effects that pressure and speed have on the traction coefficient of a traction fluid from test data generated in reference 45.

## Creep

In the linear region of the traction curve, the transfer of torque will cause a small difference in velocity to be developed between the surfaces of the driver and driven rollers. This small velocity difference, generally less than 1 percent of the rolling velocity, is often referred to as creep rather than slip. This is because in creep only part of the contact is experiencing sliding while in slip there is total relative motion.

Creep is always present to some extent between rolling bodies that are transmitting torque, whether lubricated or not. Carter in 1926 was one of the first to identify the creep occurring between a locomotive's driving wheel and the rail (ref. 46). Typically, a region of microslip will occur between the surfaces in the trailing region of the contact while the surfaces in the leading region will be locked together without relative motion (ref. 47). As the tangential traction force is increased, the microslip region will encompass more and more of the contact until, at some point, the whole contact is in total slip. This is the point of impending gross slip. It occurs when the ratio of traction force to normal load is equal to the maximum available traction coefficient. When a mechanism to increase the
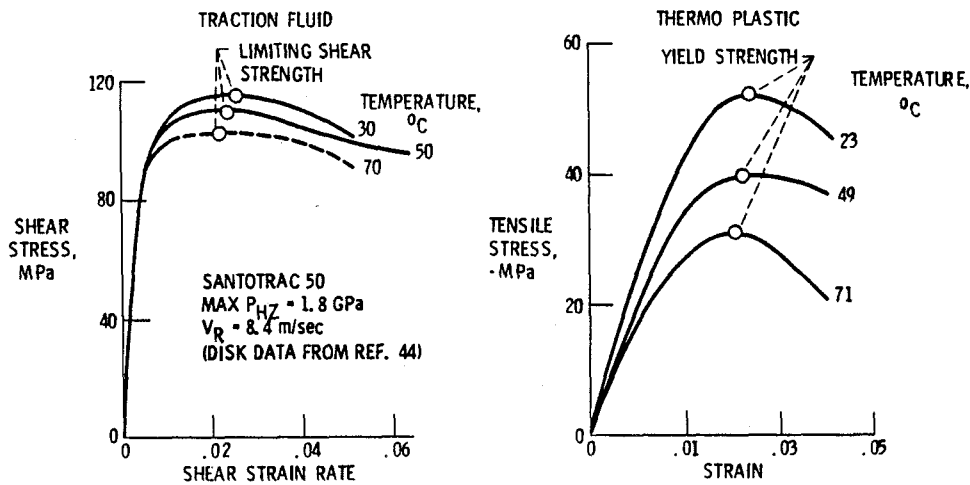
TRACTION FLUID



Figure 11. - Plastic behavior of a traction fluid.



CS-80-2487
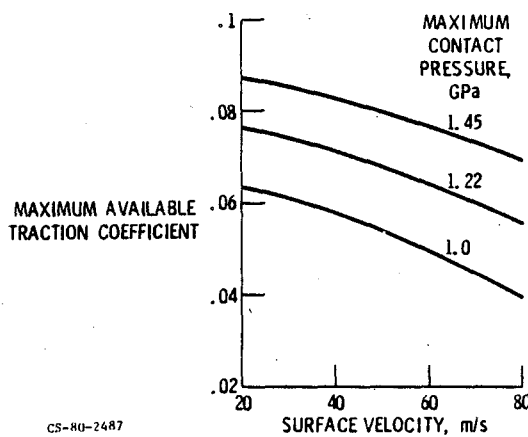
Figure 12. - Typical maximum available traction coefficient as function of
surface velocity and maximum contact pressure. Synthetic hydrocarbon
traction fluid; a/b = 5; zero spin; temperature, 343 K. Data obtained on a
twin-disk machine (ref. 45).

normal load with increasing traction is present, the point of impending gross slip is not reached.

Creep is typically the result of the elastic stretching of the solidified lubricant film and that of the roller material. The lubricant film gets stiffer with increasing pressure and because it is so thin relatively little strain occurs. In fact, as pointed out by Tevaarwerk (ref. 48), for many traction drives that regularly operate at contact pressures above 1.2 GPa, most of the creep actually takes place in the steel rollers and not in the EHD film. Johnson, et al. (ref. 49), have developed relatively simple methods to determine how much of the elastic effects are due to the roller material and how much are due to the film.

The amount of creep in a lubricated traction-drive contact can vary from as little as 0.1 percent of the rolling velocity at high pressures and low speeds to 3 or 4 percent or more when the pressures are low, speeds are high, and sideslip (misalinement) or spin (circumferential contact slip) is appreciable. Although these creep values are quite small relative to gears, where sliding velocities can be 30 or 40 percent of the pitch-line velocity at the tooth engagement and disengagement points, it is nevertheless important to minimize the creep value through the proper selection of operating conditions, geometry, and lubricant. Every percentage point loss in creep represents a percentage point loss in speed and a corresponding percentage point loss in mechanical efficiency.

131

# Traction Fluids

Because of the importance that the coefficient of traction has on the life, size, and performance of a traction drive, considerable attention has been given to identifying fluids with high traction properties, starting in the late 50's with Lane's experiments (ref. 50). Using a modified two-ball tester, Lane found an apparent inverse relationship between the traction coefficient and temperature-viscosity index for naphthenic and paraffinic mineral oils.

In a comprehensive investigation into traction phenomena, Hewko (ref. 42) obtained traction performance data for both compounded and uncompounded mineral oils as well as for a group of synthetic fluids. He also investigated the effect of oil additives on traction as well as the effects of operating conditions, roller geometry, and surface topography. His results indicated that the lubricant composition and surface topography had the greatest overall effects on traction and that naphthenic-based mineral oils gave better performance than paraffinic oils. He also observed that many common types of additives can markedly reduce traction (ref. 42).

The research of reference 51 describes the development of a formulated traction fluid, designated as Sunoco Traction Drive Fluid-86. This fluid was subsequently field tested in the General Motors turbine bus toric drive and in an automatic transmission for the Oldsmobile Toronado with reportedly good results.

Hammann, et al. (ref. 52), examined some 26 test fluids and, unlike Lane (ref. 50), could not find any obvious relationship between the coefficient of traction and the viscosity index. However, his tests did identify several synthetic fluids that had up to 50 percent higher coefficients of traction, depending on test conditions, than those reported for the best naphthenic base oils (ref. 52). This research laid the ground work for the development of Monsanto's family of commercial traction fluids, Santotrac 30, 40, 50, and 70. These fluids are the most widely used traction oils today. The results of accelerated five-ball fatigue tests (ref. 53) indicated that these synthetic cycloaliphatic traction fluids have good fatigue-life performance, comparable with the reference tetraester oil used in this experiment.

In an unusually complete doctorial investigation into the nature of traction power transfer, Gaggermeier (ref. 44), in one part of his work, measured the coefficient of traction of 17 lubricants on a twin-disk traction tester at both high and low contact pressures and surface speeds. The traction fluids in his tests showed substantially higher coefficients of traction than all of the commercial naphthenic mineral oils tested. The greatest differences occur at relatively low pressures and high surface speeds (fig. 13). At relatively high pressures and low speeds the traction fluids show less of an advantage. Under such conditions a good quality naphthenic mineral oil would serve almost as well. However, for most traction-drive applications there is considerable incentive to using a traction fluid, with expected traction improvements falling somewhere between the two examples of figure 13.

What is noteworthy about the traction curves in figure 13 is the way they illustrate the common and important tendency of traction fluids to solidify into a plastic material at far lower pressures and high speeds than conventional oils (e.g., see the work of Blair and Winer, ref. 54). This is the basic reason why the traction coefficient for the two traction fluids are already at high levels in figure 13(a), while those for the mineral oils need substantially higher pressure to attain high levels as indicated in figure 13(b). The tendency for early solidification has a lot to do with what makes a traction fluid a traction fluid.

# Capacity and Durability

### Failure Criteria

Traction drives, like rolling-element bearings are generally sized on the basis of rolling-element fatigue life. This is because, for most applications, other than those that are particularly short-lived, the stress levels required for acceptable fatigue life are generally well below those for static yield failure. Because of these relatively low maximum operating stress levels, traction drives can generally tolerate shock loads several times the maximum design value without plastic deformation or other ill effects. This is contrary to the misbelief that traction drives are particularly vulnerable to sudden overloads. Furthermore, if these transient overloads are brief and do not occur too frequently, only a relatively small penalty to the drive's total fatigue life will result.

LOW PRESSURE, HIGH SPEED

MAXIMUM HERTZ PRESSURE • 1. 09 GPa
SURFACE VELOCITY • 8.3 m/sec
OIL IN TEMPERATURE • 50°C

HIGH PRESSURE, LOW SPEED

MAXIMUM HERTZ PRESSURE = 1. 86 GPa
SURFACE VELOCITY • 0.83 m/sec
OIL TEMPERATURE • 50°C
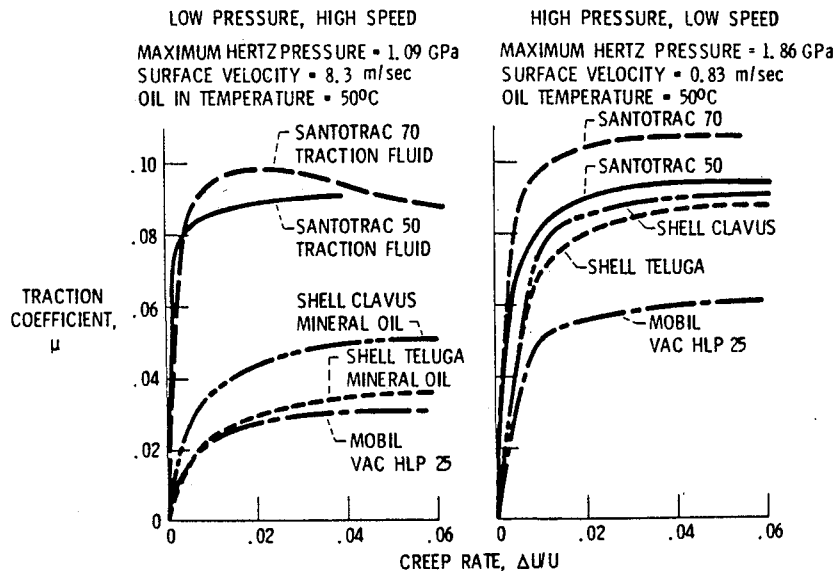
Figure 13. - Traction characteristics of a traction fluid compared with mineral oils (ref. 44).

A traction drive's sensitivity to shock loads is also dependent on the ability of the contact surface to avoid skidding or heating damage. If the drive is equipped with a fast-acting loading mechanism, skidding is unlikely. Also the transient nature of shock loads is such that there is usually insufficient time to overheat the contact, thus avoiding surface damage. However, sustained overloads can cause a thermal breakdown of the EHD film leading to failure.

## Fatigue Life

The normally expected failure mode of a properly designed traction drive will be rolling-element fatigue. This failure criterion is exactly analogous to pitting failure in gears and spalling failure in rolling-element bearings. The risk of wear or scuffing failures of traction drive contacts can be eliminated or greatly minimized through the use of proper materials and also proper lubricating and cooling design practices such as those that have been successfully applied in bearing and gear design. In view of this similarity in the failure mechanism, rolling-element bearing fatigue-life theory can be used to determine the expected service life of a traction drive.

In 1947 Lundberg and Palmgren (ref. 29) published a statiscal theory for the failure distribution of ball and roller bearings. They theorized that subsurface-originated fatigue pitting was due to high stresses developed at a subsurface defect in the bearing material. The probability of failure was related to the value of the maximum orthogonial reversing shear stress, the depth below the surface where this stress occurs and the volume of material that is being stressed. This is the theory on which bearing manufacturers, still today, base ball and roller bearing service-life ratings.

In 1971 an ASME life adjustment factors guide (ref. 55) was published to adjust the life ratings predicted by Lundberg and Palmgren analysis for recent advancements in bearing design, materials, processing, and manufacturing techniques.

In 1976 Coy, et al. (ref. 56), published a contact fatigue-life analysis for traction drives based on Lundberg-Palmgren theory. This analysis was used to predict the service life of a toroidal traction drive. In a.1980 publication, Rohn, et al. (ref. 57), presented a simplified version of this fatigue-life analysis and used it to show the effects of torque, size, speed, contact shape, traction coefficient, and number of multiple contacts on the predicted drive life. Their results show that multiple, load-sharing arrangements significantly benefit torque capacity and drive life, and that fatigue life is proportional to the 8.4 power of size for constant torque and traction coefficient.

The aforementioned Lundberg-Palmgren fatigue life analyses can be used with reasonable certainty to determine the durability characteristics of most traction drives. However, not presently considered in the analyses is a means to account for the potentially adverse effects of traction. Some

133

investigators (ref. 58) have found up to a several-fold decrease in rolling-element fatigue life when relative sliding and traction have been introduced; while others (ref. 59) have observed no change or even an improvement in fatigue life, depending on the direction of the applied traction force. A new analytical fatigue-life model, proposed by Tallian, et al. (ref. 60), considers the effects of surface traction on surface and subsurface-originated spalling. This work is significant because it addresses surface spalling, the more likely fatigue failure mode of gear and traction drive contacts. However, in its present form, the model requires many metallurgical and surface microgeometry parameters, which are not readily available. Thus, the utility of the analysis is, at present, limited. Also, there are currently insufficient test data to properly substantiate this model or to develop universal fatigue-life adjustment factors for the possible negative effects of surface traction. An element of conservatism is in order when establishing service life ratings based on current prediction methods.

## Materials

Earlier traction drives were not exploited to their full potential because of uncertainties regarding their longterm reliability. The limited durability characteristics of the materials used in these drives was a major contributing factor. The substitution of oil-lubricated, hardened steel roller components in place of rubber or reinforced plastic running dry against cast-iron parts raises their load capacity by at least an order of magnitude (ref. 27).

Because of the similarity in operating conditions, hardened bearing steels are logical choices for traction-drive rollers. Today's bearing steels are of significantly higher quality than the traditional air-melted, AISI 52100 steels used in rolling-element bearings since the 1920's. The introduction of vacuum remelting processes in the late 1950's has resulted in more homogeneous steels with fewer impurities and have extended rolling-element bearing life several-fold (ref. 61). Life improvements of eight times or more are not uncommon according to reference 55. This reference recommends that a life-improvement factor of six be applied to Lundberg-Palmgren bearing life calculations when using modern vacuum-melted AISI 52100 steel. A similar life-improvement factor is applicable to traction-drive life calculations. This improvement in steel quality in combination with improvements in lubricant traction performance have increased the torque capacity of traction drives several-fold.

# Performance Predictions

## Contact Traction

The distribution of local traction forces in the contact of an actual traction drive can be rather complicated as illustrated in figure 14. This figure shows the distribution of local traction vectors in the contact when longitudinal traction, misalinement, and spin are present. These traction forces will aline themselves with the local slip velocities. In traction-drive contacts some combination of traction, misalinement, and spin are always present. To determine the performance of a traction-drive contact, the elemental traction forces must be integrated over the contact area.

Because of the parabolic pressure distribution, the elemental traction forces are largest near the center of the contact and diminish in magnitude near the contact perimeter. As expected, in the case of longitudinal traction (fig. 14(a)), the forces aline themselves in the rolling direction. With the addition of misalinement (fig. 14(b)), a sideslip velocity is introduced causing the vectors to cock in line with the sideslip angle. Using conical rollers generally results in a circumferential slip pattern referred to as spin (fig. 14(c)). This rotary motion is due to the fact that the contact is in pure rolling only at its center. At the right hand edge of the contact the upper roller is sliding over the lower roller because of the mismatch in contact radii. At the left hand edge the situation is reversed and so is the direction of slip. Because of solid-body rotation, a complete pattern of spin exists over all of the contact.

The power throughout the contact is determined from a summation of the traction force components alined in the rolling direction times their respective rolling velocities. It is clear that in misalinement only a portion of the traction force is generating useful traction and that the remainder is generating useless side force. For pure spin no useful traction is developed, since the elemental traction forces cancel one another. Since the contact power loss is proportional to the product of the elemental traction forces and slip velocities, the presence of spin and misalinement can significantly
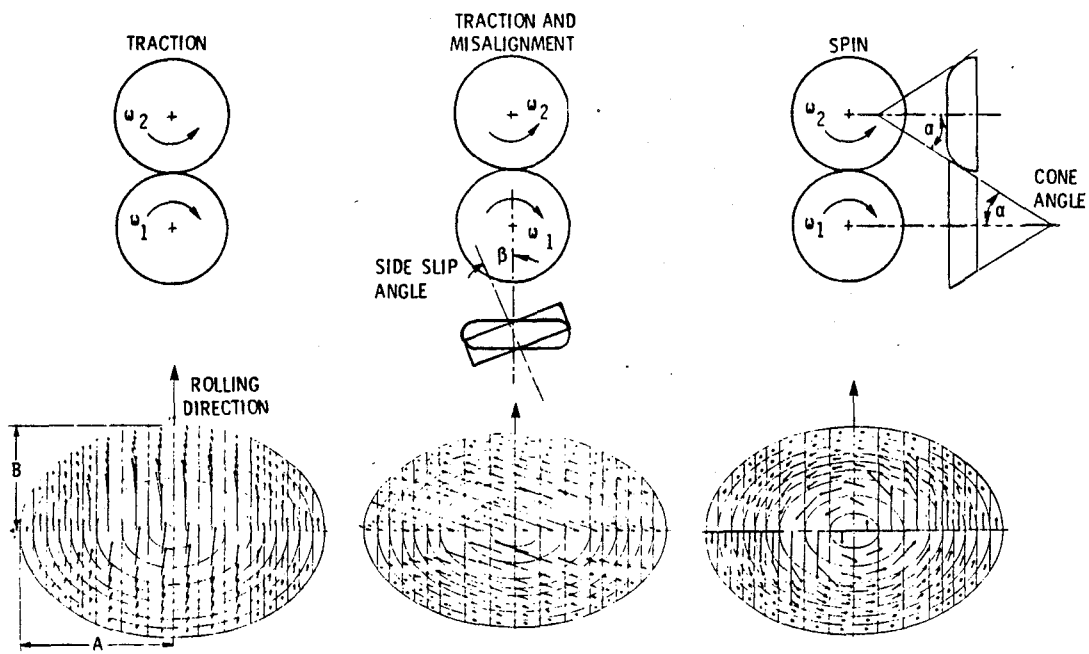
134

Figure 14. - Effect of misalinement and spin on contact traction force vectors.

decrease the efficiency of the contact. Furthermore, both conditions lower the available traction coefficient and reduce the amount of torque that can be transmitted safely. Designs that minimize spin and side slip can be quite efficient. Contact efficiency of 99 percent or higher are possible.

## Traction Experiments

Although there have been previous attempts to analyze the losses associated with ball bearings (ref. 62), the first systematic attempt to research the losses of traction-drive contacts occurred at the "Institut Fur Maschinenelemente und Forder Technik" located at the Technical University of Braunschweig in Germany between 1955 and 1960 (refs. 63 to 67). These investigations, which are summarized in an excellent manner by Wernitz (ref. 68), include analysis and test work on both simple traction contact test machines and on a commercially available Kopp ball variator. Tables and plots were developed which permit the calculation of friction losses due to creep (microslip) and spin (circumferential slip). This analysis treats the EHD film in the contact as behaving as perfectly plastic, that is, the material yields at some critical shear stress, exhibiting no elastic behavior. This model gives satisfactory results for contacts experiencing relatively high local strain rates such as those drives that have moderately high spin. In reference 69 Magi takes a similar, but more general approach and gives examples with experimental justification.

In the United States some of the earliest investigations into traction contact phenomena as they relate to traction drives were conducted by Hewko (refs. 42, 43, and 70). As mentioned earlier, Hewko (ref. 42) obtained basic traction performance data for various roller geometries, operating conditions and lubricants. He later extended much of these data to roller contacts that operate at very high surface speeds (up to 127 m/sec) (ref. 23). Much of this test information served as a data base for the construction of several fixed-ratio, simple planetary traction drives, of the type used in English life boats back in the 1930's (ref. 71). One of these units, a 6.25 to 1 speed reducer attached to a 4.5-kW electric motor, was used as the main drive for General Motors oceanographic submarine. A second, 6 to 1 reduction ratio drive delivering 373 kW at 8000 rpm was built for a turbine-powered torpedo system. In reference 70 Hewko compared the efficiency and noise characteristics of a 75-kW, 3.5 to 1 ratio, planetary tracton drive with that of a class 8, planetary gear drive of similar size, ratio, and power capacity. His test results showed that the traction drive had not only better part-load efficiency but provided substantial noise reductions as well. An overall sound pressure level of just 70 dB, about conversation noise level, was recorded for the traction drive at a particular operating condition. By contrast, at this same condition the gear drive registered 94 dB, or 16 times the noise of

135

the traction drive. The set of noise signature traces from this experiment with the integrated overall sound pressure levels appear in figure 15 (ref. 70). The quiet running characteristics of traction drives are undoubtedly appreciated by those who design drive systems for passenger carrying vehicles or for factory equipment under current OSHA noise standards.

## Theory

In the 1960's numerous papers were presented on the prediction of traction in EHD contacts. Some of these included Cheng and Sternlicht (ref. 72), Bell, Kannel, and Allen (ref. 73), and Dowson and Whitaker (ref. 74). In the early 1970's simplifications and refinements in the traction models took place as exemplified by Dyson (ref. 37), Kannel and Walowit (ref. 75), and Trachman and Cheng (ref. 39).

About this time, Poon (ref. 76) and Lingard (ref. 77) developed grid methods to predict the available traction forces of a contact experiencing spin. Poon's method utilized the basic traction data from a twin-disk machine together with contact kinematics to predict the available traction. Lingard used a theoretical approach in which the EHD film exhibited a Newtonian viscous behavior at low shear rates until a critical limiting shear stress was reached. At this point the film yielded plastically with increasing shear rate. This model showed good correlation with experimental traction data from a toroidal, variable-ratio drive of the Perbury type. This same model was also used successfully by Gaggermeier (ref. 44) in an comprehensive investigation of the losses and characteristics of traction-drive contacts. In addition to copious amounts of twin-disk traction data for numerous lubricants under various combinations of slip, sideslip, and spin, Gaggermeier (ref. 44) also investigated the sources of power losses of an Arter type toroidal drive. His findings were that, of the total power losses, the load-dependent bearing and drive idling (no-load) losses were always greater than the losses due to traction power transfer. This underscores the need to pay close attention to these tare losses in order to end up with a highly efficient traction drive.

The most recent and perhaps most comprehensive traction contact model is that proposed by Johnson and Tevaarwerk (ref. 40). Their model covers the full range of viscous, elastic, and plastic behavior of the EHD film. The type of behavior depends on the Deborah number, a relative measure of elastic to inelastic response of the lubricant film, and the strain rate. At low pressures and speeds (low Deborah number), the film exhibits linear viscous behavior at low strain rates, becoming increasingly more nonlinear with increasing strain rate. At higher pressures and speeds, more typical of traction-drive contacts, the response is linear and elastic at low rates of strain. At sufficiently high strain rates, the shear stress reaches some limiting value and the film shears plastically as in the case, of some of the earlier traction analytical models.
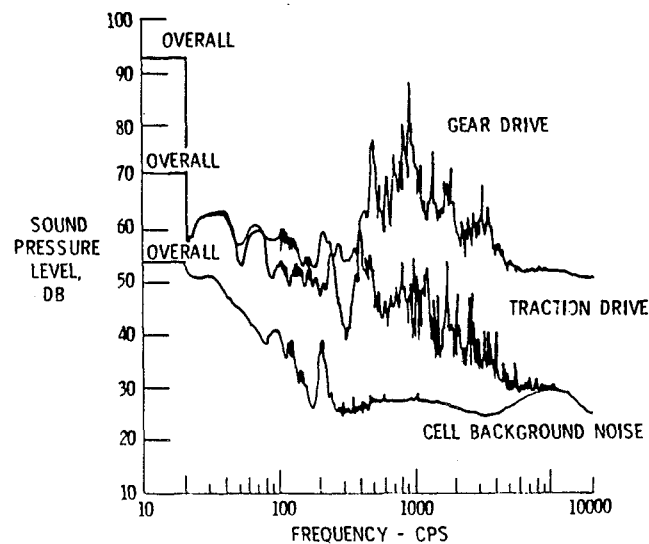


Figure 15. - External noise spectra for traction drive compared with planetary gear reducer at 2000 rpm input speed and 136 N-m input torque (ref. 70).

136

In reference 48 Tevaarwerk presents graphical solutions developed from the Johnson and Tevaarwerk elastic-plastic traction model. These solutions are of practical value in the design and optimization of traction-drive contacts. By knowing the initial slope (shear modulus) and the maximum traction coefficient (limiting shear stress) from a zero-spin/zero-sideslip traction curve, the traction, creep, spin torque, and contact power loss can be found over a wide range of spin values and contact geometries.

Figure 16 shows that this analysis compares favorably with test data, taken from experiments of Gaggermeier (ref. 44). The observed, pronounced reduction in the available traction coefficient with just a few degrees of misalinement, underscores the need to maintain accurate alinement of roller components in traction drives.

The Johnson and Tevaarwerk model, like many of the previous theories, provides an isothermal solution to the ascending portion of the traction curve. Under most circumstances the results from this isothermal analysis are quite satisfactory from a design standpoint. However, at higher surface speeds and for substantial spin, thermal effects start to become important. In reference 78 Daniels introduces a temperature-dependent elastic shear modulus term into the model, but this seems to have a rather weak effect on the results. Using an elaborate heat balance computer analysis, Tevaarwerk (ref. 79) in 1979 was able to correctly predict the heating effects occurring in a traction contact; but his solution is a bit too formidable for general design purposes. In reference 80 Tevaarwerk presents a simple, empirical technique to predict the thermally influenced, large-spin, traction curve from the large slip portion of a no-spin traction curve, but this requires knowledge of the full curve, which is not always available. Simpler analytical techniques are now being investigated (refs. 81 and 82) to better predict how heat generation within the contact affects the available traction coefficient.

## Fluid Traction Data

To be able to apply the aforementioned traction drive, certain fundamental fluid properties, namely, the lubricant's shear modulus and limiting yield shear stress, must first be known under the required operating speeds, pressures, and temperatures. Because of the difficulty of simulating the highly transient nature of an actual traction contact, the most reliable basic fluid property data are deduced, using methods described in reference 44, from the initial slope and maximum traction coefficient of an experimental traction curve. Unfortunately, there has been a general scarcity of these types of data over sufficiently broad enough operating conditions for design purposes. Recently, experimental traction data were obtained under a NASA program for both the Monsanto and Sun Oil traction fluids over a range of speeds, pressures, temperatures, spin, and sideslip values that might be encountered in traction drives (ref. 45). A regression analysis applied to the data resulted in a correlation equation that can be used to predict the initial slope and maximum traction coefficient at any intermediate operating condition (ref. 45).

# Recent Developments

During the past 5 years, several traction drives, which incorporate much of the latest technology, have reached the prototype stage. Laboratory tests and design analysis of these drives show them to have relatively high-power densities and, in some cases, to be ready for commercialization.

## Nasvytrac Drive

Although light-duty variable-ratio traction drives have been reasonably successful from a commercial standpoint, very few, if any, fixed-ratio types have progressed past the prototype stage. This is somewhat surprising in view of the outstanding ability of traction drives to provide smooth, quiet power transfer at extremely high or low speeds with good efficiency. They seem particularly well suited for high-speed machine tools, pump drives, and other turbomachinery. In other industrial applications they offer potential cost advantages because traction rollers should not be much more expensive to manufacture in quantity than ordinary rollers in roller bearings.

In terms of earlier work on fixed-ratio traction drives, the developmental effort at General Motors Research Laboratories on their planetary traction drive (as described by Hewko (ref. 70)),
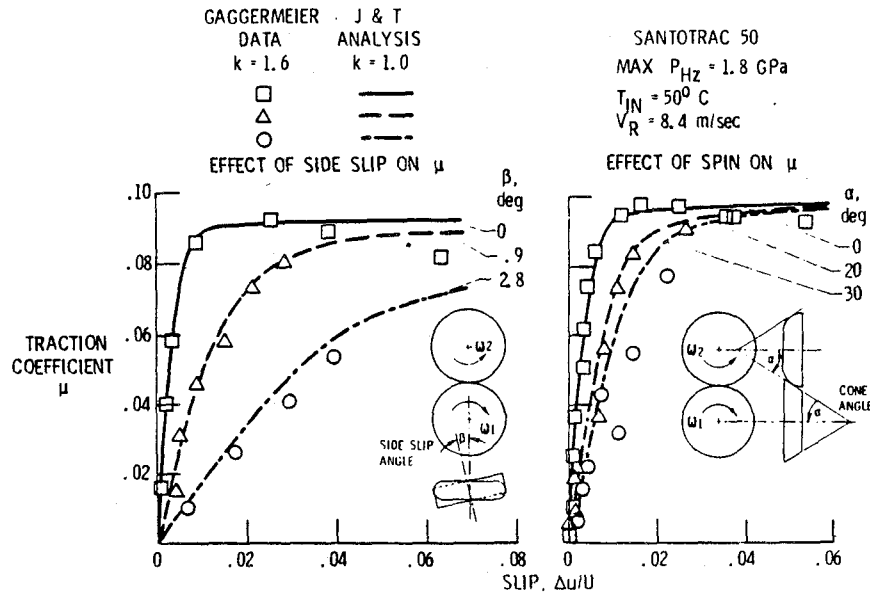
Figure 16. - Comparison of Johnson and Tevaarwerk analysis (ref. 48) with Gaggermeier test data (ref. 44).

was perhaps the most complete. As mentioned earlier, several of these drives were built and tested, including a 6-to-1 ratio, 373-kW unit for a torpedo and a 3.5-to-1 ratio, 75-kW test drive. This last drive exhibited better efficiency and lower noise then a comparable planetary gear set.

Interest in fixed-ratio traction drives is also high outside of the United States. Tests were recently conducted in Japan on a planetary traction drive of a construction similar to the General Motors unit for use with a gas-turbine auxilliary propulsion unit (APU) system (ref. 83). Planetary traction drives have also been studied in Finland.

The traction drives described thus far have a simple, single-row planet-roller format. For drives like these the number of load sharing planets is inversely related to the speed ratio. For example, a four-planet drive would have a maximum speed ratio of 6.8 before the planets interfered. A five-planet drive would be limited to a ratio of 4.8 and so on.

A remedy to the speed ratio and planet number limitations of simple, single-row planetary systems was devised by Nasvytis (ref. 84). His drive system used the sun and ring-roller of the simple planetary traction drive, but replaced the single row of equal diameter planet-rollers with two or more rows of "stepped" or dual-diameter planets. With this new "multiroller" arrangement, practical speed ratios of 250 to 1 could be obtained in a single stage with three planet rows. Furthermore, the number of planets carrying the load in parallel could be greatly increased for a given ratio. This resulted in a significant reduction in individual roller contact loading with a corresponding improvement in torque capacity and fatigue life.

In reference 84 Nasvytis reports the test results for several versions of his multiroller drive. The first drive tested was a 373-kW (500-hp) torpedo drive of three-planet row construction with a reduction ratio of 48.2 and an input speed of 53 000 rpm. The outside diameter of the drive itself was 43 cm (17 in.), and it weighed just 930 N (210 lb) including its lightweight magnesium housing. It demonstrated a mechanical efficiency above 95 percent. To investigate ultrahigh-speed operation, Nasvytis tested a 3.7-kW (5-hp), three-row, 120-to-1 ratio speed increaser. The drive was preloaded and operated without torque at 480 000 rpm for 15 min and ran for 43 consecutive hr at 360 000 rpm without lubrication but with air cooling. Two back-to-back drives were operated for 180 hr at speeds varying from 1000 to 120 000 rpm and back to 1000 rpm. They transmitted between 1.5 and 2.2 kW (2 and 3 hp). Another 3.7-kW (5-hp), three-row speed increaser, with a speed ratio of 50, was tested for more than 5 hr at the full rated speed of 150 000 rpm with oil-mist.lubrication and air cooling. It successfully transmitted 3.7 kW (5 hp) at 86 percent efficiency (ref. 84).

138

The basic geometry of the Nasvytis traction (Nasyvtrac) drive is shown in figure 17. Two rows of stepped planet-rollers are contained between the concentric, high-speed sun roller and low-speed ring rollers. In the drive shown the planet rollers do not orbit but are grounded to the case through relatively low-speed and lightly loaded reaction bearings that are contained in the outer planet row only. The high-speed sun-roller and other planet bearings have been eliminated. The sun-roller and first row rollers float freely in three-point contact with adjacent rollers for location. Because of this floating roller construction, an excellent force balance situation exists even with thermal or mechanical housing distortion or with slight mismatches in roller dimensions.

Based on the inherent qualities of the Nasvytrac drive, a NASA program was initiated (refs. 85 and 86) to parametrically test two versions of the drive. These drives of nominally 14-to-1 ratio were tested at speeds to 73 000 rpm and power levels to 180 kW. Parametric tests were also conducted with the Nasvytis drive retrofitted to an automotive gas-turbine engine. The drives exhibited good performance, with a nominal peak efficiency of 94 to 96 percent and a maximum speed loss due to creep of approximately 3.5 percent. The drive package size of approximately 25 cm diameter by 11 cm wide (excluding shafting) and total weight of about 26 kg (58 lb) makes the Nasvytrac drive, with a rated mean life of about 12 000 hr at 75 kW and 75 000 rpm, size competitive with the best commercial gear drive systems.

A 70 000 rpm, 10.8-to-1-reduction-ratio Nasvytrac drive weighing just 4 kg was designed and built for a long-life, rocket-engine pump drive system to drive the low-speed liquid-oxygen and liquid-hydrogen boost pumps (ref. 87). Either an auxilliary turbine or a gear drive off the main pump can be used. Use of an auxilliary turbine complicates the design, while gear drives were not well suited for this application because they wore badly in a matter of 20 min or so in this hostile cryogenic environment. This fell far short of the 10-hr life requirement envisioned for future, reuseable rocket engines. The relatively low sliding characteristics of the Nasvytrac drive, coupled with its demonstrated ability to run for long periods of time unlubricated, make it an excellent candidate for this application. Preliminary tests on this drive in liquid oxygen, including tests in which the drive was repeatedly accelerated under full power (15 kW) to 70 000 rpm in 5-sec intervals, showed it to perform satisfactorily (ref. 87). Cumulative operating times up to an hour have been recorded. Future work is needed to realize the 10-hr life goal, but the potential of this transmission for this application has been clearly demonstrated.

Current work with variations of the Nasvytis traction-drive concept are underway at NASA. A recently fabricated, 370-kW (500-hp) helicopter main rotor transmission combines the best features of gears with traction rollers. This experimental hybrid transmission, which offers potential cost, noise, and reliability benefits, will be tested shortly. Test of a 2240-kW (3000-hp) hybrid, twin-engine helicopter transmission is also planned. This 81-to-1-reduction-ratio, traction transmission will be the most powerful ever tested, carrying an output torque in excess of 73 000 N·m (650 000 in·lb) in an estimated 515-kg package. Hybrid and pure-traction Nasvytis drives are also being considered for wind-turbine applications where a low-cost but highly reliable speed increaser is needed to drive the high-speed alternator. Also, tests are being conducted on an infinitely variable-ratio Nasvytis drive, but the performance data are still too preliminary to be reported here.

## Promising Variable Speed Drives

Taking advantage of the latest technology, several designers have attempted to develop traction CVT's for automotive use. The potential of improving the city fuel mileage 20 to 25 percent, or more, of cars normally equipped with three- or four-speed automatic transmissions (ref. 88) or of doubling the fuel mileage in the case of flywheel equipped cars (ref. 89) has been the major incentive for the resurgence in automotive CVT research and development. These applications represents a significant challenge, since compactness, efficiency, cost, and reliability are all at a premium.

*Perbury CVT.* – One such automotive effort is that being conducted by BL Technology, Ltd., formerly British Leyland, on a Perbury, double-cavity toroidal drive. This concept is rather old (first patented in the U.S. by C. W. Hunt in 1877). It is also rather well-explored, as mentioned earlier, having been investigated by the General Motors Research Laboratory in the early 30's and late 50's, demonstrated in a 1934 Austin-Hayes, later in a 1957 Hillman-Minx, and also in a 1973 Ford Pinto, but with offset rollers.

FIRST ROW OF PLANET ROLLERS

SUN ROLLER

SECOND ROW OF PLANET ROLLERS

KING ROLLERS

AUTOMATIC LOADING MECHANISM
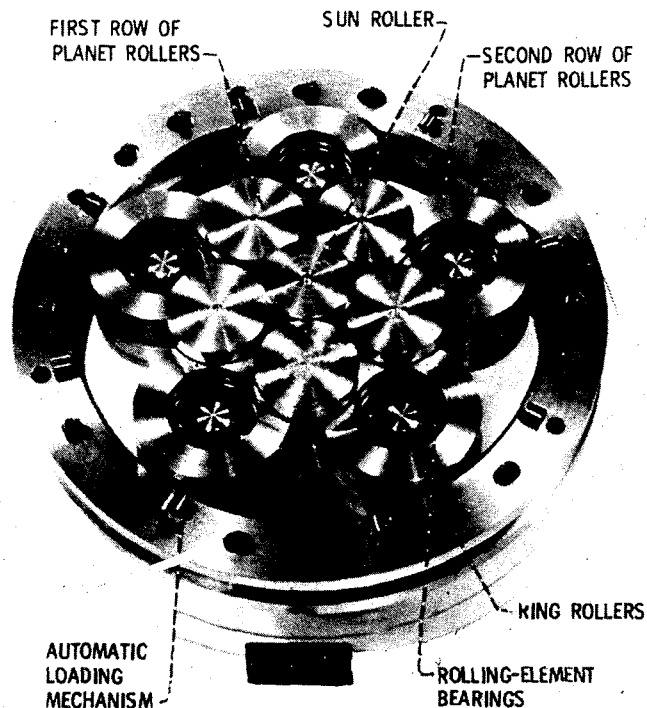
ROLLING-ELEMENT BEARINGS

Figure 17. - Geometry of the Nasvytis traction (Nasvytrac) test drive (ref. 85).

In 1977 Lucas Aerospace in England adapted the Perbury drive for maintaining constant frequency of the AC generators on the Sidley Hawker Harrier, a VSTOL jet fighter. This single cavity, toroidal drive is suitable for driving aircraft generators having output ratings up to 30 kV A. More than 20 years before this, Avco Lycoming, in the U.S., also offered a line of mechanical constant-speed drives based on the toroidal traction-drive principle. They were used on several aircraft in the 50's, including the Douglas A-4E fighter, but have long since been discontinued.

In the case of the Leyland-Perbury automotive CVT (fig. 18; ref. 90), the double-toroidal drive cavities have six tiltable transfer rollers between input and output toroids. A hydraulically controlled linkage system can tilt these rollers from one extreme position to another. By combining this toroidal drive with a two-range, output planetary gear system, the overall transmission ratio range is greatly expanded.

The BL/Perbury transmission was installed in a medium size test car having a four-cylinder, 60-kW engine. The test car showed fuel mileage improvement of 15 to 20 percent for an average mix of European driving (ref. 90). Also, acceleration times were comparable with a manual transmission car having 10 percent higher power to weight ratio and driven by a skilled driver. However, the future production picture for this transmission is not clear.

*Vadetec CVT.* – A promising traction CVT that is of a rather new vintage is the nutating drive being developed by Vadetec Corp. As shown in figure 19 (refs. 91 and 92) a double-conical-roller assembly, complete with an automatic loading mechanism, is mounted at an angle in a drive cylinder that is driven by the input shaft. As the input shaft rotates, the double-cones perform a nutating motion and at the same time are forced to rotate about their own axis as they make drive contact with a pair of moveable control rings. These rings are grounded to the housing but can be axially moved together or apart. A gear pinion attached to the end of the cone shaft orbits the output shaft axis at input shaft speed, while spinning about its own axis, due to cone rotation, in the opposite direction. By varying the axial position of the control rings, the rolling radius of the cones can be synchronously changed. This, in turn, causes a change in rotational speed of the cone shaft pinion but does not affect the pinion's rotating speed, which occurs at input shaft frequency.

Since the cone shaft pinion is in driving engagement with the ouput shaft through one of several possible interchangeable gear arrangements, the variation in pinion rotational speed causes a
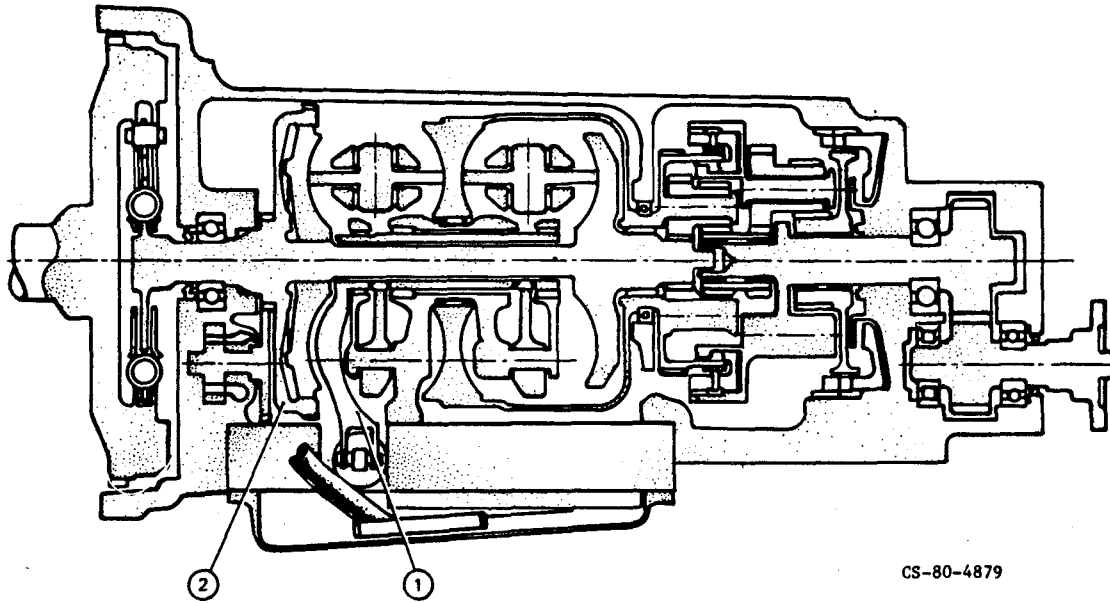
Figure 18. - BL Technology/Perbury traction CVT, 60-kW passenger car test installation (ref. 90).
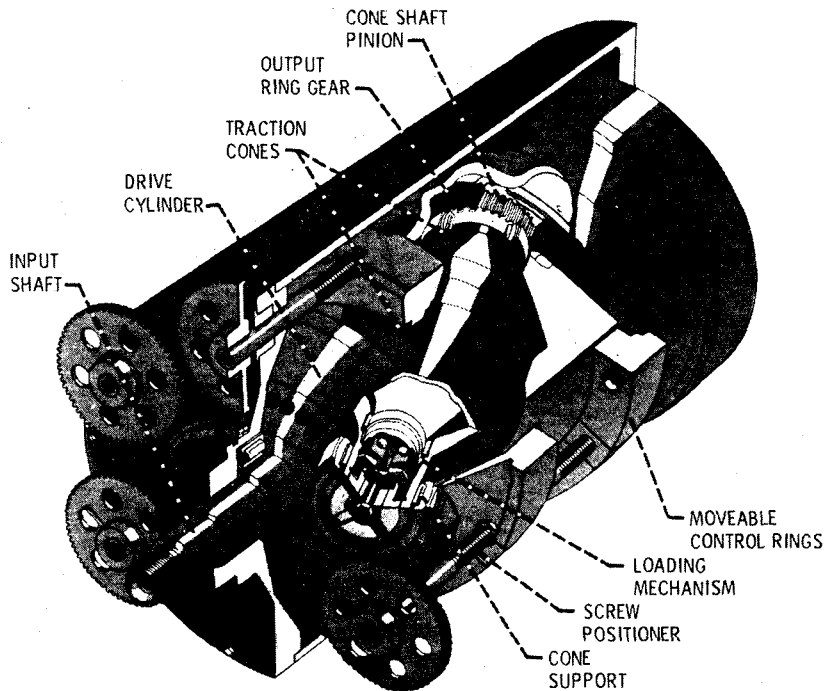


Figure 19. - Vadetec nutating traction CVT. (Courtesy of Vadetec Corp., Troy, Michigan.)

corresponding variation in output shaft speed. By changing the output gearing, the pinion speed can either vectorially subtract from pinion/input shaft orbital speed, allowing the ouput shaft speed to reach zero, if desired, or vectorially add to input orbital speed. The latter arrangement results in a transmission with only overdrive capability.

A couple of Vadetec CVT's have already been built and tested. One of these prototypes has shown successful operation as part of a tractor drive train. Although this transmission is still in the development and acceptance stage, it is a good example of the new breed of traction drive.

141

*Fafnir CVT.* – A planetary, cone roller type CVT under development by the Fafnir Bearing Division of Textron appears in figure 20 (ref. 93). This transmission is directed toward the mobile equipment market, particularly as a replacement to hydrostatic transmission in garden and light-duty tractors up to about 37 kW (50 hp). A set of double-sided, conical traction rollers are trapped between a pair of inner races and a pair of outer races. The conical rollers are mounted in a carrier that drives the planet gears in the output gear differential. The gear differential serves the purpose of expanding the limited ratio range of the traction drive to cover output speeds from forward to reverse, if desired. This is an example of power-recirculating transmission. The traction inner races are splined to the sun gear shaft of the planetary which is, in turn, keyed to the input shaft. To change the ratio, the outer traction race halves, which are grounded to the housing, can be either manually or hydraulically, in a later version, pushed together or spread apart. This causes the cone rollers' rolling radii at the outer-race contact to increase or decrease while simultaneously causing the opposite to occur at the inner-race contact. The change in rolling radii causes a corresponding change in the orbit speed of the cones and, thus, output-shaft speed. Because the inner-race load-springs, the transmission automatically "down shifts" with increased load. The current design was specifically intended to be one of low cost with maximum flexibility, so a single range output planetary was selected. Consequently, a high degree of power recirculation exists, limiting efficiency to about 85 percent maximum for the current design (ref. 6). A more efficient version would be needed for automotive applications.

*Other traction CVT's.* – The traction developments previously cited are by no means the only efforts underway. Many of the industrial manufacturers are no doubt upgrading the ratings of their systems by taking advantage of the latest technology. Furthermore, variations of older concepts are being re-evaluated and upgraded with design improvements. Two notable examples are the AiResearch toroidal drive and the Bales-McCoin cone-roller CVT. Both of these systems were carried to the preliminary design stage under a NASA contract for DOE to develop CVT's for use in advanced electric vehicles.

The AiResearch design (ref. 94) is a double-cavity toroidal CVT, containing two power rollers per cavity. The double toroidal drive elements, similar in many respects to the toroidal drive units mentioned earlier, are permanently connected to differential gearing.

The Bales-McCoin unit (ref. 95) consist of a central input traction roller surrounded by four cone-rollers which in turn are connected to the output planetary differential via idler gears. The cones are hydraulically loaded against the central roller using a novel microprocessor control system. Based on current slip rate signals, the control system adjusts the normal load between rollers to the minimum required to prevent significant roller slip at any given oprating condition.

Both of the above CVT's are in early stages of development. Estimated weights and sizes of these transmissions are comparable with equivalent conventional automatic transmissions, and calculated efficiencies are generally in the low 90's. General information on these CVT's can be found in reference 96.
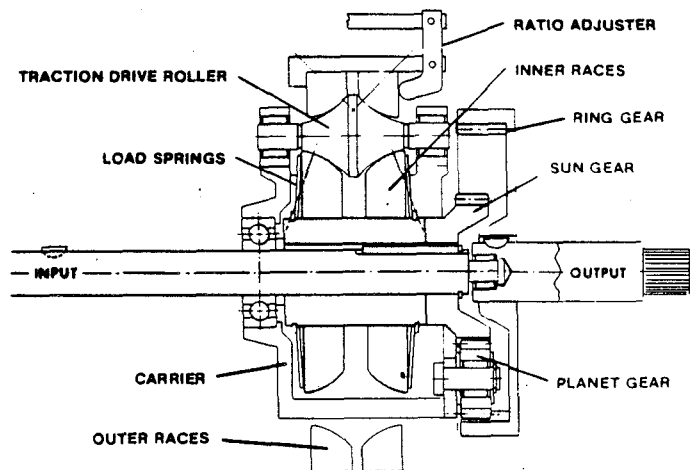


Figure 20. - Fafnir Bearing Division's planetary cone roller traction drive (ref. 93).

# Future Technology Requirements

Although there has been significant progress within the last decade in the development of technology for traction drives, future refinements in certain areas are still needed.

## Traction Fluids

Today's traction fluids are far superior to the earlier lubricants used in traction drives. However, modern traction fluids generally have poor viscosity index characteristics. At temperatures well below freezing, traction fluids can be too viscous to pour properly. Pour-point suppressents such as those incorporated in conventional oils for Arctic service might help.

Traction fluids and the additives that they contain have a tendency to capture and retain air at temperatures below about 70° C. Aeration of the oil is undesirable from both a cooling and hydraulic control system standpoint. This problem is minimized when the oil is subjected to some nominal pressure which tends to significantly condense trapped air bubbles, as occurs in the contact between rollers.

The key to faster and more powerful traction drives is the development of traction fluids whose coefficient of traction shows less degradation with higher surface speeds, operating temperatures, and contact spin. Higher traction at lower contact pressures is also desirable for drives that have extra long life requirements. Today's synthetic traction fluids appear to be reasonably stable but further work may be needed for "sealed-for-life" drive systems.

## Materials

Although today's bearing steels are well suited for traction drives, durability improvements and lower material costs are always welcome. Studies are required to determine if special coatings or nonmetallic materials might be useful in certain applications.

## Sizing and Design Criteria

Fatigue-life prediction methods based on Lundberg-Palmgren theory are available to size traction drives. These methods are well established for determining life ratings of rolling-element bearings. However, they tend to underestimate the fatigue life obtained with today's bearings. As a result, life-adjustment factors have been identified (ref. 55) to more accurately reflect the longer lives attendant with improved bearing materials, design, and manufacturing techniques. It is anticipated that many of these same life factors are also applicable to traction drives, but endurance test data are needed to corroborate this and to identify what life adjustment factors, if any, are needed.

The upper limit of power transfer for traction drives is relatively unexplored. Drives having power capacities of thousands of kilowatts can theoretically be constructed. Not enough is known about the practical thermal limits of traction contacts or their ability to tolerate transient slips under unusual circumstances. The fact that gear teeth regularly experience momentary slips of 30 or 40 percent on entering or leaving mesh suggest that transient slip values can be remarkably high.

Another important task is the establishment of a consistent, universally accepted design standard for traction drives, similar to those that currently exist for gear drives, bearings, and other mechanical components. The design guides of Wernitz (ref. 27) and Kraus (ref. 97), published about 20 years ago, were most welcome contributions to the field, but our basic understanding of traction phenomena has greatly improved during the interim. A clear, practical, and comprehensive guide for the design and assessment of traction transmissions would benefit the designer and user alike. The bulk of such a guide can probably be assembled from the wide spectrum of information that currently exists.

## Manufacturing

In principle, traction drives should be relatively inexpensive to make in large quantities. Manufacturing techniques are essentially the same as those used in the production of rolling-element bearings. To date, traction drives have been produced in relatively limited quantities or on special order and as a result have not yet realized their low cost potential.

# Summary

The evolution of traction-drive technology has been traced over the past 100 years. Some of the more prominent events in the development of traction drives appears in table II. This list is by no means intended to be comprehensive but, rather, to give the reader some appreciation of the scope of activities leading to traction drives of today.

The earliest of traction drives, constructed of wood, leather, or fiber-covered disks running in dry contact, found first use in factory equipment before the turn of the century. The ability of traction drives to smoothly and efficiently vary speed made them natural choices as main transmissions for several early vintage cars, such as those produced by Cartercar, Sears, Lambert, and Metz. Apparently, durability problems with the soft-material-covered disks used in these drives foreshortened their commercial success. In the 1920's traction drives equipped with oil-lubricated, hardened, steel rollers started to appear. These drives had much greater power capacity, and by the 1930's several industrial adjustable speed traction drives were being marketed both here and in Europe. About this time, there were several projects to develop toroidal traction car transmissions, notably the Hayes and later, the Perbury efforts in England and the General Motors' work in the United States. In the 1940's modern lubrication and fatigue theories for rolling-contact elements were developed, and these were later adapted to the design of traction drives. In the 1950's work began on identifying fluids with high traction properties and experiments on how these fluids actually behaved within the traction contact. A basic understanding was also obtained on how the fluid film within the contact was compressed into a thin, stiff, tenacious solid-like film across which considerable torque transfer could safely occur. By the end of the 1960's high-quality bearing steels and traction fluids were commercially available. The power capacity of traction drives using the new steels and fluids virtually tripled. In the 1970's improved traction models and fatigue-life prediction methods were developed. This all lead to the development of a new generation of traction drives—drives with a bright potential role to play in the power transmission industry.

In 1980 the Power Transmission and Gearing Committee of ASME took a major step in recognizing the potential viability of traction drives by establishing a subcommittee to follow the developments in the technology for these transmissions. A primary function of this subcommittee is to assist in the dissemination of technology related to traction drives and to foster their potential use in industry.

### TABLE II. - LIMITED CHRONOLOGY OF TRACTION DRIVE DEVELOPMENTS

| Date | Event |
|---|---|
| 1870 | Wooden friction drives used on wood-working machinery |
| 1877 | Hunt toroidal friction drive patented |
| 1906 | Friction drive equipped Cartercar introduced |
| 1921 | Automatic contact loading mechanism patented by Erban in Germany |
| 1923 | Oil lubricated, Arter industrial drive marketed in Switzerland |
| 1926 | Carter analyses creep between locomotive wheel and rail |
| 1928 - 1933 | General Motors Research Labs. road tests toric traction transmission |
| 1935 | Austin Motor Company offers Hayes Self-Selector toroidal transmission on Austin Sixteen |
| 1939 | EHD lubrication theory advanced by Ertel and, later, Grubin |
| 1947 | Lundberg and Palmgren develop fatigue theory for rolling elements |
| 1949 | Kopp Ball Variator commercially introduced in Switzerland |
| 1951 | Clark, et al., theorize oil solidifies in EHD contact |
| 1955 - 1962 | Braunschweig University experiments on traction contact phenomena in Germany |
| 1955 | Vacuum-melted bearing steels introduced |
| 1957 | Lane's experiments to identify high traction oils in England |
| 1962 - 1968 | Hewko's investigations into traction contact performance |
| 1965 | Nasvytis devises fixed-ratio, multiroller planetary drive |
| 1968 | Monsanto and Sun Oil introduce commercial traction fluids |
| 1976 | Coy, et al., apply Lundberg-Palmgren fatigue life theory to traction drive contacts |
| 1978 | Johnson and Tevaarwerk traction model applied to the design of traction drives |
| 1980 | ASME establishes traction drive committee |

Field experience has been gathered by industrial traction-drive manufacturers, some of whom have been making traction drives for more than 40 years. However, traction-drive technology is relatively young. The latest generation of traction drives has reached a high level of technical readiness. As these drives find their way into industrial service and as work continues in the laboratories, further improvements and increased usage of these drives can be expected.

## Concluding Remarks

In reviewing traction-drive developments through the years, it becomes evident that relatively few developments resulted from basic research. Technical advancements were largely due to individual organizations striving to perfect their own specific systems. As a consequence, meager fundamental information was left behind for those who followed. Of course, as this review has attempted to point out, there have been notable exceptions to this, but, by and large, relatively little is known about the reasons for the many commercial diasappointments that occurred along the way.

It is encouraging, at least to this writer, that there currently seems to be greater communication among people working in the field. Admittedly, their numbers are miniscule compared with those working in the bearing and gear disciplines. Nonetheless, traction-drive technology of late seems to be making good progress. This is due, in no small measure, to much of the fine work that has been performed on tribological fundamentals, common to all rolling-element components. It is likely, in the years to come, that traction drives will find an increasingly larger role to play in the power transmission industry.

## References

1. Knights, Edward H.: Knight's American Mechanical Dictionary. Vol. I. Hurd and Houghton, 1876, p. 680.
2. Trobridge: Census Office Report on Power and Machinery used by Manufacturer. Washington, 1888, p. 220.
3. Appleton's Cyclopedia of Applied Mechanics. Vol. II. D. Appleton and Co., 1880, pp. 36-37.
4. Yeaple, F.: Metal-To-Metal Traction Drives now have a New Lease on Life. Product Eng., vol. 42, no. 15, Oct. 1971, pp. 33-37.
5. Carson, R. W.: New and Better Traction Drives are Here. Mach. Des., vol. 46, no. 10, Apr. 18, 1974, pp. 148-155.
6. McCormick, D.: Traction Drives Move to Higher Powers. Des. Eng., Dec. 1980, pp. 35-39.
7. Hewko, L. O.: Traction Drives and Their Potential Role in Energy Conservation. Presented at the Joint ASLE Energy-Sources Technology Conference, New Orleans, LA, Feb. 1980.
8. Hamrock, B.; and Dowson, D.: Ball Bearing Lubrication. John Wiley & Sons, 1981.
9. Dudley, D. W.: The Evolution of the Gear Art. American Gear Manufacturers Association, 1969.
10. Drachmann, A. G.: The Mechanical Technology of Greek and Roman Antiquity. Lubrecht and Cramer, 1963, pp. 200-203.
11. Carson, R. W.: 100 Years in Review: Industrial Traction Drives. Power Transm. Des., vol. 19, no. 10, Oct. 1977, pp. 99-100.
12. Fellows, T. G.; et al.: Perbury Continuously Variable Ratio Transmission. Advances in Automobile Engineering, Pt. II, Pergamon Press (Oxford), 1964, pp. 123-142.
13. Heldt, P. M.: Automatic Transmissions. SAE J., vol. 40, no. 5, May 1937, pp. 206-220.
14. DeBono, E.: Eureca: An Illustrated History of Inventions from the Wheel to the Computer. Holt, Rinehart, and Winston, 1974, p. 33.
15. Hodges, D.; and Wise, D. B.: The Story of the Car. Hamlyn Publication Group, Ltd. (London), 1974, p. 18.
16. Sloan, Alfred P.: My Years with General Motors. Doubleday and Co., Inc., 1964.
17. Clymer, F., Historical Motor Scrapbook. Vols. 1 and 2. Clymer Motor Publications, 1944.
18. Caris, D. F.; and Richardson, R. A.: Engine-Transmission Relationships for High Efficiency. SAE Trans., vol. 61, 1953, pp. 81-96.
19. Improved Technology is Giving an Old Principle a New Drive. Monsanto Magazine, Summer 1974, pp. 14-16.
20. Carson, R. W.: Focus on Traction Drives: 100 Years of Traction Drives. Power Transm. Des., vol. 17, no. 5, May 1975, pp. 84 and 88.
21. Perry, F. G.: The Perbury Transmission. ASME Paper No. 80-GT-22, Mar. 1980.
22. Final Report on the Follow-On Phase of the Evaluation of the Wright Aeronautical Division Toroidal Drive Using a 1/4 Ton Military Truck as a Test Bed Vehicle. WAD R273-F, Curtis-Wright Corporation, Feb. 1966.
23. Carson, R. W.: Focus on Traction Drives. Power Transm. Des., vol. 17, no. 3, Mar. 1975, pp. 48-49.
24. Carson, R. W.: Today's Traction Drives. Power Transm. Des., vol. 17, no. 11, Nov. 1975, pp. 41-49.
25. Cahn-Speyer, P.: Mechanical Infinitely Variable Speed Drives. Eng. Dig. (London), vol. 18, no. 2, Feb. 1957, pp. 41-43.
26. Dvorak, D. Z.: Your Guide to Variable-Speed Mechanical Drives. Prod. Eng., vol. 34, Dec. 1963, pp. 63-74.

27. Wernitz, W.: Friction Drives. Mechanical Design and Systems Handbook, H. A. Rothbart, ed., McGraw Hill Book Co., Inc., 1964, pp. 14-1 to 14-22.

28. Grubin, A. N.: Fundamentals of the Hydrodynamic Theory of Lubrication of Heavily Loaded Cylindrical Surfaces. Investigation of the Contact of Machine Components, Kh. F. Ketova, ed., Translation of Russian Book No. 30, Central Scientific Institute for Technology and Mechanical Engineering, Moscow, 1949, Chapter 2. (Available from Department of Scientific and Industrial Research, Great Britain, Transl. CTS-235 and Special Libraries Association, Transl. R-3554.)

29. Lundberg, G. and Palmgren, A., "Dynamic Capacity of Rolling Bearings," Ingenioersvetenskapsakademian, Handlinger, No. 196, 1947.

30. Ertel, A. M.: Hydrodynamic Lubrications Based on new Principles. Prikl. Mat. Mekh., vol. 3, no. 2, 1939 (in Russian).

31. Martin, K. F.: A Review of Frictional Predictions in Gear Teeth. Wear, vol. 49, 1978, pp. 201-238.

32. Clark, O. H.; Woods, W. W.; and White, J. R.: Lubrication at Extreme Pressure with Mineral Oil Films. J. of Appl. Phys., vol. 22, no. 4, Apr. 1951, pp. 474-483.

33. Smith, F. W.: The Effect of Temperature in Concentrated Contact Lubrication. ASLE Trans., vol. 5, no. 1, Apr. 1962, pp. 142-148.

34. Plint, M. A.: Traction in Elastohydrodynamic Contacts. Proc. Inst. Mech. Eng. (London), vol. 182, no. 1, 1967, pp. 300-306.

35. Johnson, K. L.; and Cameron, R.: Shear Behavior of Elastohydrodynamic Oil Films at High Rolling Contact Pressures. Proc. Inst. Mech. Eng. (London), vol. 182, no. 1, 1967, pp. 307-318.

36. Crook, A. W.: Lubrication of Rollers. Pt. IV. Measurements of Friction and Effective Viscosity. Phil. Trans. Roy. Soc., London, Ser. A., vol. 255, no. 1056, Jan. 1963, pp. 281-312.

37. Dyson, A.: Frictional Traction and Lubricant Rheology in Elastohydrodynamic Lubrication, Phil. Trans. Roy. Soc., London, Ser. A., vol. 266, no. 1170, Feb. 1970, pp. 1-33.

38. Johnson, K. L.; and Roberts, A. D.: Observation of Visco Elastic Behavior of an Elastohydrodynamic Lubricant Film. Proc. R. Soc. (London), Ser. A., vol. 337, 1974, pp. 217-242.

39. Trachman, E. G.; and Cheng, H. S.: Thermal and Non-Newtonian Effects on Traction in Elastohydrodynamic Contacts. Symposium on Elastohydrodynamic Lubrication, Inst. of Mech. Eng. (London), 1972, pp. 142-148.

40. Johnson, K. L.; and Tevaarwerk, J. L.: Shear Behavior of Elastohydrodynamic Oil Films. Proc. R. Soc. (London), Ser. A., vol. 356, no. 1685, Aug. 1977, pp. 215-236.

41. Walowit, J. A.; and Smith, R. O.: Traction Characteristics of a MIL-L-7808 Oil. ASME Paper No. 76-Lubs-19, 1976.

42. Hewko, L. O.; Rounds, F. G., Jr.; and Scott, R. L.: Tractive Capacity and Efficiency of Rolling Contacts. Rolling Contact Phenomena, J. B. Bidwell, ed., Elsevier Publishing Co. (Amsterdam), 1962, pp. 157-185.

43. Hewko, L. O.: Contact Traction and Creep of Lubricated Cylindrical Rolling Elements at Very High Surface Speeds. ASLE Trans., vol. 12, no. 2, Apr. 1969, pp. 151-161.

44. Gaggermeier, Helmut: Investigations of Tractive Force Transmission in Variable Traction Drives in the area of Elastohydrodynamic Lubrication. Ph.D. Dissertation, Technical University of Munich, July 1977.

45. Tevaarwerk, J. L.: Traction Contact Performance Evaluation at High Speeds. NASA CR-165226, 1981.

46. Carter, F. W.: On the Action of a Locomotive Driving Wheel. Proc. R. Soc. (London), Ser. A., vol. 112, 1926, pp. 151-157.

47. Johnson, K. L.: Tangential Tractions and Micro-Slip in Rolling Contact. Rolling Contact Phenomena, J. B. Bidwell, ed., Elsevier Publishing Co. (Amsterdam), 1962, pp. 6-28.

48. Tevaarwerk, J. L.: Traction Drive Performance Prediction for the Johnson and Tevaarwerk Traction Model. NASA TP-1530, 1979.

49. Johnson, K. L.; Nayak, L.; and Moore, A. J.: Determination of Elastic Shear Modulus of Lubricants from Disc Machine Tests. Elastohydrodynamics and Related Topics: Proc. 5th Leeds-Lyon Symposium on Tribology, Mech. Eng. Publ. Ltd., 1979, pp. 204-213.

50. Lane, T. B.: The Lubrication of Friction Drives. Lubr. Eng., vol. 13, Feb. 1957, pp. 85-88.

51. Haseltine, M. W.; et al.: Design and Development of Fluids for Traction and Friction Type Transmissions. SAE Paper 710837, Oct. 1971.

52. Hamman, W. C.; et al.: Synthetic Fluids for High Capacity Traction Drives. ASLE Trans., vol. 13, 1970, pp. 105-116.

53. Loewenthal, S. H.; and Parker, R. J.: Rolling-Element Fatigue Life with Two Synthetic Cycloaliphatic Traction Fluids. NASA TN D-8124, 1976.

54. Blair, Scott; and Winer, W. O.: Shear Strength Measurements of Lubricants at High Pressures. J. Lubr. Tech., vol. 101, no. 3, July 1979, pp. 251-257.

55. Bamberger, E. N., et al.: Life Adjustment Factors for Ball and Roller Bearings—An Engineering Guide. Am. Soc. of Mech. Eng., 1971.

56. Coy, J. J.; Loewenthal, S. H.; and Zaretsky, E. V.: Fatigue Life Analysis for Traction Drives with Application to a Toroidal Type Geometry. NASA TN D-8362, 1976.

57. Rohn, D. A.; Loewenthal, S. H.; and Coy, J. J.: Simplified Fatigue Life Analysis for Traction Drive Contacts. J. Mech. Des., vol. 103, no. 2, Apr. 1981, pp. 430-439.

58. MacPherson, P. B.: The Pitting Performance of Hardened Steels. ASME Paper No. 77-DET-39, Sept. 1977.

59. Soda, N.; and Yamamoto, T.: Effect of Tangential Traction and Roughness on Crack Initiation/Propagation During Rolling Contact. NASA TM-81608, 1981.

60. Tallian, T. E.; Chiu, Y. P.; and Van Amerongen, E.: Predictions of Traction and Microgeometry Effects on Rolling Contact Fatigue Life. J. Lubr. Tech., vol. 100, no. 2, Apr. 1978, pp. 156-166.

61. Bamberger, E. N.: Materials for Rolling Element Bearings. Bearing Design—Historical Aspects, Present Technology, and Future Problems, Am. Soc. Mech. Eng., 1980, pp. 1-46.

62. Poritsky, H.; Hewlett, C. W., Jr.; and Coleman, R. E., Jr.: Sliding Friction of Ball Bearings of the Pivot Type. J. Appl. Mech., vol. 24, no. 4, Dec. 1947, pp. A-261 to A-268.

63. Lutz, O.: Grundsatzliches uber stufenlos verstellbare Walzgetriebe. Z. Konstruktion, vol. 7, 1955, p. 330; vol. 9, 1957, p. 169; vol. 10, 1958, p. 425.

64. Wernitz, W.: Walz-Bohrreibung-Bestimmung der Bohrmomente und Umfangskrafte bei Hertzscher Pressung mit Punktberuhrung. Vol. 19 of Schriftenreihe Antriebstechnik, Fr. Vieweg und Sohn, Braunschweig, 1958.

65. Maass, H.: Untersuchung uber die in elliptischen Hertzscher Flachen ubertragbaren Umfangskrafte, Dissertation, Technical University of Braunschweig, 1959.

66. Kutter, F.: Theoretische Untersuchung eines Reibgetriebes, Thesis, Technical University of Dresden, 1944.

67. Thomas, W.: Reibscheiben-Regelgetriebe (Linienberuhrung), Vol. 4 of the Schriftenreihe Antriebstechnik, Fr. Vieweg und Sohn, Braunschweig, 1954.

68. Wernitz, W.: Friction at Hertzian Contact with Combined Roll and Twist. Rolling Contact Phenomena, J. B. Biddwell, ed., Elsevier Publishing Co. (Amsterdam), 1962, pp. 132-156.

69. Magi, M.: On Efficiencies of Mechanical Coplanar Shaft Power Transmissions. Chalmers University, Gothenburg, Sweden, 1974.

70. Hewko, L. O.: Roller Traction Drive Unit for Extremely Quiet Power Transmission. J. Hydronautics, vol. 2, no. 3, July 1968, pp. 160-167.

71. New Departures in Automotive Ideas. New Departure Press, 1937, pp. 5-6.

72. Cheng, H. S.; and Sternlicht, B.: A Numerical Solution for the Pressure, Temperature, and Film Thickness Between Two Infinitely Long Lubricated Rolling and Sliding Cylinders under Heavy Loads. J. Basic Eng., vol. 87, no. 3, Sept. 1965, pp. 695-707.

73. Bell, J. C.; Kannel, J. W.; and Allen, C. M.: The Rheological Behavior of the Lubricant in the Contact Zone of a Rolling Contact System. J. Basic Eng., vol. 83, no. 3, Sept. 1964, pp. 423-425.

74. Dowson, D.; and Whitaker, B. A.: A Numerical Procedure for the Solution of the Elastohydrodynamic Problem of Rolling and Sliding Contacts Lubricated by a Newtonian Fluid. Proc. Inst. of Mech. Eng. (London), vol. 180, pt. 3B, 1965, pp. 57-71.

75. Kannel, J. W.; and Walowit, J. A.: Simplified Analysis for Tractions Between Rolling-Sliding Elastohydrodynamic Contacts. J. Lubr. Tech., vol. 93, Jan. 1971, pp. 39-46.

76. Poon, S. Y.: Some Calculations to Assess the Effect of Spin on the Tractive Capacity of Rolling Contact Drives. Proc. Inst. Mech. Eng. (London), vol. 185, no. 76/71, 1970, pp. 1015-1022.

77. Lingard, S.: Tractions at the Spinning Point Contacts of a Variable Ratio Friction Drive. Tribol. Int., vol. 7, Oct. 1974, pp. 228-234.

78. Daniels, B. K.: Traction Contact Optimization. ASLE Preprint No. 79-LC-1A-1, 1979.

79. Tevaarwerk, J. L.: Traction Calculations Using the Shear Plane Hypothesis. Thermal Effects in Tribology: Proc. 6th (1979) Leeds/Lyon Conf. on Tribology, Mech. Eng. Publ., Ltd., 1980, pp. 201-213.

80. Tevaarwerk, J. L.: A Simple Thermal Correction for Large Spin Traction Curves. J. Mech. Des., vol. 103, no. 2, Apr. 1981, pp. 440-446.

81. Johnson, K. L.; and Greenwood, J. A.: Thermal Analysis of an Eyring Fluid in Elastohydrodynamic Traction. Wear, vol. 61, 1980 pp. 353-374.

82. Tevaarwerk, J. L.: Thermal Influence on the Traction Behavior of an Elastic/Plastic Model. Presented at the Leeds/Lyon Conference on Tribology, (Leeds, England), Aug. 1981.

83. Nakamura, L.; et al.: A development of a Traction Roller System for a Gas Turbine Driven APU. SAE Paper No. 790106, Feb. 1979.

84. Nasvytis, A. L.: Multiroller Planetary Friction Drives. SAE Paper No. 660763, Oct. 1966.

85. Loewenthal, S. H.; Anderson, N. E.; and Nasvytis, A. L.: Performance of a Nasvytis Multiroller Traction Drive. NASA TP-1378, 1978.

86. Loewenthal, S. H.; Anderson, N. E.; and Rohn, D. A.: Evaluation of a High Performance Fixed-Ratio Traction Drive. J. Mech. Des., vol. 103, no. 2, Apr. 1981, pp. 410-422.

87. Meyer, S.; and Connelly, R. E.: Traction Drive for Cryogenic Boost Pump. NASA TM-81704, 1981.

88. Radtke, R. R.; Unnewehr, L. E.; and Freedman, R. J.: Optimization of a Continuously Variable Transmission with Emission Constraints. SAE Paper No. 810107, Feb. 1981.

89. Strauch, S.: Flywheel Systems for Vehicles. Proc. Electric and Hybrid Vehicle Advanced Technology Seminar, Dec. 8-9, 1980, California Institute of Technology, Pasadena, pp. 219-236.

90. Stubbs, P. W. R.: The Development of a Perbury Traction Transmission for Motor Car Applciations. J. Mech. Des., vol. 103, no. 4, Jan. 1981, pp. 29-40.

91. Kemper, Y.: A High Power Density Traction Drive. SAE Paper No. 790849, 1979.

92. Elu, P.; and Kemper, Y.: Performance of a Nutating Traction Drive. ASME Paper No. 80-C2/DET-63, Aug. 1980.

93. Dickinson, T. W.: Development of a Variable Speed Transmission for Light Ractors. SAE Paper No. 770749, Sept. 1977.

94. Raynard, A. E.; Kraus, J. H.; and Bell, D. D.: Design Study of Toroidal Traction CVT for Electric Vehicles. (Rept-80-16762, AiResearch Manufacturing Company; NASA Contract DEN3-117.) DOE/NASA/0117-80/1, NASA CR-159803, 1980.

95. Walker, R. D.; and McCoin, D. K.: Design Study of a Continuously Variable Cone/Roller Traction Transmission for Electric Vehicles. DOE/NASA/0115-80/1, NASA CR-159841, Sept. 1980.

96. Parker, R. J.; Loewenthal, S. H.; and Fischer, G. K.: Design Studies of Continuously Variable Transmissions for Electric Vehicles. DOE/NASA/10444-12, NASA TM-81642, 1981.

97. Kraus, C. E.: An Up-To-Date Guide for Designing Traction Drives. Pt. I. Mach. Des., July 2, 1964, pp. 106-112; and Pt. II. Mach. Des., July 16, 1964, pp. 147-152.

# REPORT DOCUMENTATION PAGE

Public reporting burden for this collection of information is estimated to average 1 hour per response, including the time for reviewing instructions, searching existing data sources, gathering and maintaining the data needed, and completing and reviewing the collection of information. Send comments regarding this burden estimate or any other aspect of this collection of information, including suggestions for reducing this burden, to Washington Headquarters Services, Directorate for Information Operations and Reports, 1215 Jefferson Davis Highway, Suite 1204, Arlington, VA 22202-4302, and to the Office of Management and Budget, Paperwork Reduction Project (0704-0188), Washington, DC 20503.

| 1. AGENCY USE ONLY (Leave blank) | 2. REPORT DATE<br>October 1985 | 3. REPORT TYPE AND DATES COVERED<br>Technical Memorandum |
|---|---|---|

**4. TITLE AND SUBTITLE**

Tribology: The Story of Lubrication and Wear

**5. FUNDING NUMBERS**

WU–505–44–12–00

**6. AUTHOR(S)**

Donald H. Buckley, William R. Jones, Jr., Harold E. Sliney, Erwin V. Zaretsky, Dennis P. Townsend, and Stuart H. Loewenthal

**7. PERFORMING ORGANIZATION NAME(S) AND ADDRESS(ES)**

National Aeronautics and Space Administration
Lewis Research Center
Cleveland, Ohio 44135–3191

**8. PERFORMING ORGANIZATION REPORT NUMBER**

E–4535

**9. SPONSORING/MONITORING AGENCY NAME(S) AND ADDRESS(ES)**

National Aeronautics and Space Administration
Washington, DC 20546–0001

**10. SPONSORING/MONITORING AGENCY REPORT NUMBER**

NASA TM–101430

**11. SUPPLEMENTARY NOTES**

Prepared for Seminar F–107 at the 1985 International Trade Fair, Cleveland, Ohio, October 18, 1985. This report is a compilation of papers presented at other meetings and published elsewhere.

**12a. DISTRIBUTION/AVAILABILITY STATEMENT**

Unclassified - Unlimited
Subject Category: 39

Available electronically at http://gltrs.grc.nasa.gov/GLTRS
This publication is available from the NASA Center for AeroSpace Information, (301) 621–0390.

**12b. DISTRIBUTION CODE**

**13. ABSTRACT (Maximum 200 words)**

This is a compilation of papers on the subjects of lubricants and lubricated components. The first paper addresses the fundamentals of tribology (the study of adhesion, friction, and wear). This is followed by a survey of the technology and science of boundary lubrication with liquid lubricants; another paper describes materials and methods used in solid lubrication practice. Conventional solid lubricants such as graphite and molybdenum disulfide are described, followed by a discussion of novel solid lubricants for very high temperature applications. In addition, there are three papers on the subject of lubricated mechanical components. The scope of these papers includes the lubrication and design of high speed rolling element bearings, high speed gears, and traction drives.

**14. SUBJECT TERMS**

Tribology fundamentals; Boundary lubrication; Solid lubrication;
Rolling element bearings; Gears; Traction drives

**15. NUMBER OF PAGES**
150

**16. PRICE CODE**

| 17. SECURITY CLASSIFICATION OF REPORT<br>Unclassified | 18. SECURITY CLASSIFICATION OF THIS PAGE<br>Unclassified | 19. SECURITY CLASSIFICATION OF ABSTRACT<br>Unclassified | 20. LIMITATION OF ABSTRACT |
|---|---|---|---|